NUMERICAL EVALUATION OF WAVENUMBERS OF THE ACOUSTIC WAVES PROPAGATING IN AN ICE-COVERED OCEAN

By

Mohammad M. Khan

Boris P. Belinskiy
Professor of Mathematics
(Major Advisor)

Lakmali Weerasena
Professor of Mathematics
(Co-Major Advisor)

Christopher L. Cox
Professor and Department Head
(Committee Member)

Jin Wang
Professor of Mathematics
(Committee Member)

Aniekan A. Ebiefung
Professor of Mathematics
(Committee Member)

Lani Gao
Professor of Mathematics
(Committee Member)

NUMERICAL EVALUATION OF WAVENUMBERS OF THE ACOUSTIC WAVES PROPAGATING IN AN ICE-COVERED OCEAN

By

Mohammad M. Khan

A Thesis Submitted to the University of
Tennessee at Chattanooga in Partial
Fulfillment of the Requirements of the Degree
of Doctor of Philosophy in Computational Science:
Computational and Applied Mathematics

The University of Tennessee at Chattanooga
Chattanooga, Tennessee

May 2023

ABSTRACT

We consider acoustic wave propagation in a layered ocean waveguide covered by thick ice. The standard method of separation of variables leads to a Sturm-Liouville problem in the crosssection of the waveguide. We are specifically interested in the two leading modes, the separated solutions for the maximal eigenvalues. We first consider the homogeneous waveguide. We prove the differentiability of the eigenvalues with respect to the frequency, the monotonicity of the eigenvalues with respect to the frequency, and the existence of the cut-off frequency. We compare these eigenvalues with the eigenvalues for the case of a waveguide with a free surface. To obtain some information about the influence of global warming on ice covers, we find the change in these eigenvalues with respect to air temperature. We further consider a layered medium. Assuming that the speed of propagation varies within the given limits, we develop a numerical algorithm, based on the formalism for layered media, that allows evaluating the minimum and maximum of the wavenumbers of the leading modes for a given continuous profile of the speed and the given values of Young's Modulus and ice thickness. We compare some of these numerical results with the Machine Learning results. After finding numerical results, we compare them with the results of the asymptotic considerations and find the simplified dispersion relations. We further consider the model of pack ice, a limiting case of thick ice. Like the case of thick ice, we find the analytical, numerical, and asymptotic results for this case. These results were compared with the results of the model of thick ice. With the help of our results, we hope to develop the corresponding inverse problem methods for future work to study the influence of global warming on ice covers.

DEDICATION

I would like to dedicate this to my primary advisor, Dr. Boris P. Belinskiy, who helped me at every step of my journey in the doctoral program and taught me the meaning of success.

ACKNOWLEDGEMENTS

I would like to thank the Computational Science Ph.D. program at the University of Tennessee at Chattanooga and Dr. Anthony Skjellum from the Center for Excellence in Applied Computational Science and Engineering at the University of Tennessee at Chattanooga for providing partial support for this project. This project would not have been possible without Dr. Boris P. Belinskiy and Dr. Lakmali Weerasena. I would also like to thank Dr. Christopher L. Cox, Dr. Jin Wang, Dr. Lani Gao, and Dr. Aniekan A. Ebiefung for providing thoughtful suggestions to improve the overall presentation of the material.

TABLE OF CONTENTS

LIST OF FIGURES

LIST OF ABBREVIATIONS

exp, Exponential

lim, Limit

min, Minimum

max, Maximum

LIST OF SYMBOLS

$\mathbb{R}$, set of real numbers

∇, gradient operator

$\nabla\cdot$, dot product with gradient operator

$\nabla\times$, cross product with gradient operator

$\mathscr{L}^2[0,d]$, set of square-integrable functions from 0 to d

$\oplus$, direct sum operator

$\mathbb{C}$, set of complex numbers

Δ, Laplace operator or Change

δ, delta function

$\mathbb{N}$, set of natural numbers

$\mathbb{N}_0$, set of natural numbers including 0

e, Euler's number

π, mathematical constant for the ratio of circle's circumference to its diameter

∞, infinity

$=$, equal to

$\approx$, approximately

$\implies$, implies

$\rightarrow$, approaches

$\in$, element of

$<$, less than

$<<$, much less than

$>$, greater than

$>>$, much greater than

$\leq$, less than or equal to

$\geq$, greater than or equal to

$:=$, defined as

$\sum$, sum

$\prod$, product

$\forall$, for all

CHAPTER 1

Introduction

On Earth, there are several regions where the ocean is covered by ice. We first consider acoustic wave propagation in an ocean waveguide covered by thick ice. The ocean is supposed to be layered, i.e., the speed of wave propagation varies with the depth of the ocean, but not along the waveguide (see [1] - [3]). Different types of ocean waves are actively studied: acoustic, gravity, and acoustic-gravity waves. According to [4], [5], acoustic waves propagate through longitudinal compression with the negligible effect of gravity, gravity waves are governed by gravity, and acoustic-gravity waves are compression-type waves propagating with amplitudes governed by the restoring force of gravity.

In [6], the problems of the influence of compressibility of the ocean in generating acoustic-gravity waves, along with the nonlinear interaction of waves of profoundly different wavelengths, are studied. In [7], the orthogonality relations of normal modes in moving and quiescent media are found, as well as variations in wavenumbers due to small perturbations in environmental parameters. In [8], basic equations of the acoustic-gravity surface waves are revisited, some simple approximations for the wavenumbers are found, and rich physical interpretation is given. In [9], the dispersion of ocean surface waves in sea ice is studied for diverse models. Diverse models of ice and the corresponding wave processes are discussed in [10]. We also mention [11] where the dispersion relation models, based on energy loss mechanisms, are derived. The influence of energy loss is also discussed in [10]. Some mathematical aspects of wave propagation in the ocean waveguide covered by thick ice are discussed in [12], [13].

The acoustic field in a waveguide may be represented as a series of so-called *modes*, i.e., separated solutions of the corresponding partial differential equation subject to the boundary conditions on the bottom of the ocean and the top covered by ice. We are specifically interested in the so-called *leading modes*, i.e., the solutions with the two largest wavenumbers in the direction of propagation (along the waveguide). These wavenumbers appear as the first two eigenvalues of a Sturm-Liouville problem on the cross-section of the waveguide. We study the different mathematical properties of the modes. Specifically, we find lower and upper bounds for the two first wavenumbers. For realistic parameters of the ocean waveguide and thick ice, the problem contains a large-valued parameter. We find the asymptotic formulas for the eigenvalues with respect to this parameter. We develop a numerical algorithm that allows, for a given profile of the speed, to evaluate the frequency dependence of the leading wavenumbers. The algorithm is based on matrix formalism that is natural for layered media. We compare the numerical and asymptotic results. Our results could allow tracking for long-term variations of the ice properties, such as changes in the thickness of an ice cover. Hence, we can obtain new results about the impact of global warming, seasonal changes, and other geological and environmental factors on ice covers.

We further consider a particular case of ocean ice cover, pack ice cover. These results are based on [14] and were presented at the Research Dialogues Conference and Technology Symposium at the University of Tennessee at Chattanooga and the 46th Annual New York State Regional Graduate Mathematics Conference at Syracuse University. With the same assumptions of the ocean as in the case of thick ice cover, we study the propagation of the acoustic wave in an ocean waveguide covered by pack ice. We formulate the Sturm-Liouville problem and find the first two eigenvalues, i.e., the two largest wavenumbers. Like the case of thick ice, we evaluate the minimum and maximum of these wavenumbers and present the numerical and asymptotic results. Based on the results, we note that the model of pack ice may be treated as the limiting case of the model of thick ice as the cylindrical rigidity is equal to 0. We discuss the similarities and differences between the results of these two models.

Our overall scheme is as follows: in Chapter 2, we describe the physical model of our problem; in Chapter 3, we present the qualitative results of the two positive solutions of the transcendental equations and the two eigenvalues of the Sturm-Liouville problem; Chapter 4 is dedicated to the numerical results; Chapter 5 is dedicated to the asymptotic results; in Chapter 6, we discuss a particular case of the thick ice model and present the qualitative, numerical, and asymptotic results of this case.

CHAPTER 2

The Physical Model

Different aspects of the model are discussed in [9], [10], [12], [13], [15], see also the references therein.

Let the ocean be layered, and we define the waveguide as $\mathbb{R}^2_d := \{-\infty < z < \infty,\ 0 < x < d\}$. As noted in [16], [17], we can derive the basic acoustic wave equations using fluid dynamics. The propagation of sound waves in a fluid (such as water) can be modeled by an equation of continuity (conservation of mass) and an equation of motion (conservation of momentum). Assuming for simplicity that the density of the medium is constant, we obtain

$$\frac{\partial p}{\partial t} + k\nabla \cdot \vec{u} = 0 \text{ (continuity equation)}; \tag{2.0.1}$$

$$\rho_0 \frac{\partial \vec{u}}{\partial t} + \nabla p = 0 \text{ (equation of motion)}, \tag{2.0.2}$$

where $p(\vec{x},t)$ is the acoustic pressure, $\vec{u}(\vec{x},t)$ the flow velocity vector, $\vec{x} = (z,x)$ the vector of spatial coordinates, t the time, ρ_0 the static mass density of the medium, and k the bulk modulus of the medium. The density ρ_0 is supposed to be constant. The bulk modulus k may be expressed as $k = \rho_0 c^2$, where the speed c is a function of $\vec{x}$.

Differentiating equation (2.0.1) with respect to t, we obtain

$$\frac{\partial^2 p}{\partial t^2} + k\nabla \cdot \vec{u}_t = 0. \tag{2.0.3}$$

Applying the operator $\nabla\cdot$ to equation (2.0.2), we obtain

$$\rho_0 \nabla \cdot \vec{u}_t + \Delta p = 0. \tag{2.0.4}$$

From equations (2.0.3) and (2.0.4) and from the definition of k,

$$\frac{\partial^2 p}{\partial t^2} = c^2 \Delta p, \tag{2.0.5}$$

which is the acoustic wave equation for pressure.

Differentiating equation (2.0.2) with respect to t, we obtain

$$\rho_0 \frac{\partial^2 \vec{u}}{\partial t^2} + \nabla p_t = 0. \tag{2.0.6}$$

Applying the operator ∇ to equation (2.0.1), we obtain

$$\nabla p_t + k\Delta \vec{u} = 0. \tag{2.0.7}$$

From equations (2.0.6) and (2.0.7) and from the definition of k,

$$\frac{\partial^2 \vec{u}}{\partial t^2} = c^2 \Delta \vec{u}, \tag{2.0.8}$$

which is the acoustic wave equation for the flow velocity vector.

In Acoustics, the flow velocity field is assumed to be irrotational, i.e., $\nabla \times \vec{u} = 0$. Hence, this equation may be expressed in terms of a scalar potential $\Phi(\vec{x},t)$, where $\vec{u} = \nabla\Phi$, and the acoustic wave equation is written as

$$\Phi_{tt} = c^2(z,x)\Delta\Phi, \;\; (z,x) \in \mathbb{R}^2_d, \tag{2.0.9}$$

where the speed c is a function of $\vec{x}$. Since the ocean is layered, $c = c(x)$. We assume that the bottom $S_0 = \{-\infty < z < \infty,\ x = 0\}$ is rigid and obtain

$$\Phi_x(z,0,t) = 0,\ \ z \in \mathbb{R}. \tag{2.0.10}$$

Remark 2.0.1. This text uses the term "ice cover," which means ice floe.

The thick ice cover is located at the surface $S_d = \{-\infty < z < \infty,\ x = d\}$. Let $w(z,t)$ be the vertical displacement of this surface. The velocity is continuous on the boundary of the acoustic medium and ice cover. Using this continuity condition, we obtain

$$w_t(z,t) = \Phi_x(z,d,t),\ \ z \in \mathbb{R}. \tag{2.0.11}$$

We consider the model of thick ice. On Earth, ice covers on the ocean surface are mainly found on the poles. In [9], [10], Newton's second law is used to derive the boundary condition

$$Dw_{zzzz} + mw_{tt} + \rho_2 gw + \rho_2 \Phi_t = 0, \tag{2.0.12}$$

where $D = \dfrac{Eh^3}{12(1-\sigma^2)}$ is the cylindrical rigidity of the ice cover, E is Young's Modulus for ice, σ is the Poisson's ratio, h is the thickness of the ice cover, $m = \rho_1 h$ is the surface density of the ice cover, ρ_1 is the density of ice, ρ_2 is the density of water, and g is the gravitational constant. All these quantities are positive. The value of Young's Modulus for ice varies with the temperature change. Therefore, if the temperature is constant, we have a fixed value. Here, we consider different values for E to observe the impact of global warming and seasonal changes on the ice.

Remark 2.0.2. The physical meaning of D is the force required to deform the ice cover by a given thickness value.

The overall picture of our physical model is represented by Figure 2.1.

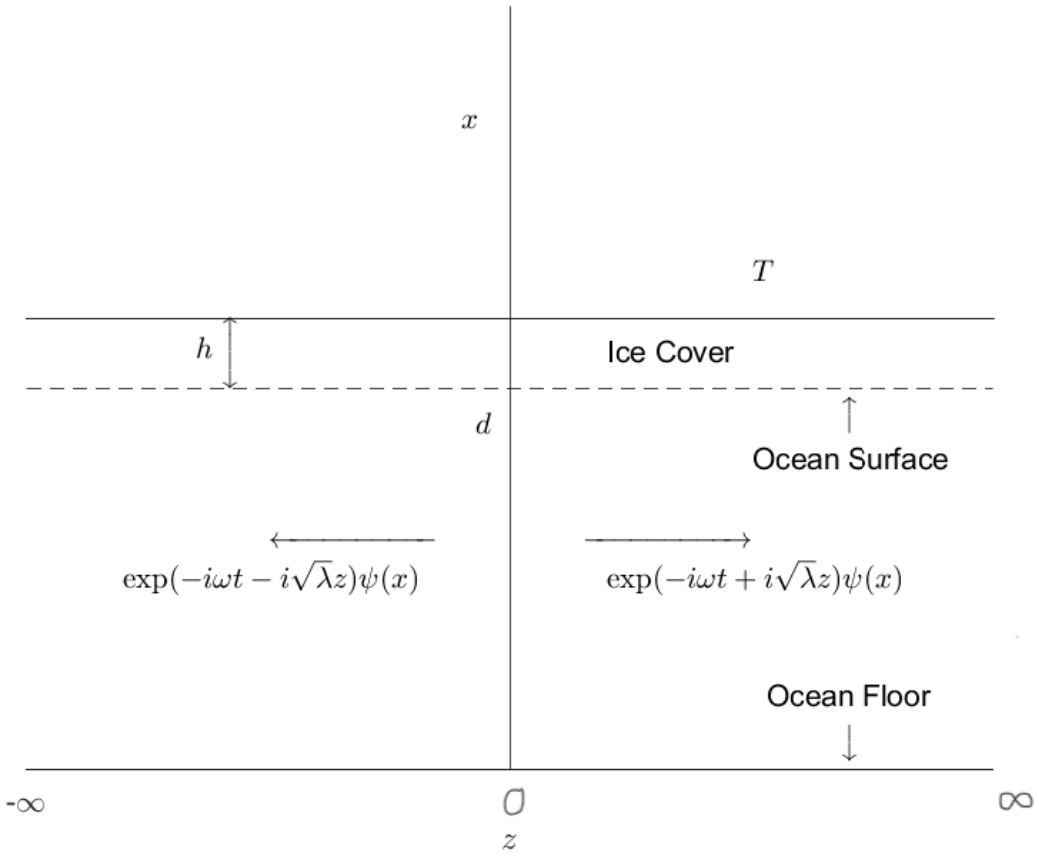

Figure 2.1 The two-dimensional geometry of the ice cover on the ocean surface (Not drawn to scale)

With the help of the separation of variables method, we obtain a solution of equations (2.0.9) and (2.0.12)

$$\Phi = \exp(-i\omega t \pm i\sqrt{\lambda}z)\psi(x), \quad w = \exp(-i\omega t \pm i\sqrt{\lambda}z)v, \tag{2.0.13}$$

where ω is the frequency of oscillations and λ is the parameter of separation. The vector $(\psi(x),\, v) \in \mathscr{L}^2[0,d] \oplus \mathbb{C}$, called the eigenfunction of the cross-section, is the solution of the Sturm-Liouville

problem

$$\psi'' + \left(\frac{\omega^2}{c^2(x)} - \lambda\right)\psi = 0, \;\; 0 < x < d, \tag{2.0.14}$$

$$\psi'(0) = 0, \tag{2.0.15}$$

$$D\lambda^2 v - m\omega^2 v + \rho_2 g v - i\omega\rho_2\psi(d) = 0, \tag{2.0.16}$$

$$-i\omega v = \psi'(d). \tag{2.0.17}$$

If $\frac{\omega^2}{c^2} = \lambda$, we have $\psi''(x) = 0$, which means that $\psi(x)$ is a linear function. From boundary condition (2.0.15), we conclude that $\psi(x)$ is constant. The remaining boundary conditions show $\psi(x) = v \equiv 0$.

The quantity $\kappa := \sqrt{\lambda}$ is called the *wavenumber*. If $\kappa > 0$, the functions (2.0.13) describe a *propagating mode*. According to [18], only propagating modes carry the energy far away from a source.

Remark 2.0.3. We briefly explain why the propagating modes are of special interest. If we look for the solution of wave equation (2.0.9) in the form $\Phi(t,z,x) = e^{-i\omega t}\Psi(z,x)$, then the function Ψ satisfies the Helmholtz equation $\left(\Delta + \frac{\omega^2}{c^2(x)}\right)\Psi = 0$. For the scattering problems in an ice-covered ocean, as well as the inverse problem, Green's function is helpful (for diverse scattering models, see, e.g., [2], [13], [19] - [23]). It is defined as the solution of the differential equation $\left(\Delta + \frac{\omega^2}{c^2(x)}\right) G(z,z_0,x,x_0) = \delta(z-z_0)\delta(x-x_0)$ subject to the appropriate boundary conditions

and radiation conditions. The following representation may be derived (see, e.g., [13])

$$G(z,z_0,x,x_0)=\sum_{n\geq 0} c_n e^{i\sqrt{\lambda_n}|z-z_0|}\psi_n(x)\psi_n(x_0), \tag{2.0.18}$$

where c_n are some coefficients that do not depend on the coordinates. We observe that for the large distances, $|z-z_0| >> 1$, only the propagating modes ($\lambda_n > 0$) present an important contribution to the field.

There are only finitely many propagating modes in our waveguide. It will be confirmed mathematically in Chapter 3 by showing that the number of positive eigenvalues λ is finite. Therefore, it is of interest to study a few maximal eigenvalues. The values of the model change from one region to another and, within the region, from one season to another. The variations of the sound speed in the ocean are discussed, e.g., in [24]. Therefore, we have the problem of finding a possible range for eigenvalues when the values of the model change within the known limits.

Eliminating v from equations (2.0.16) and (2.0.17), we obtain a new boundary condition

$$\psi'(d)=\frac{\omega^2}{g\left(1+\dfrac{D\lambda^2}{\rho_2 g}-\dfrac{\omega^2}{\omega_0^2}\right)}\psi(d), \text{ where } \omega_0^2:=\frac{\rho_2 g}{m}. \tag{2.0.19}$$

Remark 2.0.4. The physical meaning of ω_0 is the eigenfrequency of the oscillations of an ice cover in the water around the static equilibrium position (see [9], [10]).

Define

$$\tau(\omega,\lambda):=\frac{\omega^2}{g\left(1+\dfrac{D\lambda^2}{\rho_2 g}-\dfrac{\omega^2}{\omega_0^2}\right)}. \tag{2.0.20}$$

Hence, equation (2.0.19) can be written as

$$\psi'(d) = \tau(\omega, \lambda)\psi(d). \tag{2.0.21}$$

The above boundary condition (2.0.21) contains the spectral parameter λ. The physical meaning of the function $\tau(\omega, \lambda)$ will be presented in Chapter 5.

When $D = 0$, definition (2.0.20) becomes

$$\tau_0(\omega, \lambda) = \frac{\omega^2}{g\left(1 - \dfrac{\omega^2}{\omega_0^2}\right)} := \beta(\omega), \tag{2.0.22}$$

where $\beta(\omega) > 0$ if $\omega < \omega_0$ and $\beta(\omega) < 0$ if $\omega > \omega_0$. The function $\beta(\omega)$ will be used later in our study.

CHAPTER 3

Qualitative Results

In this chapter, we provide qualitative results for two cases: homogeneous ocean and non-homogeneous ocean.

Remark 3.0.1. Some of the proofs in this chapter are labeled as "in part, numerical," which means that some numerical results with a realistic set of parameters were used to prove the analytical results.

3.1 Transcendental Equations

We start our analysis of the Sturm-Liouville problem with the case of a homogeneous ocean, i.e., $c(x) = c$. The solution of equation (2.0.14) subject to boundary condition (2.0.15) is represented as

$$\psi(x) = \begin{cases} \cos\sqrt{\dfrac{\omega^2}{c^2} - \lambda}\,x & \text{if} \quad \dfrac{\omega^2}{c^2} > \lambda; \\ \\ \cosh\sqrt{\lambda - \dfrac{\omega^2}{c^2}}\,x & \text{if} \quad \dfrac{\omega^2}{c^2} < \lambda. \end{cases} \tag{3.1.1}$$

From boundary condition (2.0.21), we obtain a set of transcendental equations

$$\begin{aligned}
&\sqrt{\frac{\omega^2}{c^2}-\lambda}\tan\sqrt{\frac{\omega^2}{c^2}-\lambda}d+\tau(\omega,\lambda)=0 \quad \text{if} \quad \frac{\omega^2}{c^2}>\lambda;\\
&-\sqrt{\lambda-\frac{\omega^2}{c^2}}\tanh\sqrt{\lambda-\frac{\omega^2}{c^2}}d+\tau(\omega,\lambda)=0 \quad \text{if} \quad \frac{\omega^2}{c^2}<\lambda.
\end{aligned} \tag{3.1.2}$$

From definition (2.0.20), equations in (3.1.2) are represented as

$$\begin{aligned}
&g\left(1+\frac{D\lambda^2}{\rho_2 g}-\frac{\omega^2}{\omega_0^2}\right)\sqrt{\frac{\omega^2}{c^2}-\lambda}\tan\sqrt{\frac{\omega^2}{c^2}-\lambda}d+\omega^2=0 \quad \text{if} \quad \frac{\omega^2}{c^2}>\lambda;\\
&-g\left(1+\frac{D\lambda^2}{\rho_2 g}-\frac{\omega^2}{\omega_0^2}\right)\sqrt{\lambda-\frac{\omega^2}{c^2}}\tanh\sqrt{\lambda-\frac{\omega^2}{c^2}}d+\omega^2=0 \quad \text{if} \quad \frac{\omega^2}{c^2}<\lambda.
\end{aligned} \tag{3.1.3}$$

We introduce dimensionless variables ξ and η

$$\begin{aligned}
&\xi \coloneqq \sqrt{\frac{\omega^2}{c^2}-\lambda}d \quad \text{if} \quad \frac{\omega^2}{c^2}>\lambda;\\
&\eta \coloneqq \sqrt{\lambda-\frac{\omega^2}{c^2}}d \quad \text{if} \quad \frac{\omega^2}{c^2}<\lambda.
\end{aligned} \tag{3.1.4}$$

Hence, equations in (3.1.3) can be written as

$$\begin{aligned}
&\left[g+\frac{Dg}{\rho_2 g}\left(\frac{\omega^2}{c^2}-\frac{\xi^2}{d^2}\right)^2-\frac{g\omega^2}{\omega_0^2}\right]\frac{\xi}{d}\tan\xi+\omega^2=0;\\
&-\left[g+\frac{Dg}{\rho_2 g}\left(\frac{\omega^2}{c^2}+\frac{\eta^2}{d^2}\right)^2-\frac{g\omega^2}{\omega_0^2}\right]\frac{\eta}{d}\tanh\eta+\omega^2=0.
\end{aligned}$$

Multiplying the first equation by $\frac{d}{\xi\omega^2}$ and the second equation by $\frac{d}{\eta\omega^2}$, we obtain a set of equations

$$\begin{aligned}
&\left[1+\frac{D}{\rho_2 g d^4\left(1-\frac{\omega^2}{\omega_0^2}\right)}\left(\frac{\omega^2 d^2}{c^2}-\xi^2\right)^2\right]\tan\xi+\frac{d\omega^2}{\xi g\left(1-\frac{\omega^2}{\omega_0^2}\right)}=0;\\
&\left[1+\frac{D}{\rho_2 g d^4\left(1-\frac{\omega^2}{\omega_0^2}\right)}\left(\frac{\omega^2 d^2}{c^2}+\eta^2\right)^2\right]\tanh\eta=\frac{d\omega^2}{\eta g\left(1-\frac{\omega^2}{\omega_0^2}\right)}.
\end{aligned}\tag{3.1.5}$$

We now introduce a dimensionless parameter $P(\omega)$

$$P(\omega):=\frac{D}{\rho_2 g d^4\left(1-\frac{\omega^2}{\omega_0^2}\right)}.\tag{3.1.6}$$

From definitions (2.0.22) and (3.1.6), equations in (3.1.5) can be written as

$$\begin{aligned}
&\left[1+P(\omega)\left(\frac{\omega^2 d^2}{c^2}-\xi^2\right)^2\right]\tan\xi+\frac{\beta(\omega)d}{\xi}=0;\\
&\left[1+P(\omega)\left(\frac{\omega^2 d^2}{c^2}+\eta^2\right)^2\right]\tanh\eta=\frac{\beta(\omega)d}{\eta}.
\end{aligned}\tag{3.1.7}$$

Remark 3.1.1. Numerical results show that $P(\omega)$ is small enough. $P(\omega)$ can be lowered further by lowering E and/or h. When $P(\omega)\to 0$, we obtain a special case of the thick ice model (see Chapter 6). Then both ξ and η could be represented as power series with respect to $P(\omega)$ with the first term to be these quantities when $P(\omega)=0$.

The following proposition discusses the solutions of the first transcendental equation in (3.1.7).

Proposition 3.1.1. *The equation*

$$\xi \tan \xi = -\frac{\beta(\omega)d}{1+P(\omega)\left(\frac{\omega^2 d^2}{c^2}-\xi^2\right)^2} \tag{3.1.8}$$

has a unique solution in $\left((2n-1)\frac{\pi}{2}, n\pi\right)$*, where* $n \in \mathbb{N}$*, for* $\omega < \omega_0$ *and a unique solution in* $\left(k\pi, (2k+1)\frac{\pi}{2}\right)$*, where* $k \in \mathbb{N}_0$*, for* $\omega > \omega_0$*.*

Proof. (in part, numerical) Let $f(\xi) = \xi \tan \xi$ and $g(\xi) = -\frac{\beta(\omega)d}{1+P(\omega)\left(\frac{\omega^2 d^2}{c^2}-\xi^2\right)^2}$, for $\xi \in (0,\infty)$.

We start with the cases: (i) $\xi \in \left(0, \frac{\pi}{2}\right)$, (ii) $\xi \in \left(\frac{\pi}{2}, \frac{3\pi}{2}\right)$, and (iii) $\xi \in \left(\frac{3\pi}{2}, \frac{5\pi}{2}\right)$.

(i): In $\left(0, \frac{\pi}{2}\right)$, $f(\xi) > 0$. From numerical results, $g(\xi) < 0$ for $\omega < \omega_0$ and $g(\xi) > 0$ for $\omega > \omega_0$. Hence, there is no point of intersection in $\left(0, \frac{\pi}{2}\right)$ for $\omega < \omega_0$.

Since $f'(\xi) = \tan \xi + \xi \sec^2 \xi > 0$ and $g'(\xi) = -\frac{4\beta(\omega)dP(\omega)\left(\frac{\omega^2 d^2}{c^2}-\xi^2\right)\xi}{\left[1+P(\omega)\left(\frac{\omega^2 d^2}{c^2}-\xi^2\right)^2\right]^2} < 0$, there is a unique point of intersection in $\left(0, \frac{\pi}{2}\right)$ for $\omega > \omega_0$.

There is a jump discontinuity in $g(\xi)$ at $\omega = \omega_0$ and $f(\xi) < g(\xi)$ as $\omega \to \omega_0^+$.

Hence, equation (3.1.8) has no solution in $\left(0, \frac{\pi}{2}\right)$ for $\omega < \omega_0$ and $\omega = \omega_0$ and a unique solution in $\left(0, \frac{\pi}{2}\right)$ for $\omega > \omega_0$.

(ii): In $\left(\frac{\pi}{2}, \frac{3\pi}{2}\right)$, $f(\xi) < g(\xi)$ when $\xi \to \frac{\pi}{2}^+$ and $f(\xi) > g(\xi)$ when $\xi \to \frac{3\pi}{2}^-$. Therefore, there is at least one point of intersection in $\left(\frac{\pi}{2}, \frac{3\pi}{2}\right)$. $f(\xi) < 0$, for $\xi \in \left(\frac{\pi}{2}, \pi\right)$, and $f(\xi) > 0$, for $\xi \in \left(\pi, \frac{3\pi}{2}\right)$. For $\omega < \omega_0$, $g(\xi) < 0$, for $\xi \in \left(\frac{\pi}{2}, \frac{3\pi}{2}\right)$, so the point of intersection is in $\left(\frac{\pi}{2}, \pi\right)$. Since $f'(\xi) > 0$, $g'(\xi) < 0$, and $f(\xi) < g(\xi)$, there is a unique point of intersection in $\left(\frac{\pi}{2}, \pi\right)$. For $\omega > \omega_0$, $g(\xi) > 0$, for $\xi \in \left(\frac{\pi}{2}, \frac{3\pi}{2}\right)$, so the point of intersection is

in $\left(\pi, \frac{3\pi}{2}\right)$. Since $f'(\xi) > 0$, $g'(\xi) < 0$, and $f(\xi) < g(\xi)$ as $\omega \to \omega_0^+$, there is a unique point of intersection in $\left(\pi, \frac{3\pi}{2}\right)$.

Hence, equation (3.1.8) has a unique solution in $\left(\frac{\pi}{2}, \pi\right)$ for $\omega < \omega_0$ and a unique solution in $\left(\pi, \frac{3\pi}{2}\right)$ for $\omega > \omega_0$.

(iii): From the similar reasoning as (ii), equation (3.1.8) has a unique solution in $\left(\frac{3\pi}{2}, 2\pi\right)$ for $\omega < \omega_0$ and a unique solution in $\left(2\pi, \frac{5\pi}{2}\right)$ for $\omega > \omega_0$.

Since the tangent function is π-periodic, the result of the proposition follows for any $n \in \mathbb{N}$ and any $k \in \mathbb{N}_0$. ■

Remark 3.1.2. From Proposition 3.1.1, the first equation in (3.1.7) has infinitely many positive solutions.

The following proposition discusses the solutions of the second transcendental equation in (3.1.7).

Proposition 3.1.2. *The equation*

$$\eta \tanh \eta = \frac{\beta(\omega) d}{1 + P(\omega)\left(\frac{\omega^2 d^2}{c^2} + \eta^2\right)^2} \tag{3.1.9}$$

has a unique solution for $\eta > 0$.

Proof. Consider $\eta \in (0, \infty)$. Let $f(\eta) = \eta \tanh \eta$ and $g(\eta) = \frac{\beta(\omega) d}{1 + P(\omega)\left(\frac{\omega^2 d^2}{c^2} + \eta^2\right)^2}$.

$f(\eta) < g(\eta)$ when $\eta \to 0^+$, and $f(\eta) > g(\eta)$ when $\eta \to \infty$. There is a jump discontinuity in $g(\eta)$ at $\omega = \omega_0$, but $f(\eta) > g(\eta)$ as $\omega \to \omega_0$. We find that $f'(\eta) = \tanh \eta + \eta \operatorname{sech}^2 \eta > 0$

and $g'(\eta) = -\dfrac{4\beta(\omega)dP(\omega)\left(\dfrac{\omega^2 d^2}{c^2}+\eta^2\right)\eta}{\left[1+P(\omega)\left(\dfrac{\omega^2 d^2}{c^2}+\eta^2\right)^2\right]^2} < 0$, for $\eta \in (0,\infty)$. Therefore, the result of the proposition follows. ■

Remark 3.1.3. From Proposition 3.1.2, the second equation in (3.1.7) has a unique positive solution.

If the ocean surface is ice-free, we have $m = \rho_1 h \to 0$, which implies $D \to 0$ and $\omega_0 \to \infty$. Hence, $\beta(\omega) \to \dfrac{\omega^2}{g}$ and the transcendental equations in (3.1.7) are represented as

$$\begin{aligned} \tan \xi^f + \frac{\omega^2 d}{g\xi^f} &= 0; \\ \tanh \eta^f &= \frac{\omega^2 d}{g\eta^f}, \end{aligned} \tag{3.1.10}$$

where the super index ^{f} denotes the free surface. The roots ξ^f and η^f obtained from the above equations will later be compared with the roots ξ and η obtained from the equations in (3.1.7).

Definition 3.1.4. Let $\xi_0(\omega)$ denote the least positive solution of the first equation of (3.1.7) and $\eta_0(\omega)$ the unique positive solution of the second equation.

The eigenvalue λ has one of two forms (see definitions (3.1.4))

$$\begin{aligned} \hat{\lambda}(\omega,c) &= \frac{\omega^2}{c^2} - \frac{\xi_0^2(\omega)}{d^2}; \\ \tilde{\lambda}(\omega,c) &= \frac{\omega^2}{c^2} + \frac{\eta_0^2(\omega)}{d^2}. \end{aligned} \tag{3.1.11}$$

We note that $\hat{\lambda}(\omega,c)$ is positive and that the corresponding mode is propagating only if the frequency is high enough, $\omega > \omega_*$, but $\tilde{\lambda}(\omega,c)$ is positive, $\forall \omega > 0$. According to the wave theory

terminology, the frequency ω_* is the *cut-off frequency* for $\hat{\lambda}(\omega,c)$ and there is no cut-off frequency for $\tilde{\lambda}(\omega,c)$. The equations in (3.1.11) imply $\tilde{\lambda}(\omega,c) > \hat{\lambda}(\omega,c)$. We use the notation $\hat{\lambda}_n$, $n \geq 1$, to denote the solutions of the first equation in (3.1.7). We immediately note that the existence of the frequency ω_* is not trivial; it will be proved within Proposition 3.2.1.

3.2 Analysis of $\xi_0(\omega)$ and $\eta_0(\omega)$

In the following proposition, we start by proving some analytic properties of $\xi_0(\omega)$ and $\eta_0(\omega)$.

Remark 3.2.1. In the following text, we use the notation $O()$, which means the following. If f and g are functions and $f = O(g)$, then $|f| \leq C|g|$, for some $C > 0$.

Proposition 3.2.1. *The following analytic properties of $\xi_0(\omega)$ and $\eta_0(\omega)$ hold.*

(a) $\xi_0(\omega)$ and $\eta_0(\omega)$ are smooth functions.

(b) $\dfrac{d\xi_0}{d\omega} < 0$ *for* $\omega < M$ *and* $\dfrac{d\xi_0}{d\omega} > 0$ *for* $\omega > M$, *where* $M \approx \left(\dfrac{\rho_2 g}{D}\right)^{\frac{1}{4}} c$.

(c) $\dfrac{d\eta_0}{d\omega} > 0$ *for* $\dfrac{\omega^4 d^4}{c^4} - \eta_0^4(\omega) < \dfrac{\rho_2 g d^4}{D}$ *and* $\dfrac{d\eta_0}{d\omega} < 0$ *for* $\dfrac{\omega^4 d^4}{c^4} - \eta_0^4(\omega) > \dfrac{\rho_2 g d^4}{D}$.

(d) $\lim\limits_{\omega\to 0} \xi_0(\omega) = \pi$, $\lim\limits_{\omega\to\omega_0} \xi_0(\omega) = \dfrac{\pi}{2}$, $\lim\limits_{\omega\to\infty} \xi_0(\omega) = \pi$.

(e) $\lim\limits_{\omega\to 0} \eta_0(\omega) = 0$; $\eta_0(\omega) = O(\omega)$ for $\omega \to 0$.

(f) $\lim\limits_{\omega\to\omega_0} \eta_0(\omega) = \left(\dfrac{\rho_2\omega_0^2}{D}\right)^{\frac{1}{5}} d$, $\lim\limits_{\omega\to\omega_0} \dfrac{\eta_0(\omega)\left[1 + P(\omega)\left(\dfrac{\omega^2 d^2}{c^2} + \eta_0^2(\omega)\right)^2\right]}{\beta(\omega) d} = 1.$

(g) $\lim\limits_{\omega\to\infty} \eta_0(\omega) = 0$; $\eta_0(\omega) = O\left(\dfrac{1}{\omega}\right)$ for $\omega \to \infty$.

(h) The cut-off frequency ω_* exists and is unique if we have the condition

$$\omega_0 > \frac{\pi c}{2d}. \tag{3.2.1}$$

Proof. (in part, numerical) (a) follows from the implicit function theorem.

(b): To prove (b), we use the first transcendental equation in (3.1.7). Differentiating this equation with respect to ω, we obtain

$$\frac{d\xi_0}{d\omega} = \frac{\frac{4\omega d^2}{c^2}P(\omega)\left(\frac{\omega^2 d^2}{c^2} - \xi_0^2(\omega)\right) + P'(\omega)\left(\frac{\omega^2 d^2}{c^2} - \xi_0^2(\omega)\right)^2 + \frac{\beta'(\omega)d}{\xi_0(\omega)\tan\xi_0(\omega)}}{-\frac{\sec^2\xi_0(\omega)}{\tan\xi_0(\omega)}\left[1 + P(\omega)\left(\frac{\omega^2 d^2}{c^2} - \xi_0^2(\omega)\right)^2\right] + \frac{\beta(\omega)d}{\xi_0^2(\omega)\tan\xi_0(\omega)} + 4\xi_0(\omega)P(\omega)\left(\frac{\omega^2 d^2}{c^2} - \xi_0^2(\omega)\right)}. \tag{3.2.2}$$

Differentiating $P(\omega)$ and $\beta(\omega)$ with respect to ω, we obtain

$$P'(\omega) = \frac{2\omega}{\omega_0^2\left(1 - \frac{\omega^2}{\omega_0^2}\right)}P(\omega), \tag{3.2.3}$$

$$\beta'(\omega) = \frac{2}{\omega\left(1 - \frac{\omega^2}{\omega_0^2}\right)}\beta(\omega). \tag{3.2.4}$$

Substituting equations (3.2.3) and (3.2.4) in equation (3.2.2), we obtain

$$\frac{d\xi_0}{d\omega} = \frac{f_1(\xi_0(\omega))}{f_2(\xi_0(\omega))}, \tag{3.2.5}$$

where $f_1(\xi_0(\omega)) = \frac{4\omega d^2}{c^2}P(\omega)\left(\frac{\omega^2 d^2}{c^2} - \xi_0^2(\omega)\right) + \frac{2\omega}{\omega_0^2\left(1 - \frac{\omega^2}{\omega_0^2}\right)}P(\omega)\left(\frac{\omega^2 d^2}{c^2} - \xi_0^2(\omega)\right)^2 + \frac{2}{\omega\left(1 - \frac{\omega^2}{\omega_0^2}\right)}\frac{\beta(\omega)d}{\xi_0(\omega)\tan\xi_0(\omega)}$ and $f_2(\xi_0(\omega)) = -\frac{\sec^2\xi_0(\omega)}{\tan\xi_0(\omega)}\left[1 + P(\omega)\left(\frac{\omega^2 d^2}{c^2} - \xi_0^2(\omega)\right)^2\right] + \frac{\beta(\omega)d}{\xi_0^2(\omega)\tan\xi_0(\omega)} + 4\xi_0(\omega)P(\omega)\left(\frac{\omega^2 d^2}{c^2} - \xi_0^2(\omega)\right)$.

From the first transcendental equation in (3.1.7),

$$\frac{\beta(\omega)d}{\xi_0(\omega)\tan\xi_0(\omega)} = -\left[1+P(\omega)\left(\frac{\omega^2d^2}{c^2}-\xi_0^2(\omega)\right)^2\right]. \tag{3.2.6}$$

From the above equation,

$$f_1(\xi_0(\omega)) = \frac{2}{\omega}\left[P(\omega)\left(\frac{\omega^4d^4}{c^4}-\xi_0^4(\omega)\right)-\frac{1}{1-\dfrac{\omega^2}{\omega_0^2}}\right]. \tag{3.2.7}$$

It will be proved in (d) that $\frac{\pi}{2} < \xi_0 < \pi$. From definition (3.1.6) and using realistic values of all quantities in $f_1(\xi_0(\omega))$, we observe that $f_1(\xi_0(\omega))$ is negative for $\omega < \omega_0$ and $\frac{\omega^4d^4}{c^4} - \xi_0^4(\omega) < \frac{\rho_2gd^4}{D}$ and positive for $\omega > \omega_0$ and $\frac{\omega^4d^4}{c^4} - \xi_0^4(\omega) > \frac{\rho_2gd^4}{D}$. Since $\frac{\rho_2gd^4}{D} >> \xi_0^4(\omega)$, $f_1(\xi_0(\omega))$ is negative for $\omega < \omega_0$ and $\omega < M$ and positive for $\omega > \omega_0$ and $\omega > M$, where $M \approx \left(\frac{\rho_2g}{D}\right)^{\frac{1}{4}} c$ and $M > \omega_0$.

From equation (3.2.6),

$$f_2(\xi_0(\omega)) = \frac{\xi_0(\omega)\sec^2\xi_0(\omega)+\tan\xi_0(\omega)}{\xi_0^2(\omega)\tan^2\xi_0(\omega)}\beta(\omega)d + 4\xi_0(\omega)P(\omega)\left(\frac{\omega^2d^2}{c^2}-\xi_0^2(\omega)\right). \tag{3.2.8}$$

We know that $\frac{\xi_0(\omega)\sec^2\xi_0(\omega)+\tan\xi_0(\omega)}{\xi_0^2(\omega)\tan^2\xi_0(\omega)} = \frac{2\xi_0(\omega)+\sin 2\xi_0(\omega)}{2\xi_0^2(\omega)\sin^2\xi_0(\omega)} > 0$ for $\xi_0(\omega) > 0$. Moreover, $\beta(\omega), P(\omega) > 0$ for $\omega < \omega_0$ and $\beta(\omega), P(\omega) < 0$ for $\omega > \omega_0$. Therefore, $f_2(\xi_0(\omega))$ is positive for $\omega < \omega_0$ and negative for $\omega > \omega_0$.

Substituting equations (3.2.7) and (3.2.8) in equation (3.2.5), we obtain the result of (b).

(c): To prove (c), we use the second transcendental equation in (3.1.7). Differentiating this equation with respect to ω, we obtain

$$\frac{d\eta_0}{d\omega} = \frac{g_1(\eta_0(\omega))}{g_2(\eta_0(\omega))}, \tag{3.2.9}$$

where $g_1(\eta_0(\omega)) = \dfrac{\beta'(\omega)d}{\eta_0(\omega)\tanh\eta_0(\omega)} - P'(\omega)\left(\dfrac{\omega^2d^2}{c^2}+\eta_0^2(\omega)\right)^2 - \dfrac{4\omega d^2}{c^2}P(\omega)\left(\dfrac{\omega^2d^2}{c^2}+\eta_0^2(\omega)\right)$
and $g_2(\eta_0(\omega)) = \dfrac{\operatorname{sech}^2\eta_0(\omega)}{\tanh\eta_0(\omega)}\left[1+P(\omega)\left(\dfrac{\omega^2d^2}{c^2}+\eta_0^2(\omega)\right)^2\right] + \dfrac{\beta(\omega)d}{\eta_0^2(\omega)\tanh\eta_0(\omega)} +$
$4\eta_0(\omega)P(\omega)\left(\dfrac{\omega^2d^2}{c^2}+\eta_0^2(\omega)\right)$.

Substituting equations (3.2.3) and (3.2.4) in equation (3.2.9), we obtain

$$\frac{d\eta_0}{d\omega} = \frac{h_1(\eta_0(\omega))}{h_2(\eta_0(\omega))}, \tag{3.2.10}$$

where $h_1(\eta_0(\omega)) = \dfrac{2}{\omega\left(1-\dfrac{\omega^2}{\omega_0^2}\right)}\dfrac{\beta(\omega)d}{\eta_0(\omega)\tanh\eta_0(\omega)} - \dfrac{2\omega}{\omega_0^2\left(1-\dfrac{\omega^2}{\omega_0^2}\right)}P(\omega)\left(\dfrac{\omega^2d^2}{c^2}+\eta_0^2(\omega)\right)^2 -$
$\dfrac{4\omega d^2}{c^2}P(\omega)\left(\dfrac{\omega^2d^2}{c^2}+\eta_0^2(\omega)\right)$ and $h_2(\eta_0(\omega)) = \dfrac{\operatorname{sech}^2\eta_0(\omega)}{\tanh\eta_0(\omega)}\left[1+P(\omega)\left(\dfrac{\omega^2d^2}{c^2}+\eta_0^2(\omega)\right)^2\right] +$
$\dfrac{\beta(\omega)d}{\eta_0^2(\omega)\tanh\eta_0(\omega)} + 4\eta_0(\omega)P(\omega)\left(\dfrac{\omega^2d^2}{c^2}+\eta_0^2(\omega)\right)$.

From the second transcendental equation in (3.1.7),

$$\frac{\beta(\omega)d}{\eta_0(\omega)\tanh\eta_0(\omega)} = 1+P(\omega)\left(\frac{\omega^2d^2}{c^2}+\eta_0^2(\omega)\right)^2. \tag{3.2.11}$$

From the above equation,

$$h_1(\eta_0(\omega)) = \frac{2}{\omega}\left[\frac{1}{1-\dfrac{\omega^2}{\omega_0^2}} - P(\omega)\left(\frac{\omega^4d^4}{c^4}-\eta_0^4(\omega)\right)\right]. \tag{3.2.12}$$

It will be proved in (e), (f), and (g) that $0 < \eta_0(\omega) < \left(\frac{\rho_2\omega_0^2}{D}\right)^{\frac{1}{5}} d$. From definition (3.1.6) and using realistic values of all quantities in $h_1(\eta_0(\omega))$, we observe that $h_1(\eta_0(\omega))$ is positive for $\omega < \omega_0$ and $\frac{\omega^4 d^4}{c^4} - \eta_0^4(\omega) < \frac{\rho_2 g d^4}{D}$ and negative for $\omega > \omega_0$ and $\frac{\omega^4 d^4}{c^4} - \eta_0^4(\omega) > \frac{\rho_2 g d^4}{D}$, where $\left(\frac{\rho_2 g d^4}{D} + \eta_0^4(\omega)\right)^{\frac{1}{4}} \frac{c}{d} > \omega_0$.

From equation (3.2.11),

$$h_2(\eta_0(\omega)) = \frac{\eta_0(\omega)\operatorname{sech}^2\eta_0(\omega) + \tanh\eta_0(\omega)}{\eta_0^2(\omega)\tanh^2\eta_0(\omega)}\beta(\omega)d + 4\eta_0(\omega)P(\omega)\left(\frac{\omega^2 d^2}{c^2} + \eta_0^2(\omega)\right). \tag{3.2.13}$$

We know that $\frac{\eta_0(\omega)\operatorname{sech}^2\eta_0(\omega) + \tanh\eta_0(\omega)}{\eta_0^2(\omega)\tanh^2\eta_0(\omega)} = \frac{2\eta_0(\omega) + \sinh 2\eta_0(\omega)}{2\eta_0^2(\omega)\sinh^2\eta_0(\omega)} > 0$ for $\eta_0(\omega) > 0$. Therefore, $h_2(\eta(\omega))$ is positive for $\omega < \omega_0$ and negative for $\omega > \omega_0$.

Substituting equations (3.2.12) and (3.2.13) in equation (3.2.10), we obtain the result of (c).

(d): To prove (d), we take the limit as $\omega \to 0$ of the first transcendental equation in (3.1.7). Taking this limit, we obtain

$$\lim_{\omega\to 0} \xi_0(\omega)\left(1 + \frac{D}{\rho_2 g d^4}\xi_0^4(\omega)\right)\tan\xi_0(\omega) = 0.$$

Since $\xi_0(\omega) > 0$ and $\xi_0(\omega)$ is a real solution, the above equation is only true if $\lim_{\omega\to 0}\tan\xi_0(\omega) = 0$, and the first result of (d) follows.

We now take the limit as $\omega \to \omega_0$ of the first transcendental equation in (3.1.7). From this limit,

$$\lim_{\omega\to\omega_0} \xi_0(\omega)\tan\xi_0(\omega) = -\lim_{\omega\to\omega_0} \frac{\rho_2\omega_0^2 d^5}{D\left(\frac{\omega_0^2 d^2}{c^2} - \xi_0^2(\omega)\right)^2}.$$

Let $f(\xi_0(\omega)) = \xi_0(\omega)\tan\xi_0(\omega)$ and $g(\xi_0(\omega)) = -\dfrac{\rho_2\omega_0^2 d^5}{D\left(\dfrac{\omega_0^2 d^2}{c^2} - \xi_0^2(\omega)\right)^2}$. The functions $f(\xi_0(\omega))$ and $g(\xi_0(\omega))$ have infinitely many points of intersection. Moreover, $f(\xi_0(\omega))$ has the first positive vertical asymptote at $\xi_0(\omega) = \dfrac{\pi}{2}$ and $g(\xi_0(\omega))$ has the vertical asymptote at $\xi_0(\omega) = \dfrac{\omega_0 d}{c}$. Since $\dfrac{\omega_0 d}{c} > \dfrac{\pi}{2}$, the first point of intersection is just after $\dfrac{\pi}{2}$, and the second result of (d) follows.

We now take the limit as $\omega \to \infty$ of the first transcendental equation in (3.1.7). From this limit,

$$\lim_{\omega\to\infty} \xi_0(\omega)\tan\xi_0(\omega) = 0,$$

which implies the third result of (d).

(e): To prove (e), we take the limit as $\omega \to 0$ of the second transcendental equation in (3.1.7). From this limit,

$$\lim_{\omega\to 0} \eta_0(\omega)\left(1 + \frac{D}{\rho_2 g d^4}\eta_0^4(\omega)\right)\tanh\eta_0(\omega) = 0.$$

Since $\eta_0(\omega)$ is a real-valued solution, the above equation is true if $\lim\limits_{\omega\to 0}\tanh\eta_0(\omega) = 0$, and the first result of (e) follows.

From the second transcendental equation in (3.1.7),

$$\eta_0(\omega)\tanh\eta_0(\omega) = \frac{\omega^2 d}{g\left(1 - \dfrac{\omega^2}{\omega_0^2}\right)\left[1 + \dfrac{D}{\rho_2 g d^4\left(1 - \dfrac{\omega^2}{\omega_0^2}\right)}\left(\dfrac{\omega^2 d^2}{c^2} + \eta_0^2(\omega)\right)^2\right]}.$$

Since $\omega \to 0$ and $\eta_0(\omega)$ is small when $\omega \to 0$,

$$\eta_0(\omega)\tanh\eta_0(\omega) \approx \frac{\omega^2 d}{g}.$$

For $\omega \to 0$, $\tanh \eta_0(\omega) \approx \eta_0(\omega)$. From this approximation,

$$\eta_0^2(\omega) \approx \frac{\omega^2 d}{g} \implies \eta_0(\omega) \approx \omega \sqrt{\frac{d}{g}}.$$

Hence, the second result of (e) follows.

(f): To prove (f), we take the limit as $\omega \to \omega_0$ of the second transcendental equation in (3.1.7). From this limit, we obtain

$$\lim_{\omega \to \omega_0} \left(\frac{\omega_0^2 d^2}{c^2} + \eta_0^2(\omega) \right)^2 \eta_0(\omega) \tanh \eta_0(\omega) = \frac{\rho_2 \omega_0^2 d^5}{D}.$$

When $\omega \to \omega_0$, η_0 approaches a constant that, based on numerical results, is large. Therefore, $\tanh \eta_0(\omega) \to 1$. Moreover, $\left(\frac{\omega_0^2 d^2}{c^2} + \eta_0^2(\omega) \right)^2 \approx \eta_0^4(\omega)$ since $\eta_0(\omega) >> \frac{\omega_0 d}{c}$. Applying these conditions to the above equation, we obtain

$$\lim_{\omega \to \omega_0} \eta_0^5(\omega) = \frac{\rho_2 \omega_0^2 d^5}{D} \implies \lim_{\omega \to \omega_0} \eta_0(\omega) = \left(\frac{\rho_2 \omega_0^2}{D} \right)^{\frac{1}{5}} d.$$

Hence, the first result of (f) follows.

As explained above, for $\omega \to \omega_0$, $\tanh \eta_0(\omega) \to 1$. Moreover, $\lim_{\omega \to \omega_0} \eta_0(\omega) \left[1 + P(\omega) \left(\frac{\omega^2 d^2}{c^2} + \eta_0^2(\omega) \right)^2 \right] = \lim_{\omega \to \omega_0} \beta(\omega) d$. From the second transcendental equation in (3.1.7),

$$\frac{\eta_0(\omega) \left[1 + P(\omega) \left(\frac{\omega^2 d^2}{c^2} + \eta_0^2(\omega) \right)^2 \right]}{\beta(\omega) d} = 1.$$

Hence, the second result of (f) follows.

(g): To prove (g), we take the limit as $\omega \to \infty$ of the second transcendental equation in (3.1.7). Taking this limit, we obtain

$$\lim_{\omega\to\infty} \eta_0(\omega)\tanh\eta_0(\omega) = 0,$$

which implies the first result of (g).

From the second transcendental equation in (3.1.7),

$$\eta_0(\omega)\tanh\eta_0(\omega) = \frac{\omega^2 d}{g\left(1-\dfrac{\omega^2}{\omega_0^2}\right)\left[1+\dfrac{D}{\rho_2 g d^4\left(1-\dfrac{\omega^2}{\omega_0^2}\right)}\left(\dfrac{\omega^2 d^2}{c^2}+\eta_0^2(\omega)\right)^2\right]}.$$

For $\omega \to \infty$, $\eta_0(\omega)$ is small. From the above equation,

$$\eta_0(\omega)\tanh\eta_0(\omega) = \frac{\omega^2 d}{O(\omega^4)} \implies \eta_0(\omega)\tanh\eta_0(\omega) = O\left(\frac{1}{\omega^2}\right).$$

For $\omega \to \infty$, $\tanh\eta_0(\omega) \approx \eta_0(\omega)$. From the above equation,

$$\eta_0^2(\omega) = O\left(\frac{1}{\omega^2}\right) \implies \eta_0(\omega) = O\left(\frac{1}{\omega}\right).$$

Hence, the second result of (g) follows.

(h): For (h), consider the first equation in (3.1.11) and let $\xi_0(\omega) = \dfrac{\omega d}{c}$. ω_* is a solution to this equation, and the existence and uniqueness of ω_* follow from (b) and (d). Since $\lim\limits_{\omega\to\omega_0} \xi_0(\omega) < \dfrac{\omega_0 d}{c}$ and $\lim\limits_{\omega\to\omega_0} \xi_0(\omega) = \dfrac{\pi}{2}$ from (d), we obtain inequality (3.2.1). ■

Remark 3.2.2. After $\dfrac{\pi}{2}$, the function $f_1(\xi_0(\omega))$ has vertical asymptotes at $\dfrac{\pi}{2}(2n-1)$, for $n \geq 2$. Therefore, the next points of intersection of $f_1(\xi_0(\omega))$ and $f_2(\xi_0(\omega))$ are just after

$\xi_0(\omega) = \frac{\pi}{2}(2n-1)$, for $n \geq 2$. Therefore, $\frac{\pi}{2}(2n-1) < \frac{\omega_0 d}{c}$, for $n \geq 2$. Hence, the existence and uniqueness of the cut-off frequencies ω_* for the higher eigenvalues $\hat{\lambda}_n$ takes place if we have the condition

$$\omega_0 > \frac{\pi c}{2d}(2n-1),\ n \geq 2. \tag{3.2.14}$$

Remark 3.2.3. The number of propagating waves is finite, and these propagating waves exist for $n \geq 2$ for a given value of ω.

Remark 3.2.4. On the interval $(0,\infty)$, the function $\xi_0(\omega)$ starts from π, it approaches $\frac{\pi}{2}$ when $\omega \to \omega_0$, and it slowly approaches π when $\omega \to \infty$. On the other hand, the function $\eta_0(\omega)$ starts from 0, approaches a finite number when $\omega \to \omega_0$, reaches a maximum value at an ω value after ω_0, and slowly approaches 0 when $\omega \to \infty$. Hence, the functions $\xi_0(\omega)$ and $\eta_0(\omega)$ are not monotonic with respect to ω. These results were verified numerically.

Remark 3.2.5. When $D \to 0$, we have a special case of the thick ice model (see Chapter 6). Then from Proposition 3.2.1 (b) and (c), there is no critical point for $\xi_0(\omega)$ and $\eta_0(\omega)$. Hence, $\xi_0(\omega)$ and $\eta_0(\omega)$ would be monotonic with respect to ω.

The following proposition discusses the change in eigenvalues $\hat{\lambda}(\omega,c)$ and $\tilde{\lambda}(\omega,c)$ with respect to ω.

Proposition 3.2.2. *If we fix c and consider ω-dependence, then*

(a) $\frac{d\hat{\lambda}(\omega)}{d\omega} > 0.$

(b) $\frac{d\tilde{\lambda}(\omega)}{d\omega} > 0.$

Proof. Consider the equations in (3.1.11). Then from Proposition 3.2.1(a), $\hat{\lambda}(\omega)$ and $\tilde{\lambda}(\omega)$ are smooth functions. Taking derivative of the equations in (3.1.11), we obtain

$$\frac{d\hat{\lambda}}{d\omega} = \frac{2\omega}{c^2} - \frac{2\xi_0}{d^2}\frac{d\xi_0}{d\omega}; \qquad \frac{d\tilde{\lambda}}{d\omega} = \frac{2\omega}{c^2} + \frac{2\eta_0}{d^2}\frac{d\eta_0}{d\omega}.$$

From the first case of Proposition 3.2.1(b), $\frac{d\xi_0}{d\omega} < 0$, so $\frac{d\hat{\lambda}}{d\omega} > 0$. From the second case of Proposition 3.2.1(b), when $\frac{d\xi_0}{d\omega} > 0$, $\frac{d\xi_0}{d\omega} \to 0$ as $\omega \to \infty$ from the third result of Proposition 3.2.1(d) and ξ_0 is bounded from Proposition 3.2.1(b) and (d), so the result of (a) follows.

From the first case of Proposition 3.2.1(c), $\frac{d\eta_0}{d\omega} > 0$, so $\frac{d\tilde{\lambda}}{d\omega} > 0$. From the second case of Proposition 3.2.1(c), when $\frac{d\tilde{\lambda}}{d\omega} < 0$, $\frac{d\eta_0}{d\omega} \to 0$ as $\omega \to \infty$ from the first result of Proposition 3.2.1(g) and η_0 is bounded from Proposition 3.2.1(c) and the first results of (e), (f), and (g) of Proposition 3.2.1, so the result of (b) follows. ■

Remark 3.2.6. From Proposition 3.2.2, the eigenvalues $\hat{\lambda}(\omega,c)$ and $\tilde{\lambda}(\omega,c)$ are monotonic with respect to ω. Hence, the wavenumbers are strictly increasing with respect to ω. This result will be verified numerically in Chapter 4 for variable $c(x)$.

Remark 3.2.7. From Proposition 3.2.1, we can find the lower and upper bounds of the eigenvalues $\hat{\lambda}(\omega,c)$ and $\tilde{\lambda}(\omega,c)$. From the equations in (3.1.11), we have the following results for $\hat{\lambda}(\omega,c)$ and $\tilde{\lambda}(\omega,c)$. $\hat{\lambda}(\omega,c) \to -\frac{\pi^2}{d^2}$ when $\omega \to 0$ and ∞ when $\omega \to \infty$. On the other hand, $\tilde{\lambda}(\omega,c) \to 0$ when $\omega \to 0$ and ∞ when $\omega \to \infty$. Furthermore, when $\omega \to \omega_0$, $\hat{\lambda} \to \frac{\omega_0^2}{c^2} - \frac{\pi^2}{4d^2}$ and $\tilde{\lambda} \to \frac{\omega_0^2}{c^2} + \frac{1}{d}\left(\frac{\rho_2\omega_0^2}{D}\right)^{\frac{1}{5}}$.

We now compare ξ_0 and η_0 for the ocean model with the free surface and the surface covered by thick ice.

Proposition 3.2.3. *Let $\omega \in (0,\infty)$. Then*

(a) $\xi_0 < \xi_0^f$ for $\omega < \omega_0$ and $\xi_0 > \xi_0^f$ for $\omega > \omega_0$.

(b) $\eta_0 < \eta_0^f$.

Proof. (in part, numerical) We write the first transcendental equation in (3.1.7) in the form

$$\xi_0 \tan \xi_0 + A_1 = 0, \tag{3.2.15}$$

where $A_1 = \dfrac{\omega^2 d}{g\left(1-\dfrac{\omega^2}{\omega_0^2}\right)\left[1+P(\omega)\left(\dfrac{\omega^2 d^2}{c^2}-\xi_0^2\right)^2\right]}$.

We write the second transcendental equation in (3.1.7) as

$$\eta_0 \tanh \eta_0 = A_2, \tag{3.2.16}$$

where $A_2 = \dfrac{\omega^2 d}{g\left(1-\dfrac{\omega^2}{\omega_0^2}\right)\left[1+P(\omega)\left(\dfrac{\omega^2 d^2}{c^2}+\eta_0^2\right)^2\right]}$.

We further write the transcendental equations (3.1.10) as

$$\xi_0^f \tan \xi_0^f + A^f = 0,\ \eta_0^f \tanh \eta_0^f = A^f, \tag{3.2.17}$$

where $A^f = \dfrac{\omega^2 d}{g}$.

Numerical results imply that $A^f < A_1$ for $\omega < \omega_0$ and $A^f > A_1$ for $\omega > \omega_0$. On the other hand, numerical results imply that $A^f > A_2\ \forall \omega$. We differentiate equations (3.2.15) and (3.2.16) with respect to the parameters A_1 and A_2, respectively. Differentiating these equations, we obtain

$$\frac{d\xi_0}{dA_1}\left(\tan \xi_0 + \xi_0 \sec^2 \xi_0\right) + 1 = 0, \quad \frac{d\eta_0}{dA_2}\left(\tanh \eta_0 + \eta_0 \operatorname{sech}^2 \eta_0\right) = 1.$$

$$\implies \quad \frac{d\xi_0}{dA_1} = -\frac{1}{\tan\xi_0 + \xi_0 \sec^2\xi_0} = -\frac{2\cos^2\xi_0}{\sin 2\xi_0 + 2\xi_0} < 0,$$

$$\frac{d\eta_0}{dA_2} = \frac{1}{\tanh\eta_0 + \eta_0 \operatorname{sech}^2\eta_0} = \frac{2\cosh^2\eta_0}{\sinh 2\eta_0 + 2\eta_0} > 0.$$

Since $A^f < A_1$ for $\omega < \omega_0$ and $A^f > A_1$ for $\omega > \omega_0$, $\xi_0 < \xi_0^f$ for $\omega < \omega_0$ and $\xi_0 > \xi_0^f$ for $\omega > \omega_0$ by comparing equations (3.2.15) and (3.2.17). Since $A^f > A_2$, $\eta_0 < \eta_0^f$ by comparing equations (3.2.16) and (3.2.17). ■

Remark 3.2.8. Proposition 3.2.3 shows that ξ_0 is below ξ_0^f for $\omega < \omega_0$ and ξ_0 is above ξ_0^f for $\omega > \omega_0$. However, numerical results show that there is a jump discontinuity in A_1 at $\omega = \omega_0$, so ξ_0 and ξ_0^f do not coincide at $\omega = \omega_0$.

Remark 3.2.9. From numerical results, the functions A_1 and $\xi_0 \tan\xi_0$ have a jump discontinuity at $\omega = \omega_0$. However, the function $\xi_0(\omega)$ is continuous in $(0,\infty)$. Hence, $\hat{\lambda}(\omega)$ is continuous in $(0,\infty)$.

Remark 3.2.10. Based on Proposition 3.2.3, we conclude that the presence of thick ice instead of the free surface results in a decrease of ξ_0 with respect to ω for $\omega < \omega_0$ and an increase of ξ_0 with respect to ω for $\omega > \omega_0$. Moreover, it results in a decrease of η_0 with respect to ω. According to the equations in (3.1.11), $\hat{\lambda}$ increases with respect to ω in the presence of thick ice for $\omega < \omega_0$ and decreases with respect to ω in the presence of thick ice for $\omega > \omega_0$. Moreover, $\tilde{\lambda}$ decreases with respect to ω in the presence of thick ice.

Remark 3.2.11. From the definition of ω_0 in (2.0.19), $\omega_0 = \left(\frac{\rho_2 g}{\rho_1 h}\right)^{\frac{1}{2}}$, which is a function of h. We have the following results for a given value of ω. When $h \to 0$, $\omega_0(h) \to \infty$ and $P(\omega,h) \to 0$ from definition (3.1.6). There is a jump discontinuity in A_1 at $h = \frac{\rho_2 g}{\rho_1 \omega^2}$. From numerical results, A_1 is positive and increases with respect to h when $h < \frac{\rho_2 g}{\rho_1 \omega^2}$ and becomes negative right after $h = \frac{\rho_2 g}{\rho_1 \omega^2}$ before it continues to increase with respect to h and approaches 0 as $h \to \infty$. From numerical results, A_2 decreases when $h \to \infty$. Hence, ξ_0 increases with respect to h when $h < \frac{\rho_2 g}{\rho_1 \omega^2}$ and decreases

with respect to h when $h > \frac{\rho_2 g}{\rho_1 \omega^2}$ from equation (3.2.15). On the other hand, η_0 decreases with respect to h from equation (3.2.16). These results were verified numerically. From the first equation in (3.1.11), $\hat{\lambda}$ decreases with respect to h when $h < \frac{\rho_2 g}{\rho_1 \omega^2}$ and increases with respect to h when $h > \frac{\rho_2 g}{\rho_1 \omega^2}$. From the second equation in (3.1.11), $\tilde{\lambda}$ decreases with respect to h. If we measure the variation of wavenumbers, we could find the variation in the ice cover thickness h. For future work, we expect that this variation will provide us with information about the influence of global warming.

3.3 Air Temperature and Eigenvalues

To understand the influence of global warming, we first need to study the impact of the change in air temperature on the eigenvalues $\hat{\lambda}$ and $\tilde{\lambda}$, which are related to ξ_0 and η_0, respectively, from the equations in (3.1.11). Global warming is the long-term heating of the planet, i.e., the global average air temperature is increasing.

To understand T-dependence of $\xi_0(\omega, T)$ and $\eta_0(\omega, T)$, where T is the air temperature 1 to 2 m above the ice cover surface, we consider the tree diagrams in Figure 3.1.

Using the chain rule on the tree diagrams in Figure 3.1, we obtain

$$\begin{aligned}
\frac{\partial \xi_0}{\partial T} &= \frac{\partial \xi_0}{\partial P}\left[\frac{\partial P}{\partial D}\left(\frac{\partial D}{\partial E}\frac{dE}{dT} + \frac{\partial D}{\partial h}\frac{dh}{dT}\right) + \frac{\partial P}{\partial \omega_0}\frac{d\omega_0}{dh}\frac{dh}{dT}\right] + \frac{\partial \xi_0}{\partial \omega_0}\frac{d\omega_0}{dh}\frac{dh}{dT}; \\
\frac{\partial \eta_0}{\partial T} &= \frac{\partial \eta_0}{\partial P}\left[\frac{\partial P}{\partial D}\left(\frac{\partial D}{\partial E}\frac{dE}{dT} + \frac{\partial D}{\partial h}\frac{dh}{dT}\right) + \frac{\partial P}{\partial \omega_0}\frac{d\omega_0}{dh}\frac{dh}{dT}\right] + \frac{\partial \eta_0}{\partial \omega_0}\frac{d\omega_0}{dh}\frac{dh}{dT}.
\end{aligned} \tag{3.3.1}$$

The following text uses the term "accumulated thawing degree days" (ATDD), which is defined as the difference between daily average air temperature and freezing temperature, T_f. In the case of ATDD, the daily average air temperature is above freezing temperature, i.e., $T > T_f$ (see [25]). In our study, T is the air temperature in the case of ATDD.

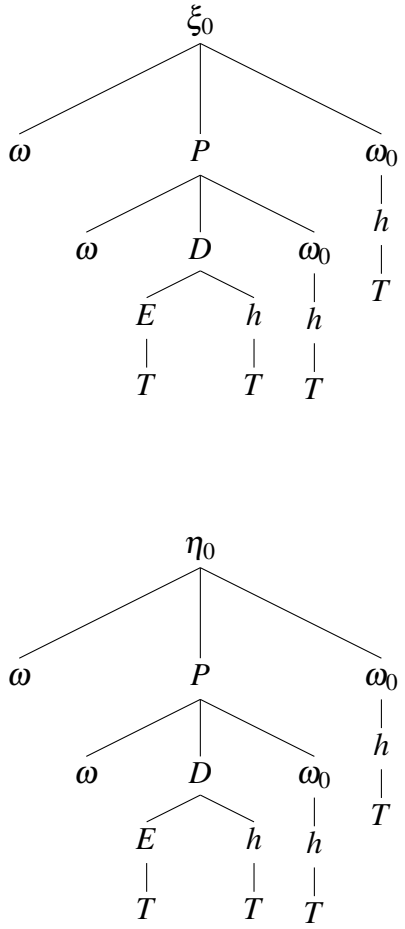

Figure 3.1 Tree diagrams of ξ_0 and η_0

From [26], the relation between Young's Modulus of ice and the surface temperature of ice cover can be represented as

$$E = E_0 - BT_s \exp\left(-\frac{T_0}{T_s}\right), \tag{3.3.2}$$

where E_0 is Young's Modulus of ice at absolute zero, T_s is the surface temperature of ice cover, and B and T_0 are positive empirical constants for ice.

Remark 3.3.1. B is defined as the slope of Young's Modulus-temperature curve as the temperature is lowered, i.e., B decreases from a constant value to 0 at absolute zero (see [27]). B is related to

the Gruneisen constant, which is related to the volume thermal expansion (see [26]). On the other hand, T_0 correlates with Debye temperature, which is related to the specific heat (see [26]). On the right side of equation (3.3.2), the factor $\exp\left(-\frac{T_0}{T_s}\right)$ appearing in the second term is a single Boltzmann factor which is suggested in [27] for the degree of excitation of the vibrational modes in non-metallic crystals. At high temperatures, this factor approaches 1, and equation (3.3.2) gives a linear dependence. In [27], some values of B and T_0 have been found by analyzing single-crystal specimens of several oxides.

Remark 3.3.2. Equation (3.3.2) satisfies the third law of thermodynamics, which requires that the derivative of any elastic constant with respect to temperature must approach 0 as the temperature approaches absolute zero.

Remark 3.3.3. For approximate calculations, we can consider $T_s \approx T_f$.

For heat transfer from air to the ice cover, the heat-transfer convection equation can be represented as

$$Q = HS_a(T - T_s), \tag{3.3.3}$$

where Q is the amount of heat transferred, H is the heat transfer coefficient, and S_a is the surface area of ice cover.

From [28], ice decay can be calculated based on the empirical Bilello equation

$$h = h_{max} - A_0(T - T_f), \tag{3.3.4}$$

where h_{max} is the maximum ice cover thickness at the start of decay and A_0 is a positive empirical constant (also referred to as ice thinning rate or melting factor).

In [25], the data points of ice thickness decrease with respect to ATDD have been plotted. This plot shows a positive correlation between these two quantities, and the slope of the line rep-

resenting the linear approximation of these data points is defined as A_0. In [25] and [29], some values of A_0 have been found for the sea ice in the Canadian Arctic Archipelago and the lake ice on the North Slope of Alaska, respectively, based on the recorded temperature values.

Using the definition of ω_0 in (2.0.19) and equation (3.3.4), we obtain a relation between ω_0 and T

$$\omega_0 = \left[\frac{\rho_2 g}{\rho_1 h_{max} - \rho_1 A_0 (T - T_f)}\right]^{\frac{1}{2}}. \tag{3.3.5}$$

Remark 3.3.4. For a given value of ω, we have $\omega < \omega_0$ or $\omega > \omega_0$. Therefore, equation (3.3.5) implies that $T < \Omega$ or $T > \Omega$, where $\Omega = \dfrac{\rho_1 \omega^2 (h_{max} + A_0 T_f) - \rho_2 g}{\rho_1 A_0 \omega^2}$ and T is the air temperature 1 to 2 m above the ice cover surface in the case of ATDD.

The next proposition demonstrates the behavior of ξ_0 and η_0 with respect to T.

Proposition 3.3.1. *If we fix ω and consider T-dependence of $\xi_0(\omega, T)$ and $\eta_0(\omega, T)$, then*

(a) $\dfrac{d\xi_0}{dT} < 0$ *for* $T < \Omega$ *and* $\dfrac{d\xi_0}{dT} > 0$ *for* $T > \Omega$.

(b) $\dfrac{d\eta_0}{dT} > 0$ *for* $T < \Omega$ *and* $\dfrac{d\eta_0}{dT} < 0$ *for* $T > \Omega$.

Proof. (in part, numerical) We consider the equations in (3.3.1). To prove (a), we start with the first transcendental equation in (3.1.7). Using this equation, we find

$$\frac{\partial \xi_0}{\partial P} = \frac{\left(\dfrac{\omega^2 d^2}{c^2} - \xi_0^2(\omega)\right)^2}{\dfrac{\xi_0(\omega)\sec^2\xi_0(\omega) + \tan\xi_0(\omega)}{\xi_0^2(\omega)\tan^2\xi_0(\omega)}\beta(\omega)d + 4\xi_0(\omega)P(\omega)\left(\dfrac{\omega^2 d^2}{c^2} - \xi_0^2(\omega)\right)}, \tag{3.3.6}$$

which is positive for $\omega < \omega_0$ and negative for $\omega > \omega_0$ from the proof of Proposition 3.2.1(b). From Remark 3.3.4, $\dfrac{\partial \xi_0}{\partial P} < 0$ for $T < \Omega$ and $\dfrac{\partial \xi_0}{\partial P} > 0$ for $T > \Omega$.

Using definition (3.1.6), we find

$$\frac{\partial P}{\partial D} = \frac{1}{\rho_2 g d^4 \left(1 - \dfrac{\omega^2}{\omega_0^2}\right)}, \tag{3.3.7}$$

which is positive for $\omega < \omega_0$ and negative for $\omega > \omega_0$. From Remark 3.3.4, $\dfrac{\partial P}{\partial D} < 0$ for $T < \Omega$ and $\dfrac{\partial P}{\partial D} > 0$ for $T > \Omega$.

Using the definition of D, we find

$$\frac{\partial D}{\partial E} = \frac{h^3}{12\,(1-\sigma^2)} > 0. \tag{3.3.8}$$

From equation (3.3.2),

$$\frac{dE}{dT} = -B\exp\left(-\frac{T_0}{T_s}\right)\frac{dT_s}{dT}\left(1+\frac{T_0}{T_s}\right). \tag{3.3.9}$$

From equation (3.3.3), $\dfrac{dT_s}{dT} = 1$. From the above equation,

$$\frac{dE}{dT} = -B\exp\left(-\frac{T_0}{T_s}\right)\left(1+\frac{T_0}{T_s}\right) < 0. \tag{3.3.10}$$

Using the definition of D, we find

$$\frac{\partial D}{\partial h} = \frac{Eh^2}{4(1-\sigma^2)} > 0. \tag{3.3.11}$$

From equation (3.3.4),

$$\frac{dh}{dT} = -A_0 < 0. \tag{3.3.12}$$

Using definition (3.1.6), we find

$$\frac{\partial P}{\partial \omega_0} = -\frac{2D\omega^2}{\rho_2 g d^4 \omega_0^3 \left(1-\frac{\omega^2}{\omega_0^2}\right)^2} < 0. \tag{3.3.13}$$

Using the definition of ω_0, we find

$$\frac{d\omega_0}{dh} = -\frac{1}{2h^{\frac{3}{2}}}\sqrt{\frac{\rho_2 g}{\rho_1}} < 0. \tag{3.3.14}$$

From the first transcendental equation in (3.1.7),

$$\frac{\partial \xi_0}{\partial \omega_0} = \frac{\frac{2\omega^2}{\omega_0^3\left(1-\frac{\omega^2}{\omega_0^2}\right)}\left[1+P(\omega)\left(\frac{\omega^2 d^2}{c^2}-\xi_0^2(\omega)\right)^2\right]}{\frac{\xi_0(\omega)\sec^2\xi_0(\omega)+\tan\xi_0(\omega)}{\xi_0^2(\omega)\tan^2\xi_0(\omega)}\beta(\omega)d+4\xi_0(\omega)P(\omega)\left(\frac{\omega^2 d^2}{c^2}-\xi_0^2(\omega)\right)} > 0. \tag{3.3.15}$$

From equations (3.3.6) - (3.3.8) and (3.3.10) - (3.3.15),

$$\frac{\partial \xi_0}{\partial P}\frac{\partial P}{\partial D}\left(\frac{\partial D}{\partial E}\frac{dE}{dT}+\frac{\partial D}{\partial h}\frac{dh}{dT}\right) < 0, \tag{3.3.16}$$

$$\frac{\partial \xi_0}{\partial P}\frac{\partial P}{\partial \omega_0}\frac{d\omega_0}{dh}\frac{dh}{dT} > 0 \text{ for } T < \Omega, \quad \frac{\partial \xi_0}{\partial P}\frac{\partial P}{\partial \omega_0}\frac{d\omega_0}{dh}\frac{dh}{dT} < 0 \text{ for } T > \Omega, \tag{3.3.17}$$

$$\frac{\partial \xi_0}{\partial \omega_0}\frac{d\omega_0}{dh}\frac{dh}{dT} > 0. \tag{3.3.18}$$

In terms of h, $\frac{\partial \xi_0}{\partial P}\frac{\partial P}{\partial D}\left(\frac{\partial D}{\partial E}\frac{dE}{dT}+\frac{\partial D}{\partial h}\frac{dh}{dT}\right) = O(1)$, $\frac{\partial \xi_0}{\partial P}\frac{\partial P}{\partial \omega_0}\frac{d\omega_0}{dh}\frac{dh}{dT} = O\left(\frac{1}{h}\right)$, and $\frac{\partial \xi_0}{\partial \omega_0}\frac{d\omega_0}{dh}\frac{dh}{dT} = O\left(\frac{1}{h}\right)$.

When h is large, we have the case $T < \Omega$ and we have the following limits. $\frac{\partial \xi_0}{\partial P} \to 0$, $\frac{\partial P}{\partial D} \to 0$, $\frac{\partial D}{\partial E}$ is a large positive number, $\frac{\partial D}{\partial h}$ is a large positive number, $\frac{\partial P}{\partial \omega_0}$ is a negative number with a large magnitude, $\frac{d\omega_0}{dh} \to 0$, and $\frac{\partial \xi_0}{\partial \omega_0}$ is a large positive number from equations (3.3.6) - (3.3.8), (3.3.11), and (3.3.13) - (3.3.15). From the first equation in (3.3.1), $\frac{\partial \xi_0}{\partial T} = O\left(\frac{\partial \xi_0}{\partial P}\frac{\partial P}{\partial D}\left(\frac{\partial D}{\partial E}\frac{dE}{dT} + \frac{\partial D}{\partial h}\frac{dh}{dT}\right)\right)$ and the first result of (a) follows from (3.3.16).

When $h \to 0$, we have the case $T > \Omega$ and we have the following limits.
$\frac{\partial \xi_0}{\partial P} \to \frac{\left(\frac{\omega^2 d^2}{c^2} - \xi_0^2(\omega)\right)^2}{\frac{\xi_0(\omega)\sec^2\xi_0(\omega) + \tan\xi_0(\omega)}{\xi_0^2(\omega)\tan^2\xi_0(\omega)}\frac{\omega^2 d}{g}}$, $\frac{\partial P}{\partial D} \to \frac{1}{\rho_2 g d^4}$, $\frac{\partial D}{\partial E} \to 0$, $\frac{\partial D}{\partial h} \to 0$, $\frac{\partial P}{\partial \omega_0} \to 0$, $\frac{d\omega_0}{dh} \to -\infty$, and $\frac{\partial \xi_0}{\partial \omega_0} \to 0$ from equations (3.3.6) - (3.3.8), (3.3.11), and (3.3.13) - (3.3.15). By comparing equation (3.3.15) with equations (3.3.6) and (3.3.13) , we obtain $\left|\frac{\partial \xi_0}{\partial \omega_0}\right| > \left|\frac{\partial \xi_0}{\partial P}\frac{\partial P}{\partial \omega_0}\right|$. Hence, $\left|\frac{\partial \xi_0}{\partial \omega_0}\frac{d\omega_0}{dh}\frac{dh}{dT}\right| > \left|\frac{\partial \xi_0}{\partial P}\frac{\partial P}{\partial \omega_0}\frac{d\omega_0}{dh}\frac{dh}{dT}\right|$. From the first equation in (3.3.1), $\frac{\partial \xi_0}{\partial T} = O\left(\frac{\partial \xi_0}{\partial \omega_0}\frac{d\omega_0}{dh}\frac{dh}{dT}\right)$ and the second result of (a) follows from (3.3.18).

To prove (b), we start with the second transcendental equation in (3.1.7). Using this equation, we find

$$\frac{\partial \eta_0}{\partial P} = -\frac{\left(\frac{\omega^2 d^2}{c^2} + \eta_0^2(\omega)\right)^2}{\frac{\eta_0(\omega)\operatorname{sech}^2\eta_0(\omega) + \tanh\eta_0(\omega)}{\eta_0^2(\omega)\tanh^2\eta_0(\omega)}\beta(\omega)d + 4\eta_0(\omega)P(\omega)\left(\frac{\omega^2 d^2}{c^2} + \eta_0^2(\omega)\right)}, \quad (3.3.19)$$

which is negative for $\omega < \omega_0$ and positive for $\omega > \omega_0$ from the proof of Proposition 3.2.1(c). From Remark 3.3.4, $\frac{\partial \eta_0}{\partial P} > 0$ for $T < \Omega$ and $\frac{\partial \eta_0}{\partial P} < 0$ for $T > \Omega$.

From the second transcendental equation in (3.1.7),

$$\frac{\partial \eta_0}{\partial \omega_0} = -\frac{\dfrac{2\omega^2}{\omega_0^3\left(1-\frac{\omega^2}{\omega_0^2}\right)}\left[1+P(\omega)\left(\dfrac{\omega^2 d^2}{c^2}+\eta_0^2(\omega)\right)^2\right]}{\dfrac{\eta_0(\omega)\operatorname{sech}^2\eta_0(\omega)+\tanh\eta_0(\omega)}{\eta_0^2(\omega)\tanh^2\eta_0(\omega)}\beta(\omega)d+4\eta_0(\omega)P(\omega)\left(\dfrac{\omega^2 d^2}{c^2}+\eta_0^2(\omega)\right)}. \quad (3.3.20)$$

From numerical results, $\left[1+P(\omega)\left(\dfrac{\omega^2 d^2}{c^2}+\eta_0^2(\omega)\right)^2\right] > 0$ for $\omega < \omega_0$ and $\left[1+P(\omega)\left(\dfrac{\omega^2 d^2}{c^2}+\eta_0^2(\omega)\right)^2\right] < 0$ for $\omega > \omega_0$. From Remark 3.3.4, $\dfrac{\partial \eta_0}{\partial \omega_0} > 0$ for $T < \Omega$ and $\dfrac{\partial \eta_0}{\partial \omega_0} < 0$ for $T > \Omega$.

From equations (3.3.7), (3.3.8), (3.3.10) - (3.3.14), (3.3.19), and (3.3.20),

$$\frac{\partial \eta_0}{\partial P}\frac{\partial P}{\partial D}\left(\frac{\partial D}{\partial E}\frac{dE}{dT}+\frac{\partial D}{\partial h}\frac{dh}{dT}\right) > 0, \quad (3.3.21)$$

$$\frac{\partial \eta_0}{\partial P}\frac{\partial P}{\partial \omega_0}\frac{d\omega_0}{dh}\frac{dh}{dT} < 0 \text{ for } T < \Omega, \quad \frac{\partial \xi_0}{\partial P}\frac{\partial P}{\partial \omega_0}\frac{d\omega_0}{dh}\frac{dh}{dT} > 0 \text{ for } T > \Omega, \quad (3.3.22)$$

$$\frac{\partial \eta_0}{\partial \omega_0}\frac{d\omega_0}{dh}\frac{dh}{dT} > 0 \text{ for } T < \Omega, \quad \frac{\partial \eta_0}{\partial \omega_0}\frac{d\omega_0}{dh}\frac{dh}{dT} < 0 \text{ for } T > \Omega. \quad (3.3.23)$$

In terms of h, $\dfrac{\partial \eta_0}{\partial P}\dfrac{\partial P}{\partial D}\left(\dfrac{\partial D}{\partial E}\dfrac{dE}{dT}+\dfrac{\partial D}{\partial h}\dfrac{dh}{dT}\right) = O(1)$, $\dfrac{\partial \eta_0}{\partial P}\dfrac{\partial P}{\partial \omega_0}\dfrac{d\omega_0}{dh}\dfrac{dh}{dT} = O\left(\dfrac{1}{h}\right)$, and $\dfrac{\partial \eta_0}{\partial \omega_0}\dfrac{d\omega_0}{dh}\dfrac{dh}{dT} = O\left(\dfrac{1}{h}\right)$.

When h is large, we have the case $T < \Omega$ and we have the following limits. $\dfrac{\partial \eta_0}{\partial P} \to 0$ from equation (3.3.19) and $\dfrac{\partial \eta_0}{\partial \omega_0}$ is a negative number with a large magnitude from

equation (3.3.20). From the second equation in (3.3.1), $\frac{\partial \eta_0}{\partial T} = O\left(\frac{\partial \eta_0}{\partial P}\frac{\partial P}{\partial D}\left(\frac{\partial D}{\partial E}\frac{dE}{dT} + \frac{\partial D}{\partial h}\frac{dh}{dT}\right)\right)$ and the first result of (b) follows from (3.3.21).

When $h \to 0$, we have the case $T > \Omega$ and we have the following limits.
$\frac{\partial \eta_0}{\partial P} \to -\frac{\left(\frac{\omega^2 d^2}{c^2} + \eta_0^2(\omega)\right)^2}{\frac{\eta_0(\omega)\operatorname{sech}^2\eta_0(\omega) + \tanh\eta_0(\omega)}{\eta_0^2(\omega)\tanh^2\eta_0(\omega)}\frac{\omega^2 d}{g}}$ from equation (3.3.19) and $\frac{\partial \eta_0}{\partial \omega_0} \to 0$ from equation (3.3.20). By comparing equation (3.3.20) with equations (3.3.19) and (3.3.13) , we obtain $\left|\frac{\partial \eta_0}{\partial \omega_0}\right| > \left|\frac{\partial \eta_0}{\partial P}\frac{\partial P}{\partial \omega_0}\right|$. Hence, $\left|\frac{\partial \eta_0}{\partial \omega_0}\frac{d\omega_0}{dh}\frac{dh}{dT}\right| > \left|\frac{\partial \eta_0}{\partial P}\frac{\partial P}{\partial \omega_0}\frac{d\omega_0}{dh}\frac{dh}{dT}\right|$. From the second equation in (3.3.1), $\frac{\partial \eta_0}{\partial T} = O\left(\frac{\partial \eta_0}{\partial \omega_0}\frac{d\omega_0}{dh}\frac{dh}{dT}\right)$ and the second result of (b) follows from (3.3.23). ■

Remark 3.3.5. For small values of ω, we have $\Omega < T_f$ for realistic values of ρ_1, ρ_2, T_f, h_{max}, A_0, and g. Hence, we obtain $T < T_f$ for the case $T < \Omega$. Therefore, for small values of ω, we only have the case $T > \Omega$ in Proposition 3.3.1 since $T > T_f$ in our study.

Applying the results of Proposition 3.3.1 on equations in (3.1.11), we obtain that for a fixed value of ω, both $\hat{\lambda}(\omega, T)$ and $\tilde{\lambda}(\omega, T)$ increase with respect to T for $T < \Omega$ and decrease with respect to T for $T > \Omega$. Hence, the eigenvalues are not monotonic with respect to temperature. Since the global average air temperature is increasing, this result could enable us to find the impact of the variation of wavenumbers on the thickness of ice covers.

This completes our study of the homogeneous waveguide. We will now consider the case of a non-homogeneous waveguide.

3.4 Analysis of Non-Homogeneous Waveguide

For the non-homogeneous case, i.e., $c = c(x)$, we would not have an explicitly written transcendental equation like in (3.1.10). Hence, we would use Numerical Analysis in Chapter 4 to compute the eigenvalues of two leading propagating modes as functions of the frequency ω.

We use the notations $\hat{\lambda}(\omega, c(x))$ and $\tilde{\lambda}(\omega, c(x))$ for the case of a non-homogeneous waveguide. In [14], a particular model (see Chapter 6) of the thick ice model was considered. For this model, the comparison theory for Sturm-Liouville problems was used to prove that the eigenvalue $\hat{\lambda}_1$ satisfies the inequalities

$$\hat{\lambda}_1(\omega, c_+) = \min_{c_- \le c(x) \le c_+} \hat{\lambda}_1(\omega, c(x)) \le \hat{\lambda}_1(\omega, c(x)) \le \max_{c_- \le c(x) \le c_+} \hat{\lambda}_1(\omega, c(x)) = \hat{\lambda}_1(\omega, c_-),$$
$$\text{where } \hat{\lambda}_1(\omega, c_\pm) = \frac{\omega^2}{c_\pm^2} - \frac{\xi_0^2(\omega)}{d^2}. \tag{3.4.1}$$

Similarly, $\tilde{\lambda}(\omega, c(x))$ is bounded as

$$\tilde{\lambda}(\omega, c_+) = \min_{c_- \le c(x) \le c_+} \tilde{\lambda}(\omega, c(x)) \le \tilde{\lambda}(\omega, c(x)) \le \max_{c_- \le c(x) \le c_+} \tilde{\lambda}(\omega, c(x)) = \tilde{\lambda}(\omega, c_-),$$
$$\text{where } \tilde{\lambda}(\omega, c_\pm) = \frac{\omega^2}{c_\pm^2} + \frac{\eta_0^2(\omega)}{d^2}. \tag{3.4.2}$$

Conjecture 3.4.1. *The inequalities (*3.4.1*) and (*3.4.2*) also hold for the general case, the thick ice model.*

From the inequalities in (3.4.1), a propagating mode associated with $\hat{\lambda}_1(\omega, c(x))$ exists if $\hat{\lambda}_1(\omega, c_+) > 0$. From this condition,

$$F(\omega) := \omega - \frac{\xi_0(\omega) c_+}{d} > 0. \tag{3.4.3}$$

If the frequency ω is low enough, $\hat{\lambda}_1(\omega, c(x)) < 0$. Then, only $\tilde{\lambda}(\omega, c(x))$ provides a propagating mode.

Taking the derivative of $F(\omega)$ with respect to ω, we obtain

$$\frac{dF}{d\omega} = 1 - \frac{c_+}{d} \frac{d\xi_0(\omega)}{d\omega}. \tag{3.4.4}$$

From Proposition 3.2.1(b), $\frac{dF}{d\omega} > 1$ for $\omega < M$ and $\frac{dF}{d\omega} < 1$ for $\omega > M$, where $M \approx \left(\frac{\rho_2 g}{D}\right)^{\frac{1}{4}} c$ for any c value in (c_-, c_+).

For $\omega > 0$, we always have that $\tilde{\lambda}(\omega, c(x)) > \hat{\lambda}_1(\omega, c(x))$. While $\tilde{\lambda}(\omega, c(x))$ is always positive and therefore corresponds to a propagating mode, $\hat{\lambda}_1(\omega, c(x))$ becomes negative below some frequency ω_*, i.e., for $\omega < \omega_*$, from the inequalities in (3.4.1). As a result, we have the following proposition.

Proposition 3.4.1. *For the layered ocean covered by ice, there exists a cut-off frequency ω_* such that the following holds.*

(a) When $0 < \omega < \omega_*$, $\hat{\lambda}_1 < 0 < \tilde{\lambda}$. Thus $\tilde{\lambda}$ corresponds to the only propagating mode.

(b) When $\omega > \omega_*$, $0 < \hat{\lambda}_1 < \tilde{\lambda}$. Hence, while both $\hat{\lambda}_1$ and $\tilde{\lambda}$ correspond to propagating modes, $\tilde{\lambda}$ is the leading propagating mode.

(c) When $\omega > \omega_*$, some higher eigenvalues, $\hat{\lambda}_n$, $n \geq 2$, may be positive.

(d) $\forall \omega > 0$, $\tilde{\lambda} > \hat{\lambda}_1$.

Proposition 3.4.1, (a), (b), and (d), is illustrated in Figure 3.2. The two modes corresponding to $\hat{\lambda}_1$ and $\tilde{\lambda}$ are the subject of our study below.

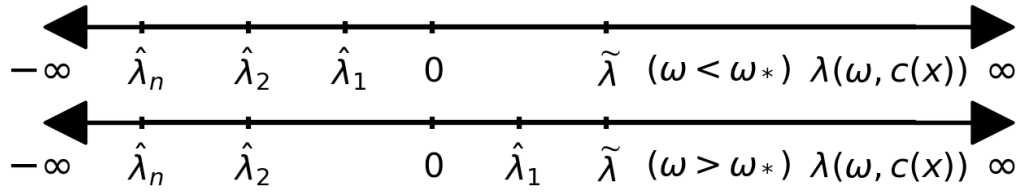

Figure 3.2 Location of the eigenvalues

The next chapter will provide the numerical observations of the dimensionless wavenumbers.

CHAPTER 4

Numerical Results

In sections 3.1 - 3.3, we considered a homogeneous waveguide, i.e., with the constant speed profile $c(x) \equiv c$, and proved that some or all of the modes associated with $\hat{\lambda}_n$ may be non-propagating and the (unique) leading mode associated with $\tilde{\lambda}$ is propagating for all values of ω. Hence, we have a chain of inequalities

$$\cdots < \hat{\lambda}_n < \hat{\lambda}_{n-1} < \cdots < \hat{\lambda}_1 < \tilde{\lambda}.$$

In this chapter, we consider a non-homogeneous waveguide. Since we are not working on the case of a homogeneous waveguide, we do not have explicit formulas like in sections 3.1 - 3.3. However, we use Numerical Analysis to study the modes. These modes are similar to the two for the homogeneous case, associated with the eigenvalues $\hat{\lambda}_1$ and $\tilde{\lambda}$. To study the Sturm-Liouville problem (2.0.14), (2.0.15), and (2.0.21), we develop a numerical algorithm and test it using several speed profiles $c(x)$. We begin with the study of $\hat{\lambda}_1$.

4.1 Analysis of $\hat{\lambda}_1$

The following implementation of the algorithm is based on the formalism known for the layered media (see [1]). We split the interval $[0,d]$ into n subintervals and let $\Delta x := d/n$; $x_j = j\Delta x$, $j = 0,\ldots,n$. Assuming that $c(x)$ is constant on each subinterval, i.e. $c(x) = c_j$ on (x_{j-1},x_j),

$j = 1, \ldots, n$, consider the function ψ, that is denoted as ψ_j with domain $[0, \Delta x]$ on each subinterval (x_{j-1}, x_j). The algorithm is similar to [14], [30] - [32].

The general solution ψ of equation (2.0.14) on the j^{th} interval is

$$\psi_j(x) = a_j \sin(\gamma_j x) + b_j \cos(\gamma_j x), \text{ where } \gamma_j := \sqrt{\frac{\omega^2}{{c_j}^2} - \hat{\lambda}}, j = 1, \ldots, n, \tag{4.1.1}$$

where a_j and b_j are arbitrary constants.

From boundary condition (2.0.15), we have that $a_1 = 0$. We choose $b_1 = 1$. From these conditions,

$$\psi_1(x) = \cos(\gamma_1 x). \tag{4.1.2}$$

From the definition of ψ_n and boundary condition (2.0.21),

$$a_n \gamma_n \cos(\gamma_n \Delta x) - b_n \gamma_n \sin(\gamma_n \Delta x) - \tau(\omega, \hat{\lambda})(a_n \sin(\gamma_n \Delta x) + b_n \cos(\gamma_n \Delta x)) = 0. \tag{4.1.3}$$

Since each ψ_j is expressed in the local coordinate $x \in [0, \Delta x]$, (4.1.3) is a condition at $x = d$ in the domain of ψ. Since $\psi(x)$ is continuous in $[0, \Delta x]$ and differentiable at $x_1, \ldots, x_n$, we obtain the system of equations

$$\begin{gathered} a_{j-1} \sin(\gamma_{j-1} \Delta x) + b_{j-1} \cos(\gamma_{j-1} \Delta x) = b_j; \\ a_{j-1} \gamma_{j-1} \cos(\gamma_{j-1} \Delta x) - b_{j-1} \gamma_{j-1} \sin(\gamma_{j-1} \Delta x) = a_j \gamma_j; \quad j = 2, \ldots, n, \\ \text{with } a_1 = 0, b_1 = 1. \end{gathered} \tag{4.1.4}$$

Since the arguments of the sine and cosine functions must be represented as dimensionless quantities, we define a new parameter α_j

$$\alpha_j := \gamma_j \Delta x = \sqrt{\frac{\omega^2}{{c_j}^2} - \hat{\lambda}}\,\Delta x. \tag{4.1.5}$$

From equation (4.1.3),

$$a_n(\alpha_n - \tau(\omega,\hat{\lambda})\Delta x \tan\alpha_n) = b_n(\alpha_n \tan\alpha_n + \tau(\omega,\hat{\lambda})\Delta x), \tag{4.1.6}$$

where, for each $j = 1,\ldots,n$, $\hat{\lambda} := \dfrac{\omega^2}{c_j^2} - \dfrac{\alpha_j^2}{\Delta x^2}$. Using definitions (2.0.20), (2.0.22), and (3.1.6), we obtain

$$a_n\left\{\alpha_n\left[1 + P(\omega)\left(\frac{\omega^2 d^2}{c_j^2} - n^2\alpha_j^2\right)^2\right] - \beta(\omega)\Delta x\tan\alpha_n\right\} = b_n\left\{\alpha_n\tan\alpha_n\left[1 + P(\omega)\left(\frac{\omega^2 d^2}{c_j^2} - n^2\alpha_j^2\right)^2\right] + \beta(\omega)\Delta x\right\}, \quad j = 1,\ldots,n. \tag{4.1.7}$$

From system (4.1.4), we can form transfer matrices

$$\begin{bmatrix} a_n \\ b_n \end{bmatrix} = \prod_{j=n}^{2}\begin{bmatrix} \dfrac{\alpha_{j-1}}{\alpha_j}\cos\alpha_{j-1} & \dfrac{-\alpha_{j-1}}{\alpha_j}\sin\alpha_{j-1} \\ \sin\alpha_{j-1} & \cos\alpha_{j-1} \end{bmatrix} \cdot \begin{bmatrix} 0 \\ 1 \end{bmatrix} := \begin{bmatrix} A_n(\alpha_1,\ldots,\alpha_n) \\ B_n(\alpha_1,\ldots,\alpha_n) \end{bmatrix}. \tag{4.1.8}$$

From system (4.1.8), equation (4.1.7) contains n unknown variables $\alpha_j, j = 1,\ldots,n$. Using definition (4.1.5), we exclude $n-1$ of them since

$$\alpha_j = \sqrt{{\alpha_n}^2 + \left(\frac{\omega\Delta x}{c_j}\right)^2 - \left(\frac{\omega\Delta x}{c_n}\right)^2}, \quad j = 1,\ldots,n-1. \tag{4.1.9}$$

Therefore, equations (4.1.7) and (4.1.8) could be viewed as a single transcendental equation for α_n. After α_n, the spectral parameter $\hat{\lambda}$ may be found from the definition (4.1.5). Since the functions $A_n(\alpha_1,\ldots,\alpha_n)$ and $B_n(\alpha_1,\ldots,\alpha_n)$ become long and complex expressions as n increases, we use Numerical Analysis to work with these formulas.

We implement the algorithm based on equation (4.1.7), system (4.1.8), and equation (4.1.9). In system (4.1.8), we use the variables, which we guess are of the order one for large $n, w_j := n\alpha_j$, so

$$w_j = \sqrt{n^2{\alpha_n}^2 + \left(\frac{\omega d}{c_j}\right)^2 - \left(\frac{\omega d}{c_n}\right)^2}, \quad j = 1,\ldots,n-1. \tag{4.1.10}$$

To solve equation (4.1.7) numerically, we use the initial approximation $\alpha_n = \dfrac{\xi_0}{n}$ for each of the n values of ξ_0 for the n transcendental equations, for a given value of ω and E. c is constant in each subinterval, so for each c_i, $i = 1,\ldots,n$, we use this initial approximation as explained in Algorithm 1. After solving for the n values of α_n, we use definition (4.1.5) to find each of the n values of the dimensionless wavenumber $\hat{\kappa}(\omega)d := \sqrt{\hat{\lambda}d^2}$ using the formula

$$\hat{\kappa}(\omega)d = \sqrt{\left(\frac{\omega d}{c_n}\right)^2 - n^2{\alpha_n}^2}. \tag{4.1.11}$$

The lower and upper bounds of $\hat{\kappa}(\omega)d$ for a given frequency ω, respectively, are given by

$$\hat{\kappa}_+(\omega)d = \sqrt{\left(\frac{\omega d}{c_+}\right)^2 - \xi_0^2(\omega)}, \quad \hat{\kappa}_-(\omega)d = \sqrt{\left(\frac{\omega d}{c_-}\right)^2 - \xi_0^2(\omega)}. \tag{4.1.12}$$

4.2 Analysis of $\tilde{\lambda}$

We now consider the study of the eigenvalue associated with the leading mode $\tilde{\lambda}$. We use the same discretization and numerical approach as used in Section 4.1. Since $\frac{\omega^2}{c^2} - \tilde{\lambda} < 0$,

$$\psi_j(x) = a_j \sinh(\Gamma_j x) + b_j \cosh(\Gamma_j x), \quad \text{where } \Gamma_j := \sqrt{\tilde{\lambda} - \frac{\omega^2}{c_j^2}},\ j = 1, \ldots, n, \tag{4.2.1}$$

where a_j and b_j are arbitrary constants. From boundary condition (2.0.15), we obtain $a_1 = 0$. We choose $b_1 = 1$. From these conditions,

$$\psi_1(x) = \cosh(\Gamma_1 x). \tag{4.2.2}$$

From the definition of ψ_n and boundary condition (2.0.21),

$$a_n \Gamma_n \cosh(\Gamma_n \Delta x) + b_n \Gamma_n \sinh(\Gamma_n \Delta x) - \tau(\omega, \tilde{\lambda})(a_n \sinh(\Gamma_n \Delta x) + b_n \cosh(\Gamma_n \Delta x)) = 0. \tag{4.2.3}$$

We need a dimensionless parameter to express the arguments of hyperbolic sine and cosine functions. Therefore, we define a dimensionless parameter ζ_j

$$\zeta_j := \Gamma_j \Delta x = \sqrt{\tilde{\lambda} - \frac{\omega^2}{{c_j}^2}} \Delta x. \tag{4.2.4}$$

We form transfer matrices

$$\begin{bmatrix} a_n \\ b_n \end{bmatrix} = \prod_{j=n}^{2} \begin{bmatrix} \frac{\zeta_{j-1}}{\zeta_j} \cosh \zeta_{j-1} & \frac{\zeta_{j-1}}{\zeta_j} \sinh \zeta_{j-1} \\ \sinh \zeta_{j-1} & \cosh \zeta_{j-1} \end{bmatrix} \cdot \begin{bmatrix} 0 \\ 1 \end{bmatrix} := \begin{bmatrix} A_n(\zeta_1, \ldots, \zeta_n) \\ B_n(\zeta_1, \ldots, \zeta_n) \end{bmatrix}. \tag{4.2.5}$$

Finally, we arrive at the system of equations

$$\begin{gathered}\left(\frac{\zeta_k}{\Delta x}\right)^2+\left(\frac{\omega}{c_k}\right)^2=\left(\frac{\zeta_j}{\Delta x}\right)^2+\left(\frac{\omega}{c_j}\right)^2,\\ \text{for all } \ k,j=1,...,n\,, \ \text{ but } \ k<j\,;\\ A_n(\zeta_1,\ldots,\zeta_n)(\zeta_n\cosh\zeta_n-\tau(\omega,\tilde{\lambda})\Delta x\sinh\zeta_n)\\ =B_n(\zeta_1,\ldots,\zeta_n)(-\zeta_n\sinh\zeta_n+\tau(\omega,\tilde{\lambda})\Delta x\cosh\zeta_n).\end{gathered} \tag{4.2.6}$$

We solve this system for $\tilde{\lambda}$

$$\tilde{\lambda}=\frac{\omega^2}{{c_j}^2}+\frac{{\zeta_j}^2}{(\Delta x)^2}. \tag{4.2.7}$$

From system (4.2.6), the last of the equations contains n unknown variables, ζ_j, $j=1,\ldots,n$, but the first group of the equations allows to exclude $n-1$ of them since

$$\zeta_j=\sqrt{\zeta_n^2+\left(\frac{\omega\Delta x}{c_n}\right)^2-\left(\frac{\omega\Delta x}{c_j}\right)^2}, \ \ j=1,\ldots,n-1. \tag{4.2.8}$$

From numerical analysis, we find that $\zeta_j >> 1$, so the values of hyperbolic functions in systems (4.2.5) and (4.2.6) are large. Therefore, it is not realistic to perform Numerical Analysis on these equations. To resolve this issue, we consider the formulas of the hyperbolic functions

$$\cosh\zeta=\frac{e^{\zeta}}{2}(1+e^{-2\zeta}), \quad \sinh\zeta=\frac{e^{\zeta}}{2}(1-e^{-2\zeta}). \tag{4.2.9}$$

Now, system (4.2.5) is expressed as

$$\begin{bmatrix}a_n\\ b_n\end{bmatrix}=P_n\cdot\prod_{j=n}^{2}\cdot\begin{bmatrix}\frac{\zeta_{j-1}}{\zeta_j}(1+e^{-2\zeta_{j-1}}) & \frac{\zeta_{j-1}}{\zeta_j}(1-e^{-2\zeta_{j-1}})\\ 1-e^{-2\zeta_{j-1}} & 1+e^{-2\zeta_{j-1}}\end{bmatrix}\cdot\begin{bmatrix}0\\ 1\end{bmatrix}=P_n\cdot\begin{bmatrix}A_n^0(\zeta_1,...,\zeta_n)\\ B_n^0(\zeta_1,...,\zeta_n)\end{bmatrix}, \tag{4.2.10}$$

where $P_n := e^{\zeta_1+\cdots+\zeta_{n-1}}/2^{n-1}$. After canceling the common factor P_n of A_n and B_n in the last of the equations (4.2.6), we obtain

$$A_n{}^0(\zeta_1,\ldots,\zeta_n)\left(\zeta_n\left(1+e^{-2\zeta_n}\right)-\tau(\omega,\tilde{\lambda})\Delta x\left(1-e^{-2\zeta_n}\right)\right)=B_n{}^0(\zeta_1,\ldots,\zeta_n)\big(-\zeta_n\left(1-e^{-2\zeta_n}\right)+\tau(\omega,\tilde{\lambda})\Delta x\left(1+e^{-2\zeta_n}\right)\big). \quad (4.2.11)$$

Using definitions (2.0.20), (2.0.22), and (3.1.6), we obtain

$$A_n{}^0(\zeta_1,\ldots,\zeta_n)\left\{\zeta_n\left(1+e^{-2\zeta_n}\right)\left[1+P(\omega)\left(\frac{\omega^2d^2}{c_j^2}+n^2\zeta_j^2\right)^2\right]-\beta(\omega)\Delta x\left(1-e^{-2\zeta_n}\right)\right\}=$$
$$B_n{}^0(\zeta_1,\ldots,\zeta_n)\left\{-\zeta_n\left(1-e^{-2\zeta_n}\right)\left[1+P(\omega)\left(\frac{\omega^2d^2}{c_j^2}+n^2\zeta_j^2\right)^2\right]+\beta(\omega)\Delta x\left(1+e^{-2\zeta_n}\right)\right\},$$
$$j=1,\ldots,n. \quad (4.2.12)$$

Now, the system (4.2.10) (without the factor P_n) and equation (4.2.12) are stable, and it is easy to perform Numerical Analysis.

We implement the algorithm based on equation (4.2.8), system (4.2.10), and equation (4.2.12). In system (4.2.10), we use the variables, which we guess are of the order one for large n, $w_j := n\zeta_j$, which are expressed as

$$w_j=\sqrt{n^2\zeta_n^2+\left(\frac{\omega d}{c_n}\right)^2-\left(\frac{\omega d}{c_j}\right)^2},\ \ j=1,\ldots,n. \quad (4.2.13)$$

In order to solve equation (4.2.12) numerically, we use the initial approximation $\zeta_n=\dfrac{\eta_0}{n}$ for each of the n values of η_0 for the n transcendental equations, for a given value of ω and E. c is constant in each subinterval, so for each c_i, $i=1,\ldots,n$, we use this initial approximation as explained in Algorithm 2. After solving for the n values of ζ_n, we use definition (4.2.4) to find

each of the n values of the dimensionless wavenumber $\tilde{\kappa}(\omega)d := \sqrt{\tilde{\lambda}d^2}$ using the formula

$$\tilde{\kappa}(\omega)d = \sqrt{\left(\frac{\omega d}{c_n}\right)^2 + n^2\zeta_n^2}. \tag{4.2.14}$$

The lower and upper bounds of $\tilde{\kappa}(\omega)d$ for a given frequency ω, respectively, are given by

$$\tilde{\kappa}_+(\omega)d = \sqrt{\left(\frac{\omega d}{c_+}\right)^2 + \eta_0^2(\omega)}, \quad \tilde{\kappa}_-(\omega)d = \sqrt{\left(\frac{\omega d}{c_-}\right)^2 + \eta_0^2(\omega)}. \tag{4.2.15}$$

4.3 Computational Results

With the help of the formulas developed in sections 4.1 and 4.2, we numerically evaluate the wavenumbers with reasonable accuracy. The algorithms were implemented in MATLAB. We used the 'vpasolve' solver to solve the transcendental equations in (3.1.7), the 'fmincon' solver to solve the transcendental equation (4.1.7), and the 'fsolve' solver to solve the transcendental equation (4.2.12). In both algorithms, we set the termination tolerance on the nonlinear function (OptimalityTolerance) and the variables (StepTolerance) to 10^{-3}. The results were obtained for different values of h and E, and we observed that when $n = 15$, the numerical values of $\hat{\kappa}(\omega)d$ and $\tilde{\kappa}(\omega)d$ stopped changing for all ω that we considered. Hence, we obtain convergence at the numerical level. We observed that the α_n values were very close to the initial approximation $\frac{\xi_0}{n}$ and the ζ_n values obtained were very close to the initial approximation $\frac{\eta_0}{n} \approx \frac{\beta d}{n}$ over a range of ω values.

The 'fmincon' solver requires a lower and upper bound, and the interval from lower to upper bound is the "corridor" of α_n. The solution of the transcendental equation (4.1.7) for α_n must be within this interval. The lower bound was set as 0, and the upper bound was set as $\frac{1}{n}\sqrt{\xi_0^2(\omega) + \omega d^2\left(\frac{1}{{c_-}^2} - \frac{1}{{c_n}^2}\right)}$, which is obtained by replacing c_j with c_- in equation (4.1.9) and

using the initial approximation $\alpha_n = \dfrac{\xi_0}{n}$. The n values $c_1, \ldots, c_n$ from the interval (c_-, c_+) were chosen in such a way that $c_1, \ldots, c_n$ are the intermediate values of the interval (c_-, c_+).

We used four profiles of speed:

$$\begin{gathered} c(x) = c_- + \frac{c_+ - c_-}{d}x, \quad c(x) = c_+ - \frac{c_+ - c_-}{d}x, \\ c(x) = \frac{c_+ + c_-}{2} + \frac{c_+ - c_-}{2}\sin\frac{\pi x}{2d}, \quad c(x) = c_- + 4(c_+ - c_-)\left(\frac{x}{d} - \frac{x^2}{d^2}\right). \end{gathered} \tag{4.3.1}$$

These speed profiles are also shown in Figure 4.1. We observed that the convergence speed is about the same for all profiles $c(x)$, except the convergence is a little faster when $c(x)$ is constant.

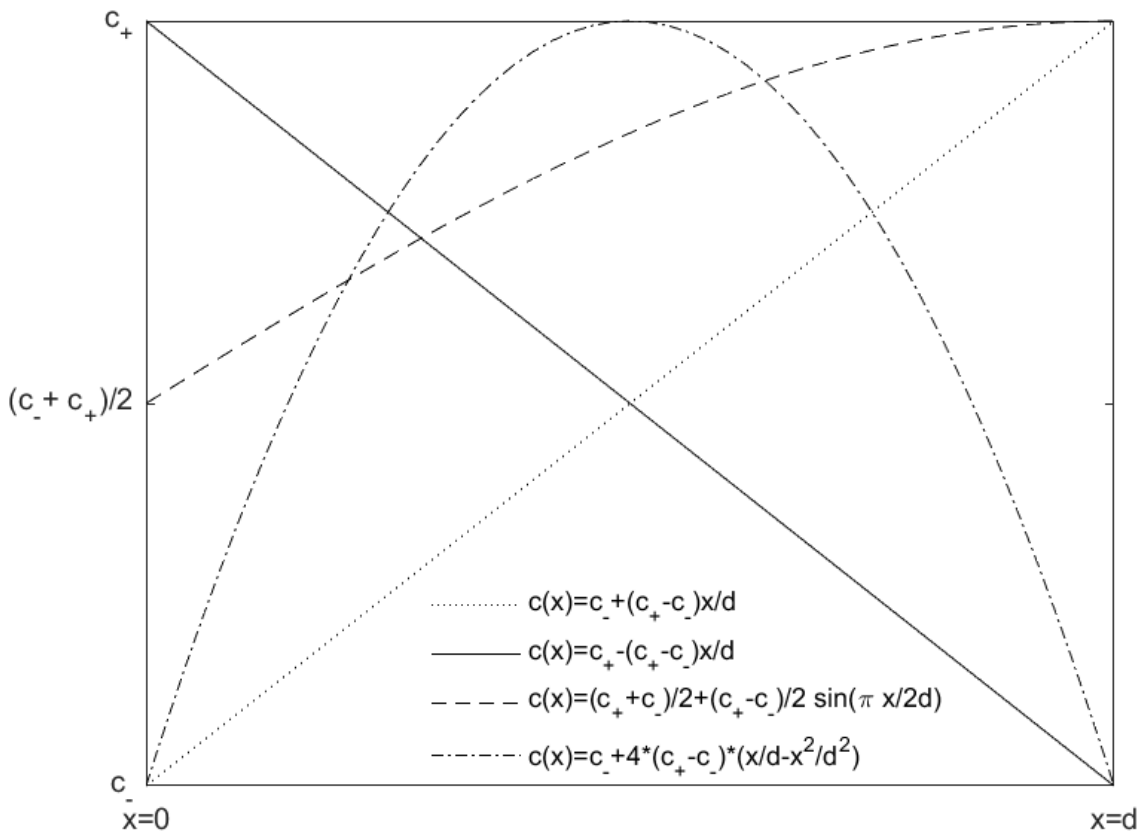

Figure 4.1 Speed profiles $c(x)$

We demonstrate the numerical results for the following set of parameters:

$$d = 500\,m;\ \ \rho_1 = 917\,kg/m^3;\ \ \rho_2 = 1024\,kg/m^3;\ \ g = 9.8\,m/s^2;\ \ h = 0.1, 1, \text{and } 2\,m;$$
$$E = 5 \text{ and } 9.1\,GPa;\ \ \sigma = 0.3;\ \ c_- = 1350\,m/s;\ \ c_+ = 1650\,m/s \tag{4.3.2}$$

We now present the algorithm that allows evaluating the dimensionless wavenumbers $\hat{\kappa}(\omega)d$ and $\hat{\kappa}_\pm(\omega)d$ for the speed profiles (4.3.1).

Algorithm 1 The steps of the numerical algorithm for $\hat{\kappa}(\omega)$

Input: n, d, ρ_1, ρ_2, g, h, E, σ, c_-, c_+
Initialize: a discrete function $c(x) = (c_1, c_2, \ldots, c_n)$
for $\omega \in (0, \infty)$ **do**
  Evaluate $\beta(\omega)$ according to definition (2.0.22) and $P(\omega)$ according to definition (3.1.6).
  Solve equation (3.1.7) for ξ_0 on $[\pi/2, \pi]$.
  Solve $F(\omega) := \omega - \dfrac{\xi_0 c_+}{d} = 0$.
  if $F(\omega) > 0$ **then**
    Set initial approximation $\alpha_n = \xi_0/n$.
    Calculate $\hat{\kappa}_+(\omega)d$ and $\hat{\kappa}_-(\omega)d$ according to formulas (4.1.12).
    for $i = 1$ to n **do**
      $w_i = \sqrt{\left(\dfrac{\omega d}{c_n}\right)^2 + n^2\alpha_n^2 - \left(\dfrac{\omega d}{c_i}\right)^2}$.
    end for
    for $j = 2$ to n **do**
      Find the 2×2 matrix u_j where
      $u_j(1,1) = \dfrac{w_{j-1}}{w_j}\cos\left(\dfrac{w_{j-1}}{n}\right)$, $u_j(1,2) = -\dfrac{w_{j-1}}{w_j}\sin\left(\dfrac{w_{j-1}}{n}\right)$,
      $u_j(2,1) = \sin\left(\dfrac{w_{j-1}}{n}\right)$, and $u_j(2,2) = \cos\left(\dfrac{w_{j-1}}{n}\right)$.
      $u(k,l)$ represents the element of matrix V in the k^{th} row and l^{th} column.
    end for
    Find the product of the matrices $V = \prod_{j=n}^{2} [u_j]$.
    for $i = 1$ to n **do**
      Evaluate $S_i(\omega) = 1 + P(\omega)\left(\dfrac{\omega^2 d^2}{c_i^2} - n^2\alpha_i^2\right)^2$.
      Solve the transcendental equation for α_n
      $v(1,2)(n\alpha_n S_i(\omega) - \beta(\omega)d\tan(\alpha_n)) - v(2,2)(n\alpha_n\tan(\alpha_n)S_i(\omega) + \beta(\omega)d) = 0$,
      $v(k,l)$ represents the element of matrix V in the k^{th} row and l^{th} column.
      Calculate $\hat{\kappa}(\omega)d = \sqrt{\left(\dfrac{\omega d}{c_n}\right)^2 - n^2\alpha_n^2}$.
    end for
  end if
end for
Output: $\hat{\kappa}_+(\omega)d, \hat{\kappa}_-(\omega)d$ and $\hat{\kappa}(\omega)d$

We further present the algorithm that allows evaluating the dimensionless wavenumbers $\tilde{\kappa}(\omega)d$ and $\tilde{\kappa}_{\pm}(\omega)d$ for the speed profiles (4.3.1).

Algorithm 2 The steps of the numerical algorithm for $\tilde{\kappa}(\omega)$

Input: n, d, ρ_1, ρ_2, g, h, E, σ, c_-, c_+
Initialize: a discrete function $c(x) = (c_1, c_2, \ldots, c_n)$
for $\omega \in (0, \infty)$ **do**
    Evaluate $\beta(\omega)$ according to definition (2.0.22) and $P(\omega)$ according to definition (3.1.6).
    Solve equation (3.1.7) for $\eta_0 > 0$.
    Set initial approximation $\zeta_n = \eta_0/n$.
    Calculate $\tilde{\kappa}_+(\omega)d$ and $\tilde{\kappa}_-(\omega)d$ according to formulas (4.2.15).
    for $i = 1$ to n **do**
        $w_i = \sqrt{\left(\frac{\omega d}{c_n}\right)^2 + n^2\zeta_n^2 - \left(\frac{\omega d}{c_i}\right)^2}$.
    end for
    for $j = 2$ to n **do**
        Let $\zeta_j = \frac{w_{j-1}}{n}$.
        Find the 2×2 matrix u_j where
        $u_j(1,1) = \frac{w_{j-1}}{w_j}\left(\frac{1+e^{-2\zeta_j}}{2}\right)$, $u_j(1,2) = -\frac{w_{j-1}}{w_j}\left(\frac{1-e^{-2\zeta_j}}{2}\right)$,
        $u_j(2,1) = \left(\frac{1+e^{-2\zeta_j}}{2}\right)$, and $u_j(2,2) = \left(\frac{1-e^{-2\zeta_j}}{2}\right)$.
        $u(k,l)$ represents the element of matrix V in the k^{th} row and l^{th} column.
    end for
    Find the product of the matrices $V = \prod_{j=n}^{2}[u_j]$.
    for $i = 1$ to n **do**
        Evaluate $T_i(\omega) = 1 + P(\omega)\left(\frac{\omega^2 d^2}{c_i^2} + n^2{\zeta_i}^2\right)^2$, define $\mathscr{E}(\zeta_n) = \frac{1-e^{-2\zeta_n}}{1+e^{-2\zeta_n}}$, and solve the transcendental equation for ζ_n
        $v(1,2)(n\zeta_n T_i(\omega) - \beta(\omega)d\mathscr{E}(\zeta_n)) - v(2,2)(-n\zeta_n\mathscr{E}(\zeta_n)T_i(\omega) + \beta(\omega)d) = 0$,
        $v(k,l)$ represents the element of matrix V in the k^{th} row and l^{th} column.
        Calculate $\tilde{\kappa}(\omega)d = \sqrt{\left(\frac{\omega d}{c_n}\right)^2 + n^2\zeta_n^2}$.
    end for
end for
Output: $\tilde{\kappa}_+(\omega)d, \tilde{\kappa}_-(\omega)d$ and $\tilde{\kappa}(\omega)d$

4.4 Observations

From Section 3.4, the wave associated with the eigenvalue $\tilde{\lambda}$ is always propagating but the wave associated with the eigenvalue $\hat{\lambda}$ propagates only on the frequencies $\omega > \omega_*$. The graph of

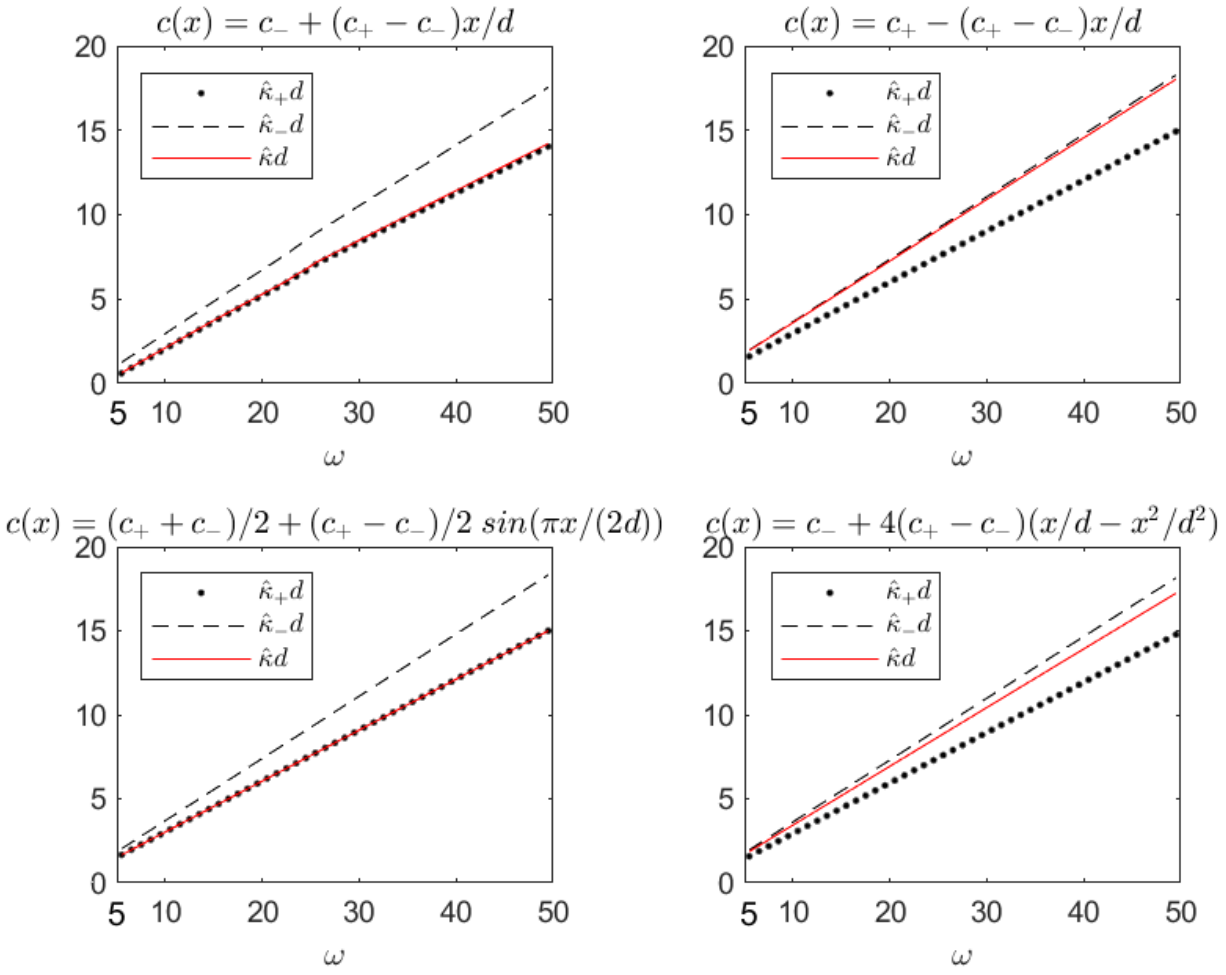

Figure 4.2 Frequency dependence of the dimensionless wavenumber $\hat{\kappa}d$ for $h = 1\ m$ and $E = 5\ GPa$

the function $F(\omega)$, as defined in inequality (3.4.3), is shown in Figure 4.7 for the set of parameters (4.3.2) and also for the similar set but with $c_+ = 1400\ m/s$.

We conclude that no propagating waves associated with the eigenvalue $\hat{\lambda}_1$ appear for the frequencies below the cut-off frequency ω_* and this frequency decays with the decrease of c_+. This result is the same for all values of E and h that we considered.

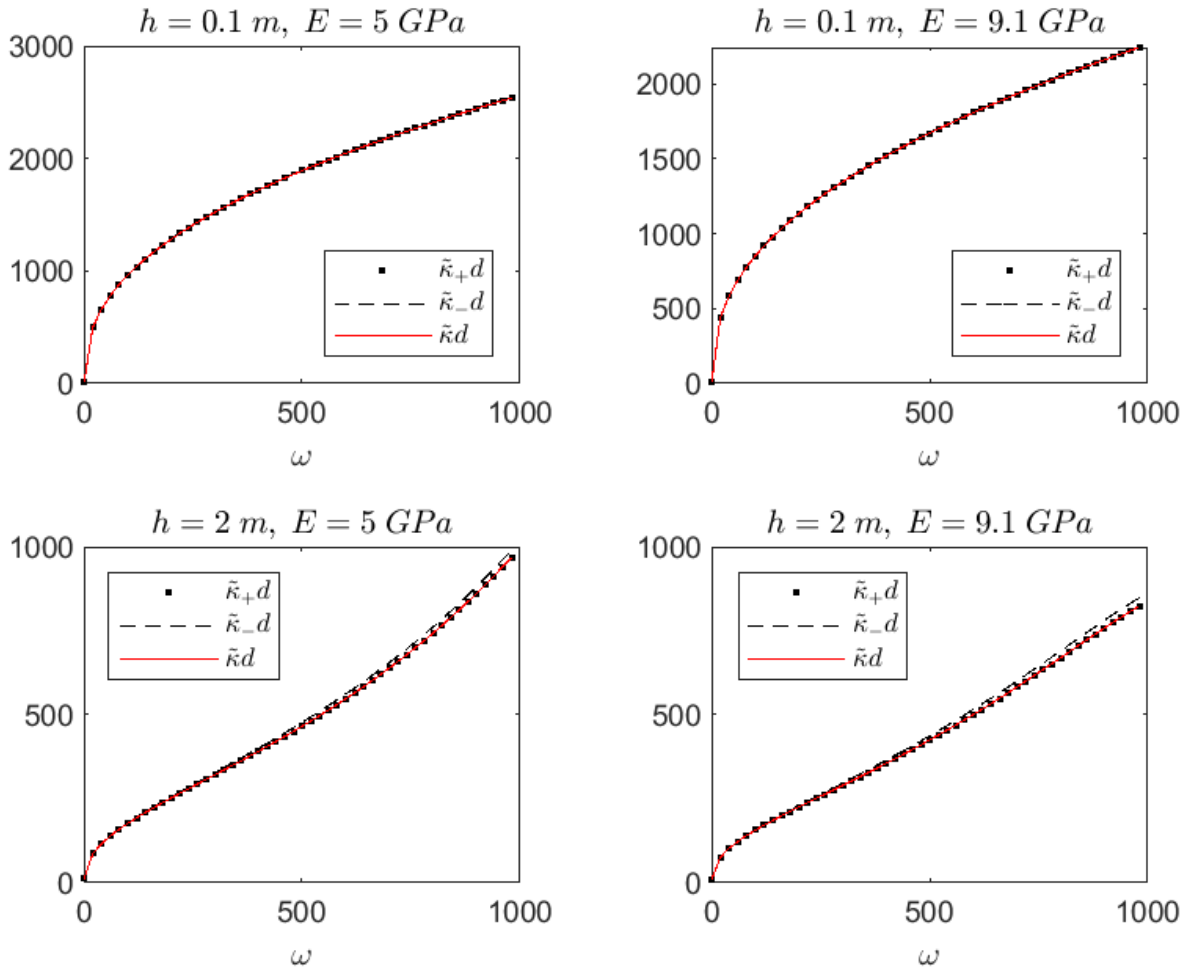

Figure 4.3 Frequency dependence of the dimensionless wavenumber $\tilde{\kappa}d$ for $c(x) = c_- + (c_+ - c_-)x/d$

The graphs from figures 4.2 - 4.6 demonstrate the numerical results. These figures show the dimensionless wavenumbers $\hat{\kappa}(\omega)d$ and $\tilde{\kappa}(\omega)d$ as functions of frequency ω for different speed profiles $c(x)$ and different values of ice thickness h and Young's Modulus E.

From the numerical results, we observe that $\hat{\kappa}(\omega)d$ is close to either $\hat{\kappa}_+(\omega)d$ or $\hat{\kappa}_-(\omega)d$ or is approximately in the middle of these bounds for different speed profiles $c(x)$. However, no change in $\hat{\kappa}(\omega)d$ was observed for the reasonable values of ice thickness and Young's Modulus. On the other hand, the $\tilde{\kappa}(\omega)d$ curve changes its shape for different speed profiles and different

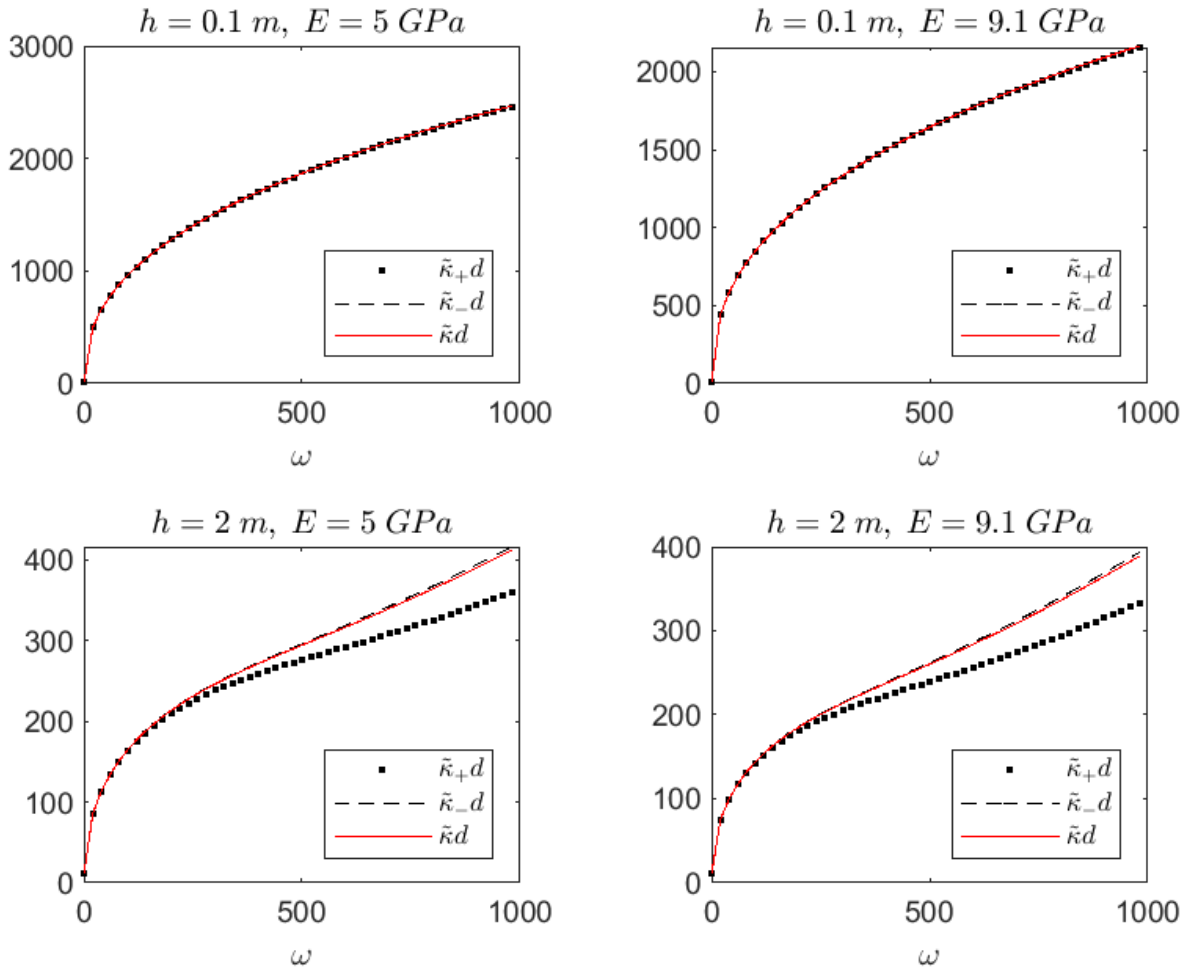

Figure 4.4 Frequency dependence of the dimensionless wavenumber $\tilde{\kappa}d$ for $c(x) = c_+ - (c_+ - c_-)x/d$

values of h. Moreover, the values of $\tilde{\kappa}(\omega)d$ get smaller as the values of E and h increase. As ω values increase, the curve $\tilde{\kappa}(\omega)d$ changes its shape and gets farther apart from its upper and lower bounds. For all values of h and E that we considered and every speed profile $c(x)$, the wavenumbers $\hat{\kappa}(\omega)$ and $\tilde{\kappa}(\omega)$ are strictly increasing with respect to ω. These results are consistent with remarks 3.2.4 and 3.2.6. The numerical results are in complete agreement with the analytical results.

Remark 4.4.1. The case of the waveguide with the free surface may be considered by changing $\beta(\omega)$ as in equations (3.1.10). Hence, only a minor modification would be required in algorithms

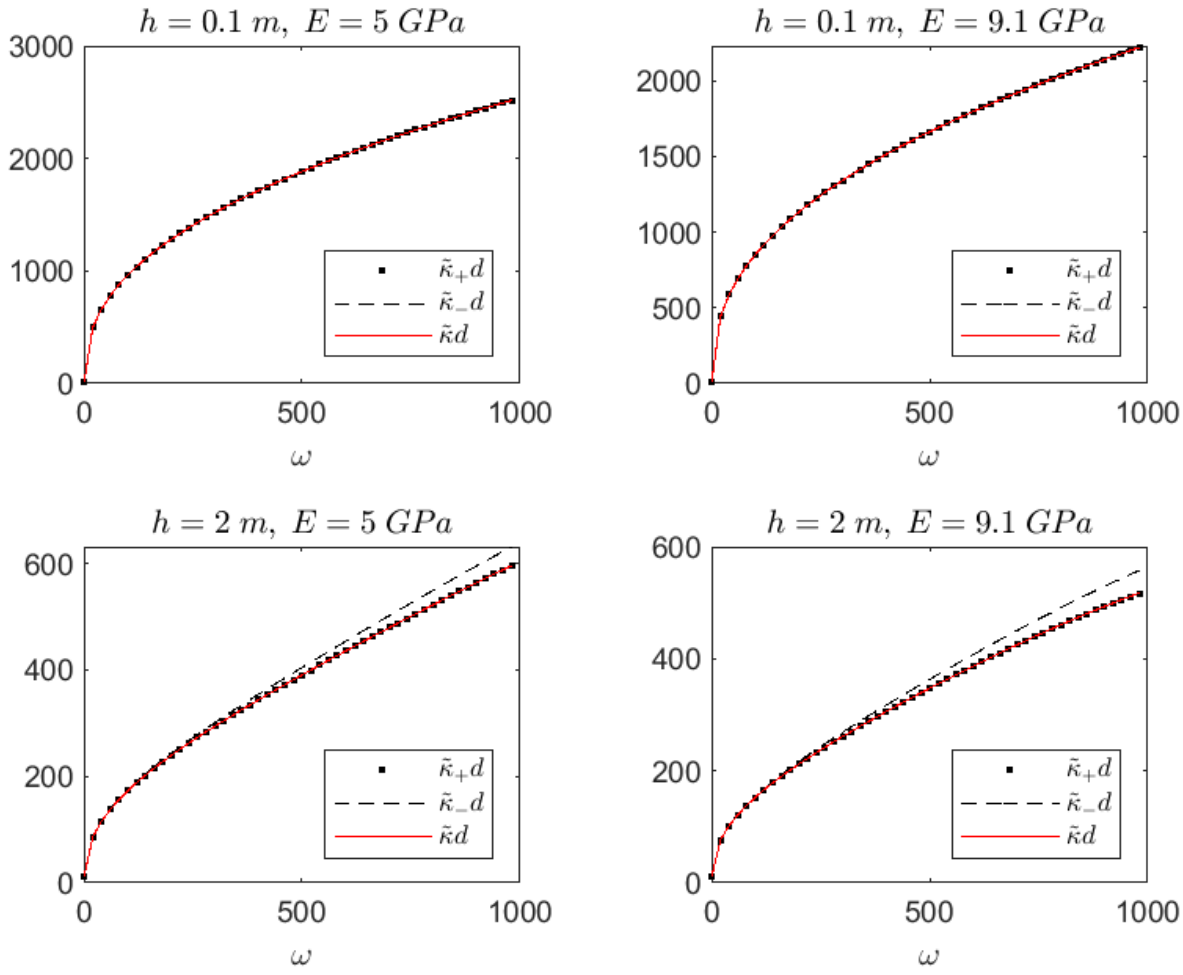

Figure 4.5 Frequency dependence of the dimensionless wavenumber $\tilde{\kappa}d$ for $c(x) = (c_+ + c_-)/2 + (c_+ - c_-)/2\ sin(\pi x/(2d))$

1 and 2 to find the dimensionless wavenumbers $\hat{\kappa}(\omega)d$ and $\tilde{\kappa}(\omega)d$, respectively. It is evident from the numerical results that the wavenumber $\hat{\kappa}(\omega)d$ for the waveguide with the free surface is a little lower than the wavenumber $\hat{\kappa}(\omega)d$ for the surface covered by thick ice, but these wavenumbers are close for a given value of ω.

In the next section, we compare some numerical results of Algorithm 1 with the results obtained from Machine Learning.

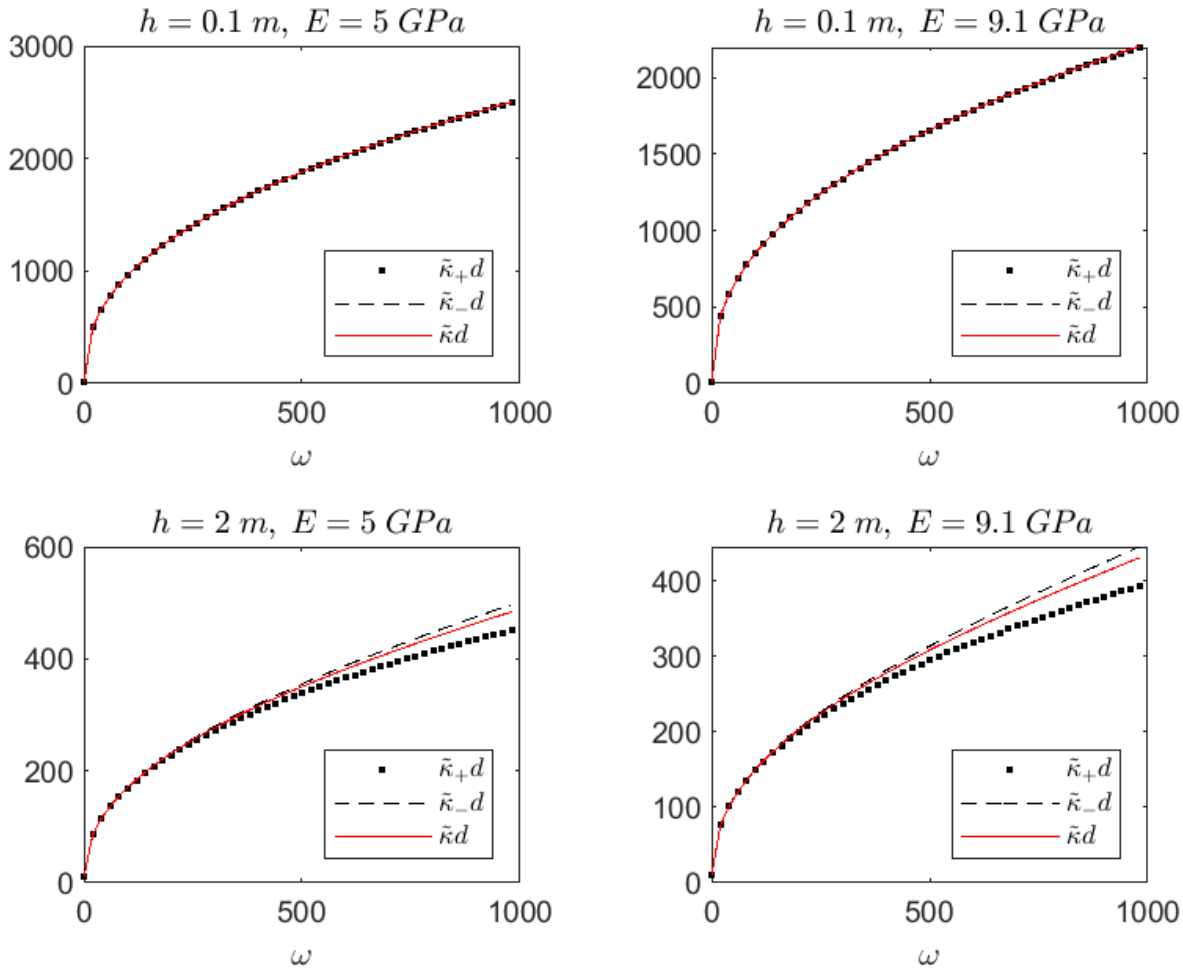

Figure 4.6 Frequency dependence of the dimensionless wavenumber $\tilde{\kappa}d$ for $c(x) = c_- + 4(c_+ - c_-)(x/d - x^2/d^2)$

4.5 Machine Learning Results

We consider the α_n values obtained from equation (4.1.7) and work with two Machine Learning models, Long Short-Term Memory (LSTM) and Random Forest Regressor, to predict these α_n values over a range of ω values. We consider the α_n values for the speed profile $c(x) = c_- + (c_+ - c_-)x/d$, ice thickness $h = 1\ m$, and Young's Modulus $E = 5\ GPa$. The goal of this study is to compare the α_n values obtained from the 'fmincon' solver used in Algorithm 1 with

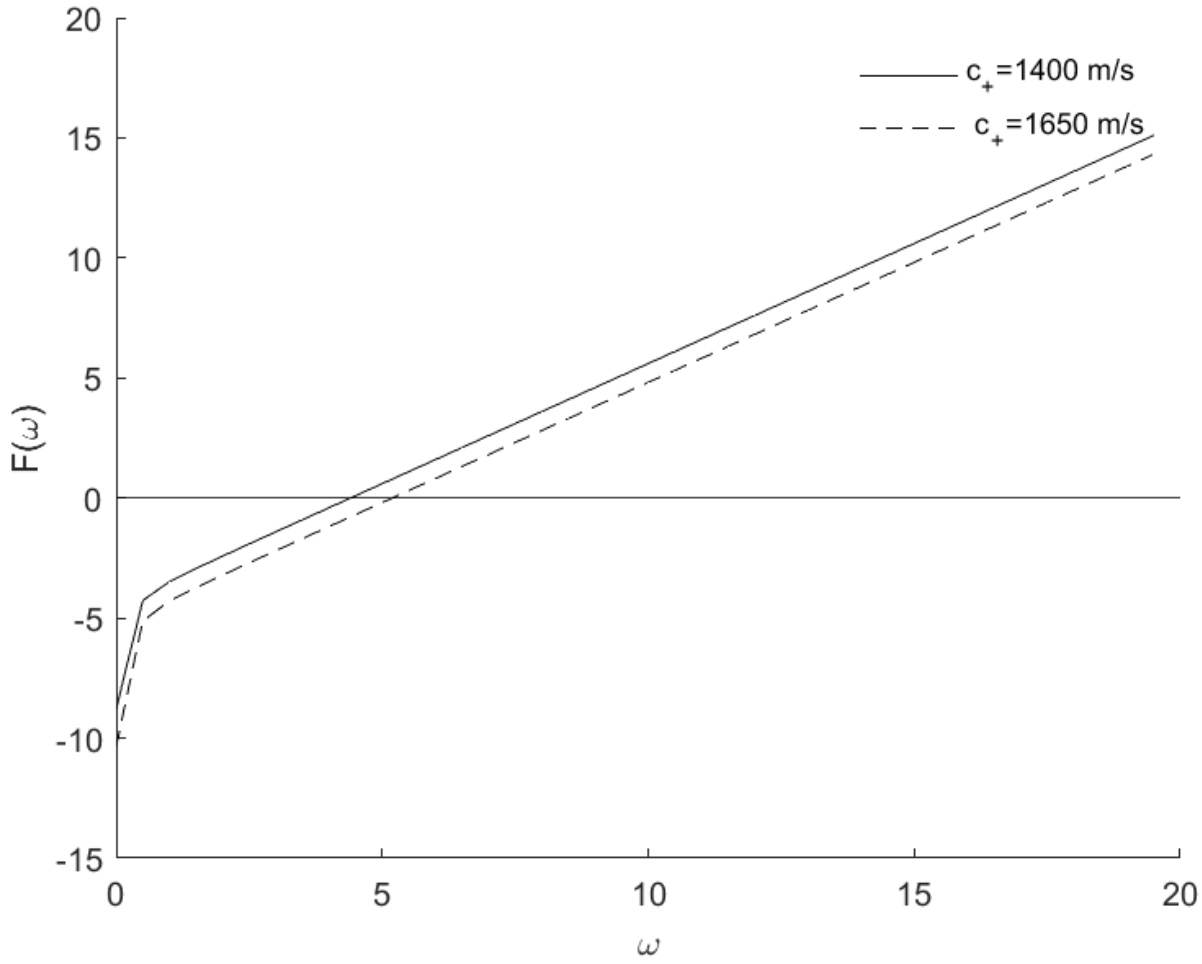

Figure 4.7 $F(\omega)$: If the lines are below the horizontal axis, it indicates that the corresponding frequencies ω do not satisfy the inequality $F(\omega) > 0$

the ones obtained by the Machine Learning models and use these Machine Learning models for the prediction of α_n values for higher values of ω.

Remark 4.5.1. In our study, it is better to use supervised methods of Machine Learning than unsupervised or reinforcement learning methods since the target α_n values are known.

Before the Machine Learning results, we provide some statistical results. After normalizing the α_n values using min-max rescaling, we find that the covariance between the normalized α_n values and the ω values is 3.228. Since the covariance is positive, there is a correlation between

α_n and ω. We find that the Pearson correlation is 0.756. Figure 4.8 shows this strong positive correlation with a few outliers.

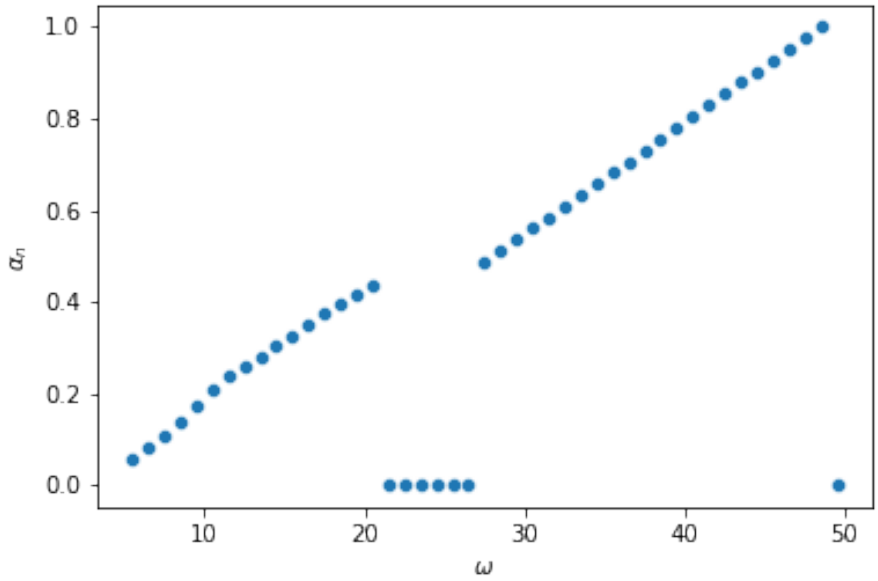

Figure 4.8 Scatter plot of α_n and ω values

We further view the count of α_n values in Figure 4.9, which shows that the α_n values are uniformly distributed over a range of ω values.

From these statistical results, we conclude that it is possible to implement Machine Learning models for predicting α_n values. In sections 4.5.1 and 4.5.2, we discuss the implementation of LSTM and Random Forest Regressor, respectively.

4.5.1 Long Short-Term Memory (LSTM)

We first used a time series model, LSTM. The Python library used in this model was PyTorch. This model contained one LSTM layer and one fully connected layer. In the training method, the number of epochs was set to 2,000 with an input size of 1, a hidden size of 2, and the number of classes as 1. The dataset was divided into training and testing sets using PyTorch

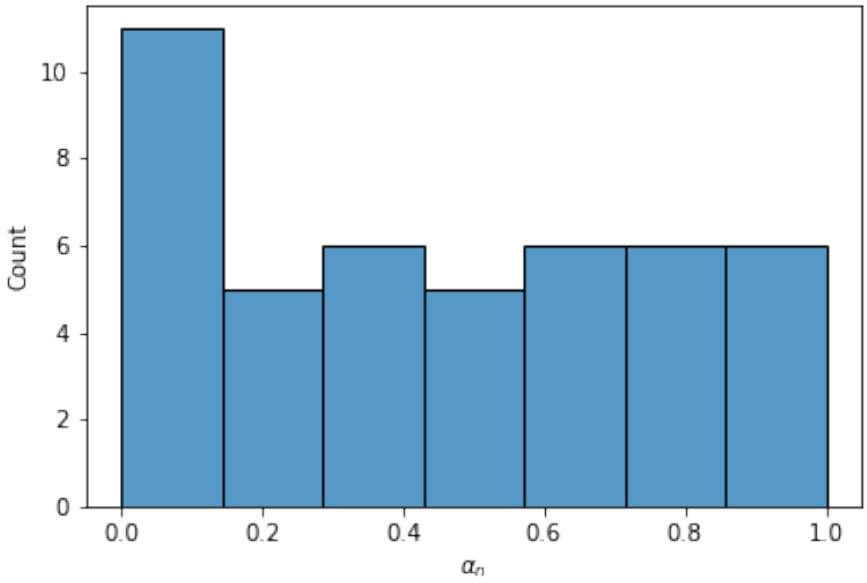

Figure 4.9 Histogram of α_n values

tensors, and the training set was split and randomized using the train_test_split function. The prediction from this model was compared with the actual values saved in the testing data set. The accuracy of the time series analysis was computed using the Mean Average Percentage Error (MAPE) score, where $100(1-\text{MAPE})$ was used to calculate the error. In general, LSTM is an unsupervised model. However, we used supervised methods since we trained our model using the target α_n values to compare the predictions.

4.5.2 Random Forest Regressor

We now consider Random Forest Regressor, which is a supervised regression model. We used the Scikit-learn library of Python, and the training set was split and randomized using the train_test_split function. The training size was 80% of the data while 20% was held out for testing. The model was trained using the 'fit' method, and the data points from the model were plotted

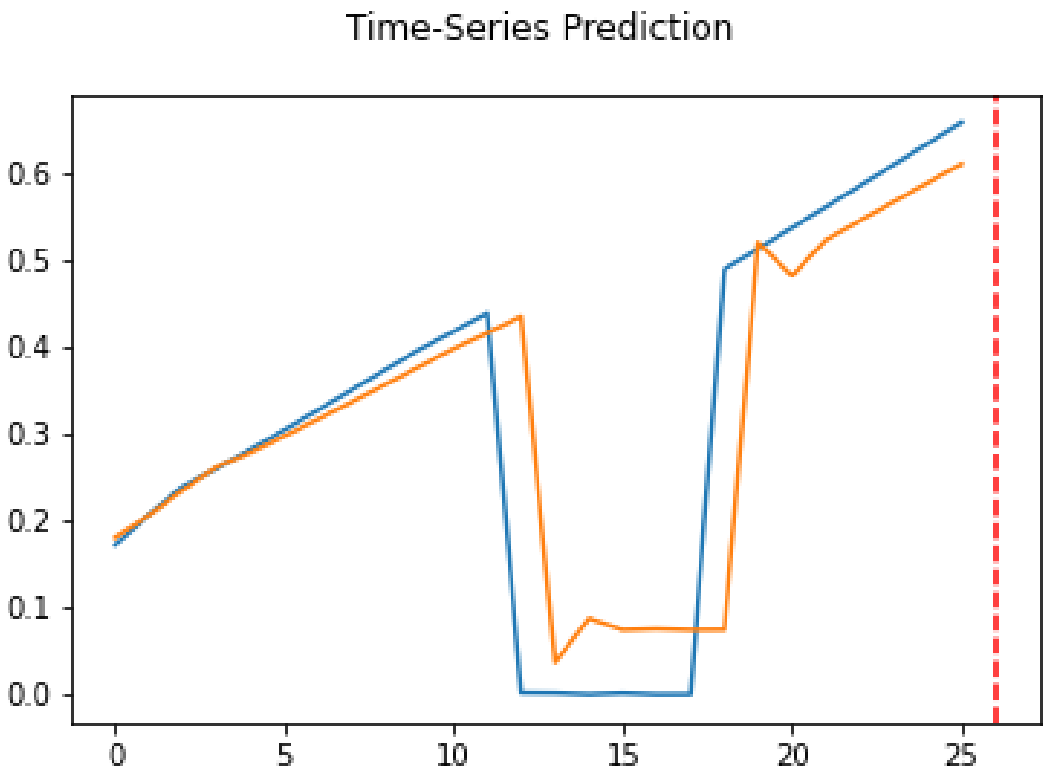

Figure 4.10 Training data of α_n

against the testing data to illustrate the accuracy of this model. The number of estimators (or trees in the forest) used was 100, with a maximum depth of 50.

4.5.3 Computational Results and Observations

The LSTM results for the training and testing data are shown in figures 4.10 and 4.11, respectively. These two figures show that in the LSTM model, there is a close fit between the two curves. This observation was verified by calculating the accuracy, which was 91.47%. The Mean Absolute Error (MAE) was 0.072, and the Mean Squared Error (MSE) was 0.005. Hence, the errors in this model are close to 0. The explained variance score was found to be 0.976.

The results of the Random Forest Regressor model are given in Figure 4.12. We observe that the data points obtained from the model are very close to the testing data values of α_n. This

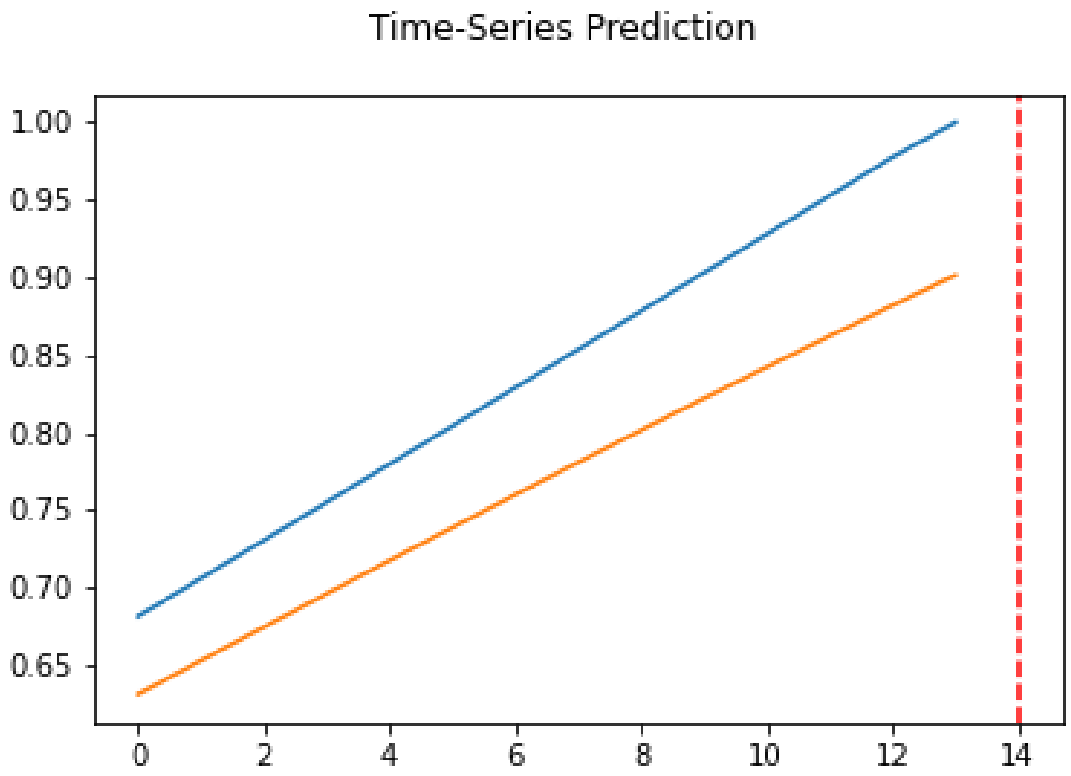

Figure 4.11 Testing data of α_n

observation was verified by calculating the accuracy, which was 99.90%. The MAE was 0.076, and the MSE was 0.020. Hence, the errors are close to 0. The explained variance score was found to be 0.833.

We conclude that both models performed very well in predicting the testing values. However, we observe that Random Forest Regressor performed better than LSTM. These two models can predict an α_n value for a higher ω value. For this study, we can also use other Machine Learning models, for example, LSTM with an attention mechanism (Transformer) or other regression models.

From Figure 4.8 and the explained variance score calculated in both models, we observe that the dispersion in the data is small. Due to this observation, our study did not consider a large dataset for the training data.

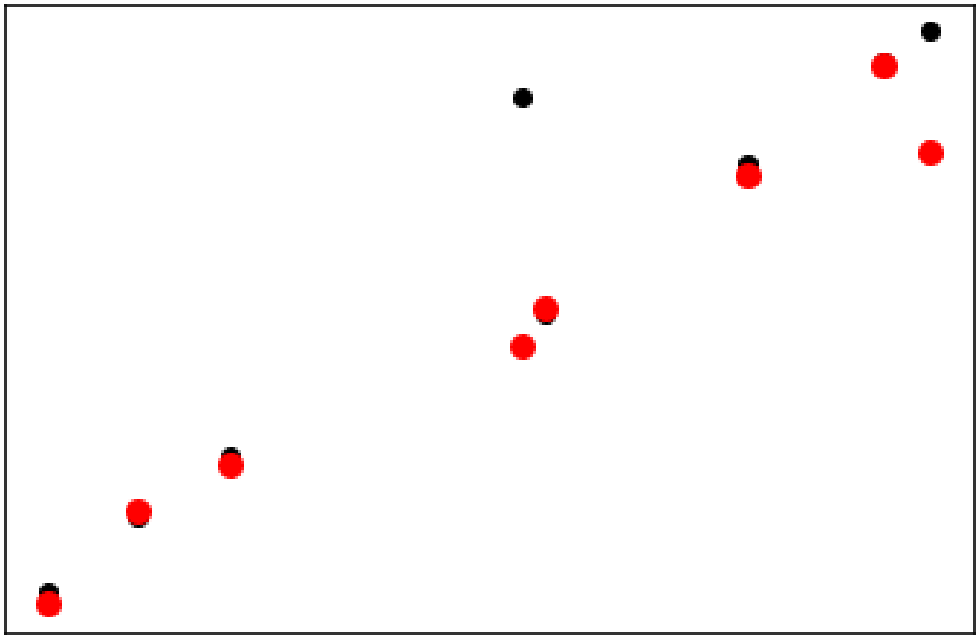

Figure 4.12 Comparison of α_n values from Random Forest Regressor (red) with the testing data (black)

Remark 4.5.2. Although we obtained accurate results with small training data, a larger interval of ω would yield a large training dataset. This training dataset would result in a better performance of the models and better shapes of the curves. Moreover, this large training dataset would ignore the outliers we observe in Figure 4.8.

This completes our study of the numerical results of the dimensionless wavenumbers $\hat{\kappa}(\omega)d$ and $\tilde{\kappa}(\omega)d$. The next chapter will discuss the asymptotic properties of these dimensionless wavenumbers.

CHAPTER 5

Asymptotic Considerations

In this chapter, we find asymptotic representations of the dimensionless wavenumbers $\hat{\kappa}(\omega)d$, $\tilde{\kappa}(\omega)d$ and the solutions ξ, η of the transcendental equations (3.1.7) obtained from our analytical results and compare these asymptotic results with the numerical results. We use Asymptotic Analysis but proceed at the formal level.

We begin with the function $\tau(\omega,\lambda)$. If $c(x) >> 1$, then the solution of equation (2.0.14) subject to boundary condition (2.0.15) is $\psi(x) = \cosh(\sqrt{\lambda}x)$. Then from boundary condition (2.0.21),

$$\sqrt{\lambda}\tanh(\sqrt{\lambda}d) = \tau(\omega,\lambda), \tag{5.0.1}$$

where the function $\tau(\omega,\lambda)$ is defined by (2.0.20). If, in addition, the ocean is deep, i.e., $d >> 1$, we have $\tanh(\sqrt{\lambda}d) \to 1$. Therefore, the above equation can be approximately represented in the dimensionless form

$$\sqrt{\lambda}d \approx \tau(\omega,\lambda)d. \tag{5.0.2}$$

In our study, for the homogeneous waveguide, we use the representation for λ (equations (3.1.11))

$$\lambda = \begin{cases} \dfrac{\omega^2 d^2}{c^2} - \xi_0^2 & \text{if} \quad \lambda = \hat{\lambda}, \\ \\ \dfrac{\omega^2 d^2}{c^2} + \eta_0^2 & \text{if} \quad \lambda = \tilde{\lambda}. \end{cases}$$

Substituting these formulas in definition (2.0.20), we obtain

$$\tau(\omega,\lambda) \coloneqq \tau(\omega) = \begin{cases} \dfrac{\omega^2}{g\left[1 + \dfrac{D\left(\dfrac{\omega^2 d^2}{c^2} - \xi_0^2\right)^2}{\rho_2 g} - \dfrac{\omega^2}{\omega_0^2}\right]} & \text{if} \quad \lambda = \hat{\lambda}, \\ \\ \dfrac{\omega^2}{g\left[1 + \dfrac{D\left(\dfrac{\omega^2 d^2}{c^2} + \eta_0^2\right)^2}{\rho_2 g} - \dfrac{\omega^2}{\omega_0^2}\right]} & \text{if} \quad \lambda = \tilde{\lambda}. \end{cases}$$

Since $\kappa = \sqrt{\lambda}$, from approximation (5.0.2), the function $\tau(\omega)$ approximately represents the wavenumber. Since ξ_0 is the first positive solution and η_0 is the unique positive solution of the first and second transcendental equations in (3.1.7), respectively, the function $\tau(\omega)$ is a higher function, and the wavenumber is approximately represented as a higher function.

Remark 5.0.1. The approximate equation (5.0.1) makes sense if $\tau(\omega,\lambda) > 0$, which was verified numerically for the set of parameters (4.3.2). D is large for all realistic values of E and h, and the denominator of $\tau(\omega,\lambda)$ is of the order ω^4. Therefore, $\tau(\omega,\lambda) > 0$ even for $\omega > \omega_0$.

Remark 5.0.2. Based on the numerical results, the dimensionless quantity $\tau(\omega,\lambda)d$ is small, i.e. $\tau(\omega,\lambda)d << 1$. Hence, the asymptotic consideration on boundary condition (2.0.21) implies that $\psi(d)$ is large. This result implies that the ocean is covered by thick ice.

The first equation in (3.1.2) yields

$$\xi_0 \tan \xi_0 = -\tau(\omega, \hat{\lambda})d.$$

If $\tau(\omega, \hat{\lambda})d << 1$, we obtain

$$\xi_0 \approx \pi.$$

Now, the bounds in (3.4.1) can be expressed as

$$\hat{\lambda}_1(\omega, c_+) \approx \frac{\omega^2}{c_+^2} - \frac{\pi^2}{d^2}, \qquad \hat{\lambda}_1(\omega, c_-) \approx \frac{\omega^2}{c_-^2} - \frac{\pi^2}{d^2}. \tag{5.0.3}$$

Since $\hat{\kappa}d = \sqrt{\hat{\lambda}_1}d$, we obtain

$$\hat{\kappa}_+ d \approx \sqrt{\frac{\omega^2 d^2}{c_+^2} - \pi^2}, \qquad \hat{\kappa}_- d \approx \sqrt{\frac{\omega^2 d^2}{c_-^2} - \pi^2}. \tag{5.0.4}$$

The curves described by the above approximations are very close to the curves in Figure 4.2.

The second equation in (3.1.2) yields

$$\eta_0 \tanh \eta_0 = \tau(\omega, \tilde{\lambda})d.$$

If $\tau(\omega, \tilde{\lambda})d << 1$, we obtain

$$\eta_0^2 \approx \tau(\omega, \tilde{\lambda})d \implies \eta_0 \approx \sqrt{\tau(\omega, \tilde{\lambda})d}.$$

Remark 5.0.3. From numerical results, the function $\tau(\omega, \tilde{\lambda})d$ is very small except when both $\omega \to 0$ and $h \to 0$.

Now, the bounds in (3.4.2) can be expressed as

$$\tilde{\lambda}(\omega, c_+) \approx \frac{\omega^2}{c_+^2} + \frac{\tau(\omega,\tilde{\lambda})}{d}, \qquad \tilde{\lambda}(\omega, c_-) \approx \frac{\omega^2}{c_-^2} + \frac{\tau(\omega,\tilde{\lambda})}{d}. \tag{5.0.5}$$

Since $\tilde{\kappa}d = \sqrt{\tilde{\lambda}}d$, we obtain

$$\tilde{\kappa}_+ d \approx \sqrt{\frac{\omega^2 d^2}{c_+^2} + \tau(\omega,\tilde{\lambda})d}, \qquad \tilde{\kappa}_- d \approx \sqrt{\frac{\omega^2 d^2}{c_-^2} + \tau(\omega,\tilde{\lambda})d}. \tag{5.0.6}$$

The curves described by the above approximations are very close to the curves in figures 4.3 - 4.6.

Comparing approximations (5.0.4) and (5.0.6), we obtain

$$\tilde{\kappa}d > \hat{\kappa}d, \tag{5.0.7}$$

which is verified by comparing Figure 4.2 with figures 4.3 - 4.6.

Now, we will find the dispersion relations for deep ocean and open water cases. For deep ocean, $d >> 1$, and $c(x) >> 1$, $\tau(\omega,\lambda) := \tau(\omega) \approx \kappa$. Therefore, from definition (2.0.20),

$$\kappa \approx \frac{\omega^2}{g\left(1 + \frac{D\lambda^2}{\rho_2 g} - \frac{\omega^2}{\omega_0^2}\right)}. \tag{5.0.8}$$

Since $\kappa = \sqrt{\lambda}$ and from the definition of ω_0, the above approximation becomes

$$\kappa g \approx \frac{\omega^2}{1 + \frac{D\kappa^4}{\rho_2 g} - \frac{m\omega^2}{\rho_2 g}}. \tag{5.0.9}$$

We know that $m = \rho_{ice} h$, and let $\rho = \rho_2$. From the above approximation,

$$\frac{D}{\rho g - \rho_{ice} h \omega^2} \kappa^5 + \kappa \approx \frac{\omega^2}{g - \dfrac{\rho_{ice} h \omega^2}{\rho}}. \tag{5.0.10}$$

If $D = 0$, we have a particular case of the thick ice model (see Chapter 6), and we obtain the dispersion relation (equation (3)) presented in [9].

For open water (ice-free), $m = 0$ and $D = 0$. From definition (2.0.20),

$$\omega^2 = g\tau(\omega, \lambda). \tag{5.0.11}$$

From equation (5.0.1) and the fact that $\kappa = \sqrt{\lambda}$, we obtain

$$\tau(\omega, \lambda) = \kappa \tanh(\kappa d). \tag{5.0.12}$$

Substituting equation (5.0.12) in equation (5.0.11), we obtain

$$\omega^2 = g\kappa \tanh(\kappa d), \tag{5.0.13}$$

which is the open water dispersion relation (equation (1)) presented in [9].

When $d >> 1$, $\tanh(\kappa d) \to 1$. From the above equation,

$$\kappa = \frac{\omega^2}{g}, \tag{5.0.14}$$

which is the dispersion relation for the open water wavenumber (equation (2)) presented in [9].

Now, we consider the first equation in (3.1.7). From Remark 3.1.2, there are infinitely many positive solutions to this equation. Therefore, we can find an asymptotic representation for

the solutions ξ_n as $n \to \infty$. We rewrite the first equation in (3.1.7) as

$$\tan\xi = -\frac{\beta(\omega)d}{\xi + \xi^5 P(\omega) - 2P(\omega)\dfrac{\omega^2 d^2}{c^2}\xi^3 + P(\omega)\dfrac{\omega^4 d^4}{c^4}\xi}. \tag{5.0.15}$$

$$\implies \quad \left[\xi + \xi^5 P(\omega) - 2P(\omega)\frac{\omega^2 d^2}{c^2}\xi^3 + P(\omega)\frac{\omega^4 d^4}{c^4}\xi\right]\sin\xi + \beta(\omega)d\cos\xi = 0. \tag{5.0.16}$$

Since $\left[\xi + \xi^5 P(\omega) - 2P(\omega)\dfrac{\omega^2 d^2}{c^2}\xi^3 + P(\omega)\dfrac{\omega^4 d^4}{c^4}\xi\right]\sin\xi + \beta(\omega)d\cos\xi$ is entire and has infinitely many zeros, the only point of accumulation is ∞. Since the right side of equation (5.0.15) approaches 0 when $\xi \to \infty$,

$$\tan\xi \approx 0 \implies \xi_n \approx \pi n + \varepsilon_n, \tag{5.0.17}$$

where $\varepsilon_n \to 0$ as $n \to \infty$.

From equation (5.0.15),

$$\tan(\pi n + \varepsilon_n) = -\frac{\beta(\omega)d}{\pi n + \varepsilon_n + (\pi n + \varepsilon_n)^5 P(\omega) - 2P(\omega)\dfrac{\omega^2 d^2}{c^2}(\pi n + \varepsilon_n)^3 + (\pi n + \varepsilon_n)P(\omega)\dfrac{\omega^4 d^4}{c^4}}.$$

Since $\tan(\pi n + \varepsilon_n) = \tan\varepsilon_n$, we obtain

$$\tan\varepsilon_n = -\frac{\beta(\omega)d}{\pi n + \varepsilon_n + (\pi n + \varepsilon_n)^5 P(\omega) - 2P(\omega)\dfrac{\omega^2 d^2}{c^2}(\pi n + \varepsilon_n)^3 + (\pi n + \varepsilon_n)P(\omega)\dfrac{\omega^4 d^4}{c^4}}.$$

Since $\varepsilon_n \to 0$ as $n \to \infty$, we can express the above equation asymptotically as

$$\tan\varepsilon_n = -\frac{\beta(\omega)d}{\pi^5 n^5 P(\omega) - 2\pi^3 n^3 P(\omega)\dfrac{\omega^2 d^2}{c^2} + \pi n P(\omega)\dfrac{\omega^4 d^4}{c^4} + \pi n}.$$

Remark 5.0.4. When n is not large enough, we can ignore the terms containing $P(\omega)$ in the above equation since $P(\omega)$ is small enough.

Remark 5.0.5. From numerical results, the first root is far away from the first root in the case $P(\omega) \to 0$ (see Chapter 6) even though $P(\omega)$ is small enough.

For ε_n small enough, $\tan \varepsilon_n \approx \varepsilon_n$. From the above equation,

$$\varepsilon_n \approx -\frac{\beta(\omega)d}{\pi^5 n^5 P(\omega) - 2\pi^3 n^3 P(\omega)\dfrac{\omega^2 d^2}{c^2} + \pi n P(\omega)\dfrac{\omega^4 d^4}{c^4} + \pi n}. \tag{5.0.18}$$

Substituting approximation (5.0.18) in approximation (5.0.17), we obtain

$$\xi_n \approx \pi n - \frac{\beta(\omega)d}{\pi^5 n^5 P(\omega) - 2\pi^3 n^3 P(\omega)\dfrac{\omega^2 d^2}{c^2} + \pi n P(\omega)\dfrac{\omega^4 d^4}{c^4} + \pi n}. \tag{5.0.19}$$

From the above approximation,

$$\xi_n = \pi n + O\left(\frac{1}{n^5}\right).$$

Now, we will represent the formulas for the minimum and maximum of the dimensionless wavenumber $\hat{\kappa}(\omega)d$. Substituting approximation (5.0.19) in formulas (4.1.12), we obtain

$$\hat{\kappa}_+(\omega)d \approx \sqrt{\left(\frac{\omega d}{c_+}\right)^2 - \left(\pi n - \frac{\beta(\omega)d}{\pi^5 n^5 P(\omega) - 2\pi^3 n^3 P(\omega)\dfrac{\omega^2 d^2}{c^2} + \pi n P(\omega)\dfrac{\omega^4 d^4}{c^4} + \pi n}\right)^2};$$

$$\hat{\kappa}_-(\omega)d \approx \sqrt{\left(\frac{\omega d}{c_-}\right)^2 - \left(\pi n - \frac{\beta(\omega)d}{\pi^5 n^5 P(\omega) - 2\pi^3 n^3 P(\omega)\dfrac{\omega^2 d^2}{c^2} + \pi n P(\omega)\dfrac{\omega^4 d^4}{c^4} + \pi n}\right)^2}. \tag{5.0.20}$$

Remark 5.0.6. In formulas (5.0.20), we note that the corresponding waves propagate only for moderate values of n, i.e., when n is not large enough.

We now consider the second equation in (3.1.7). From Remark 3.1.3, this equation has a unique positive solution for a given value of ω. Therefore, there is no asymptotic representation for η. Hence, the formulas for the minimum and maximum of the dimensionless wavenumber $\tilde{\kappa}(\omega)d$ are represented by (4.2.15).

CHAPTER 6

Pack Ice Model - Special Case

This chapter discusses a special case of the thick ice model. The assumptions about the ocean are the same as in Chapter 2. If we consider boundary condition (2.0.12) and take the limit $D \to 0$, then we obtain a new boundary condition as derived in [10] using Newton's second law

$$mw_{tt} + \rho_2 gw + \rho_2 \Phi_t = 0. \tag{6.0.1}$$

Hence, the Sturm-Liouville problem from Chapter 2 now becomes

$$\psi'' + \left(\frac{\omega^2}{c^2(x)} - \lambda \right) \psi = 0, \;\; 0 < x < d, \tag{6.0.2}$$

$$\psi'(0) = 0, \tag{6.0.3}$$

$$-m\omega^2 v + \rho_2 g v - i\omega\rho_2 \psi(d) = 0, \tag{6.0.4}$$

$$-i\omega v = \psi'(d). \tag{6.0.5}$$

Eliminating v from equations (6.0.4) and (6.0.5) yields a new boundary condition

$$\psi'(d) = \frac{\omega^2}{g\left(1 - \dfrac{\omega^2}{{\omega_0}^2}\right)}\psi(d), \text{ where } \omega_0^2 := \frac{\rho_2 g}{m}. \tag{6.0.6}$$

From Remark 2.0.4, $\omega < \omega_0$ in the pack ice model.

Using the definition of $\beta(\omega)$ from (2.0.22), the above equation can be written as

$$\psi'(d) = \beta(\omega)\psi(d). \tag{6.0.7}$$

The physical meaning of the function $\beta(\omega)$ will be presented in Section 6.3. The following section will discuss the qualitative results of both cases: the homogeneous and non-homogeneous ocean.

6.1 Qualitative Results

We start our analysis of the Sturm-Liouville problem with the case of a homogeneous ocean, i.e., $c(x) = c$. The solution of equation (6.0.2) subject to boundary condition (6.0.3) is given by (3.1.1), and boundary condition (6.0.7) leads to the transcendental equations

$$\begin{aligned} &\sqrt{\frac{\omega^2}{c^2} - \lambda}\tan\sqrt{\frac{\omega^2}{c^2} - \lambda}d + \beta(\omega) = 0 \quad \text{if} \quad \frac{\omega^2}{c^2} > \lambda; \\ &-\sqrt{\lambda - \frac{\omega^2}{c^2}}\tanh\sqrt{\lambda - \frac{\omega^2}{c^2}}d + \beta(\omega) = 0 \quad \text{if} \quad \frac{\omega^2}{c^2} < \lambda. \end{aligned} \tag{6.1.1}$$

Using the dimensionless variables ξ and η as defined in (3.1.4), the above equations can be expressed as

$$\begin{aligned} \tan\xi + \frac{\beta(\omega)d}{\xi} &= 0; \\ \tanh\eta &= \frac{\beta(\omega)d}{\eta}. \end{aligned} \tag{6.1.2}$$

Remark 6.1.1. Elementary calculus considerations show that the first equation has infinitely many positive solutions, though the second one has a unique positive solution.

If the ocean surface is ice-free, the above transcendental equations have the form (3.1.10). Using $\xi_0(\omega)$ and $\eta_0(\omega)$ from Definition 3.1.4, the eigenvalue λ is represented by equations in (3.1.11).

In the following proposition, we start by proving some analytic properties of $\xi_0(\omega)$ and $\eta_0(\omega)$.

Proposition 6.1.1. *The following analytic properties of $\xi_0(\omega)$ and $\eta_0(\omega)$ hold.*

(a) $\xi_0(\omega)$ and $\eta_0(\omega)$ are smooth functions.

(b) $\dfrac{d\xi_0}{d\omega} < 0$ *and* $\dfrac{d\eta_0}{d\omega} > 0$.

(c) $\lim\limits_{\omega\to 0} \xi_0(\omega) = \pi, \ \lim\limits_{\omega\to\omega_0} \xi_0(\omega) = \dfrac{\pi}{2}$.

(d) $\lim\limits_{\omega\to 0} \eta_0(\omega) = 0; \ \eta_0(\omega) = O(\omega)$ for $\omega \to 0$.

(e) $\lim\limits_{\omega\to\omega_0} \eta_0(\omega) = \infty, \ \lim\limits_{\omega\to\omega_0} \dfrac{\eta_0(\omega)}{\beta(\omega)d} = 1$.

(f) The cut-off frequency ω_* exists and is unique if we have the condition

$$\omega_0 > \frac{\pi c}{2d}. \tag{6.1.3}$$

Proof. (a) follows from the implicit function theorem. To prove (b), we use the first transcendental equation in (6.1.2). Differentiating this equation with respect to ω, we obtain

$$\frac{d\xi_0}{d\omega} = \frac{\beta'(\omega)d}{-\tan\xi_0 - \xi_0\sec^2\xi_0} = \frac{2\beta'(\omega)d\cos^2\xi_0}{-\sin 2\xi_0 - 2\xi_0} < 0, \tag{6.1.4}$$

since $\beta'(\omega) > 0$. Now, we consider the second transcendental equation in (6.1.2). Differentiating this equation with respect to ω, we obtain

$$\frac{d\eta_0}{d\omega} = \frac{2\beta'(\omega)d\cosh^2\eta_0}{\sinh 2\eta_0 + 2\eta_0} > 0. \tag{6.1.5}$$

(c) - (e) are trivial. For (f), consider the first equation in (3.1.11). Let the frequency ω_* be a solution to the equation $\xi_0(\omega) = \dfrac{\omega d}{c}$. Now, the existence and uniqueness of ω_* follow from (b) and (c). Since $\lim\limits_{\omega\to\omega_0}\xi_0(\omega) < \dfrac{\omega_0 d}{c}$ and $\lim\limits_{\omega\to\omega_0}\xi_0(\omega) = \dfrac{\pi}{2}$ from (c), we obtain inequality (6.1.3). ■

Remark 6.1.2. When $D = 0$, we note that the statements of Proposition 3.2.1(b) - (f) are reduced to Proposition 6.1.1(b) - (e).

Remark 6.1.3. The existence and uniqueness of the cut-off frequencies ω_* for the higher eigenvalues $\hat{\lambda}_n$ takes place if we have the condition

$$\omega_0 > \frac{\pi c}{2d}(2n-1),\ n \geq 2. \tag{6.1.6}$$

Remark 6.1.4. The number of propagating waves is finite, and these propagating waves exist for $n \geq 2$ for a given value of ω.

Remark 6.1.5. From Proposition 6.1.1(b), $\xi_0(\omega)$ and $\eta_0(\omega)$ are monotonic with respect to ω, and there is no critical point in the pack ice model.

The next proposition will discuss the change in eigenvalues $\hat{\lambda}(\omega, c)$ and $\tilde{\lambda}(\omega, c)$.

Proposition 6.1.2. *If we fix c and consider ω-dependence, then*

(a) $\dfrac{d\hat{\lambda}(\omega)}{d\omega} > 0.$

(b) $\dfrac{d\tilde{\lambda}(\omega)}{d\omega} > 0.$

Proof. Consider the equations in (3.1.11). Then from Proposition 6.1.1(a), $\hat{\lambda}(\omega)$ and $\tilde{\lambda}(\omega)$ are smooth functions. Taking derivative of the equations in (3.1.11), we obtain

$$\frac{d\hat{\lambda}}{d\omega} = \frac{2\omega}{c^2} - \frac{2\xi_0}{d^2}\frac{d\xi_0}{d\omega}; \qquad \frac{d\tilde{\lambda}}{d\omega} = \frac{2\omega}{c^2} + \frac{2\eta_0}{d^2}\frac{d\eta_0}{d\omega}.$$

Since $\dfrac{d\xi_0}{d\omega} < 0$ and $\dfrac{d\eta_0}{d\omega} > 0$ from Proposition 6.1.1(b), the results of (a) and (b) follow. ■

Remark 6.1.6. From Proposition 6.1.2, the eigenvalues $\hat{\lambda}(\omega,c)$ and $\tilde{\lambda}(\omega,c)$ are monotonic with respect to ω. Hence, the wavenumbers are strictly increasing with respect to ω. This result will be verified numerically in Section 6.2 for variable $c(x)$. From propositions 3.2.2 and 6.1.2, we conclude that the wavenumbers are strictly increasing with respect to ω in both thick ice and pack ice models.

Remark 6.1.7. From Proposition 6.1.1, we can find the lower and upper bounds of the eigenvalues $\hat{\lambda}(\omega,c)$ and $\tilde{\lambda}(\omega,c)$. From equations in (3.1.11), we have the following results about $\hat{\lambda}(\omega,c)$ and $\tilde{\lambda}(\omega,c)$. $\hat{\lambda}(\omega,c) \to -\dfrac{\pi^2}{d^2}$ when $\omega \to 0$ and $\dfrac{\omega_0^2}{c^2} - \dfrac{\pi^2}{4d^2}$ when $\omega \to \omega_0$. On the other hand, $\tilde{\lambda}(\omega,c) \to 0$ when $\omega \to 0$ and ∞ when $\omega \to \omega_0$.

We now compare ξ_0 and η_0 for the ocean model with the free surface and the surface covered by pack ice.

Proposition 6.1.3. *Let* $\omega < \omega_0$. *Then* $\xi_0 < \xi_0^f$ *and* $\eta_0 > \eta_0^f$.

Proof. We may write the transcendental equations (6.1.2) and (3.1.10) in the form

$$\begin{gathered}\xi_0 \tan \xi_0 + A = 0,\ \eta_0 \tanh \eta_0 = A \ \text{ and} \\ \xi_0^f \tan \xi_0^f + A^f = 0,\ \eta_0^f \tanh \eta_0^f = A^f, \\ \text{where } A = \frac{\omega^2 d}{g\left(1 - \dfrac{\omega^2}{\omega_0^2}\right)} \text{ and } A^f = \frac{\omega^2 d}{g}.\end{gathered} \tag{6.1.7}$$

We observe that $A^f < A$. We further differentiate two first equations in (6.1.7) with respect to the parameter A

$$\frac{d\xi_0}{dA}\left(\tan \xi_0 + \xi_0 \sec^2 \xi_0\right) + 1 = 0, \quad \frac{d\eta_0}{dA}\left(\tanh \eta_0 + \eta_0 \operatorname{sech}^2 \eta_0\right) = 1.$$

$$\implies \quad \frac{d\xi_0}{dA} = -\frac{1}{\tan \xi_0 + \xi_0 \sec^2 \xi_0} = -\frac{2\cos^2 \xi_0}{\sin 2\xi_0 + 2\xi_0} < 0,$$

$$\frac{d\eta_0}{dA} = \frac{1}{\tanh \eta_0 + \eta_0 \operatorname{sech}^2 \eta_0} = \frac{2\cosh^2 \eta_0}{\sinh 2\eta_0 + 2\eta_0} > 0.$$

Hence, ξ_0 decreases with respect to A. Since $A^f < A$, $\xi_0 < \xi_0^f$. Moreover, η_0 increases with respect to A. Since $A^f < A$, $\eta_0 > \eta_0^f$. ■

We conclude that the presence of pack ice instead of the free surface results in the decrease of ξ_0 and the increase of η_0 with respect to ω. According to the equations in (3.1.11), both $\hat{\lambda}$ and $\tilde{\lambda}$ increase with respect to ω in the presence of pack ice. From propositions 3.2.3 and 6.1.3, we conclude that as the thick ice model is reduced to pack ice, the result for ξ_0 and hence for $\hat{\lambda}$ remains the same for $\omega < \omega_0$ but the result for η_0 and hence for $\tilde{\lambda}$ becomes opposite.

If we fix ω and consider T-dependence of $\xi_0(\omega,T)$ and $\eta_0(\omega,T)$, where T is the air temperature 1 to 2 m above the ice cover surface in the case of ATDD, we only have the results for the case $T > \Omega$ in Proposition 3.3.1(a) and (b) since $\omega < \omega_0$ in the case of pack ice.

In the non-homogeneous case, the results of Proposition 3.4.1 also hold for the pack ice model. As proved in [14] and stated in Section 3.4, we would have inequalities (3.4.1) and (3.4.2) for $\hat{\lambda}_1$ and $\tilde{\lambda}$, respectively. Same as in Section 3.4, a propagating mode associated with $\hat{\lambda}_1(\omega, c(x))$ exists if $\hat{\lambda}_1(\omega, c_+) > 0$, which means $F(\omega) > 0$, where $F(\omega)$ is defined in (3.4.3) and $\xi_0(\omega)$ is the first positive solution in the pack ice model. Consider the derivative of $F(\omega)$ in equation (3.4.4). Since $\dfrac{d\xi_0(\omega)}{d\omega} < 0$ from Proposition 6.1.1(b), $\dfrac{dF}{d\omega} > 1$. This inequality was verified with the help of numerical results.

The following section will provide the numerical observations of the dimensionless wavenumbers.

6.2 Numerical Results

Similar to the case of the thick ice model in Chapter 4, we consider a non-homogeneous waveguide in this section and develop a numerical algorithm to study the Sturm-Liouville problem (6.0.2), (6.0.3), and (6.0.7). We begin with the analysis of $\hat{\lambda}_1$.

6.2.1 Analysis of $\hat{\lambda}_1$

The implementation of the algorithm is the same as in Section 4.1. Therefore, from boundary condition (6.0.7),

$$a_n\gamma_n\cos(\gamma_n\Delta x) - b_n\gamma_n\sin(\gamma_n\Delta x) - \beta(\omega)(a_n\sin(\gamma_n\Delta x) + b_n\cos(\gamma_n\Delta x)) = 0. \tag{6.2.1}$$

Using the continuity and differentiability of $\psi(x)$ and the dimensionless representation (4.1.5) as in Section 4.1, equation (6.2.1) becomes

$$a_n(\alpha_n - \beta(\omega)\Delta x \tan\alpha_n) = b_n(\alpha_n \tan\alpha_n + \beta(\omega)\Delta x). \tag{6.2.2}$$

Using the same procedure as in Section 4.1, we obtain equation (4.1.11) for the dimensionless wavenumber $\hat{\kappa}(\omega)d$ and equations (4.1.12) for the lower and upper bounds of $\hat{\kappa}(\omega)d$.

6.2.2 Analysis of $\tilde{\lambda}$

We now consider the analysis of the eigenvalue associated with the leading mode $\tilde{\lambda}$. From boundary condition (6.0.7),

$$a_n\Gamma_n\cosh(\Gamma_n\Delta x) + b_n\Gamma_n\sinh(\Gamma_n\Delta x) - \beta(\omega)(a_n\sinh(\Gamma_n\Delta x) + b_n\cosh(\Gamma_n\Delta x)) = 0. \tag{6.2.3}$$

Using the dimensionless representation (4.2.4) and transfer matrices (4.2.5), we obtain the system of equations

$$\begin{gathered}\left(\frac{\zeta_k}{\Delta x}\right)^2 + \left(\frac{\omega}{c_k}\right)^2 = \left(\frac{\zeta_j}{\Delta x}\right)^2 + \left(\frac{\omega}{c_j}\right)^2, \\ \text{for all } \; k, j = 1, ..., n, \; \text{ but } \; k < j; \\ A_n(\zeta_1, \ldots, \zeta_n)(\zeta_n\cosh\zeta_n - \beta(\omega)\Delta x\sinh\zeta_n) \\ = B_n(\zeta_1, \ldots, \zeta_n)(-\zeta_n\sinh\zeta_n + \beta(\omega)\Delta x\cosh\zeta_n.\end{gathered} \tag{6.2.4}$$

Using the same procedure as in Section 4.2, the last of the equations (6.2.4) becomes

$$\begin{aligned}{A_n}^0(\zeta_1, \ldots, \zeta_n)\left(\zeta_n\left(1 + e^{-2\zeta_n}\right) - \beta(\omega)\Delta x\left(1 - e^{-2\zeta_n}\right)\right) = {B_n}^0(\zeta_1, \ldots, \zeta_n)\big(-\zeta_n\left(1 - e^{-2\zeta_n}\right) + \\ \beta(\omega)\Delta x\left(1 + e^{-2\zeta_n}\right)\big)\end{aligned} \tag{6.2.5}$$

Using the same procedure as in Section 4.2, we obtain equation (4.2.14) for the dimensionless wavenumber $\tilde{\kappa}(\omega)d$ and equations (4.2.15) for the lower and upper bounds of $\tilde{\kappa}(\omega)d$.

6.2.3 Computational Results

The implementation of the algorithms was the same as in Chapter 4, and 'fmincon' and 'fsolve' solvers were used to solve the transcendental equations (6.2.2) and (6.2.5), respectively. We observed that when $n = 15$, the values of $\hat{\kappa}(\omega)d$ and $\tilde{\kappa}(\omega)d$ stopped changing for all ω values that we considered. Like the results of the thick ice model, we observed that the α_n values were very close to the initial approximation ξ_0/n and the ζ_n values obtained were very close to the initial approximation $\eta_0/n \approx \beta d/n$ over a range of ω values.

The speed profiles (4.3.1) were used, and we observed that the convergence speed is about the same for all speed profiles $c(x)$, except the convergence is a little faster when $c(x)$ is constant.

We demonstrate the numerical results for the following set of parameters:

$$\omega_0 = 20\,Hz;\;\; d = 500\,m;\;\; c_- = 1350\,m/s;\;\; c_+ = 1650\,m/s \tag{6.2.6}$$

We now present the algorithm that allows evaluating the dimensionless wavenumbers $\hat{\kappa}(\omega)d$ and $\hat{\kappa}_{\pm}(\omega)d$ for the speed profiles (4.3.1).

We further present the algorithm that allows evaluating the dimensionless wavenumbers $\tilde{\kappa}(\omega)d$ and $\tilde{\kappa}_{\pm}(\omega)d$ for the speed profiles (4.3.1).

6.2.4 Observations

The graphs from figures 6.1 and 6.2 demonstrate the numerical results. These figures show the dimensionless wavenumbers $\hat{\kappa}(\omega)d$ and $\tilde{\kappa}(\omega)d$ as functions of frequency ω for different speed profiles $c(x)$. From the numerical results, we observe that $\hat{\kappa}(\omega)d$ is either close to $\hat{\kappa}_+(\omega)d$ or $\hat{\kappa}_-(\omega)d$ or is in the middle of these bounds for different speed profiles $c(x)$ but no change in $\tilde{\kappa}(\omega)d$

Algorithm 3 The steps of the numerical algorithm for $\hat{\kappa}(\omega)$

Input: n, ω_0, d, c_-, c_+
Initialize: a discrete function $c(x) = (c_1, c_2, \ldots, c_n)$
for $\omega \in (0, \omega_0)$ **do**
    Evaluate $\beta(\omega)$ according to definition (2.0.22).
    Solve equation (6.1.2) for ξ_0 on $[\pi/2, \pi]$.
    Solve $F(\omega) := \omega - \dfrac{\xi_0 c_+}{d} = 0$.
    if $F(\omega) > 0$ **then**
        Set initial approximation $\alpha_n = \xi_0/n$.
        Calculate $\hat{\kappa}_+(\omega)d$ and $\hat{\kappa}_-(\omega)d$ according to formulas (4.1.12).
        for $i = 1$ to n **do**
            $w_i = \sqrt{\left(\dfrac{\omega d}{c_i}\right)^2 + n^2\alpha_n^2 - \left(\dfrac{\omega d}{c_n}\right)^2}$.
        end for
        for $j = 2$ to n **do**
            Find the 2×2 matrix u_j where
            $u_j(1,1) = \dfrac{w_{j-1}}{w_j}\cos\left(\dfrac{w_{j-1}}{n}\right)$, $u_j(1,2) = -\dfrac{w_{j-1}}{w_j}\sin\left(\dfrac{w_{j-1}}{n}\right)$,
            $u_j(2,1) = \sin\left(\dfrac{w_{j-1}}{n}\right)$ and $u_j(2,2) = \cos\left(\dfrac{w_{j-1}}{n}\right)$.
            $u(k,l)$ represents the element of matrix V in the k^{th} row and l^{th} column.
        end for
        Find the product of the matrices $V = \prod_{j=n}^{2} [u_j]$.
        Solve the transcendental equation for α_n
        $v(1,2)(n\alpha_n - \beta(\omega)d\tan(\alpha_n)) - v(2,2)(n\alpha_n\tan(\alpha_n) + \beta(\omega)d) = 0$,
        $v(k,l)$ represents the element of matrix V in the k^{th} row and l^{th} column.
        Calculate $\hat{\kappa}(\omega)d = \sqrt{\left(\dfrac{\omega d}{c_n}\right)^2 - n^2\alpha_n^2}$.
    end if
end for
Output: $\hat{\kappa}_+(\omega)d, \hat{\kappa}_-(\omega)d$ and $\hat{\kappa}(\omega)d$

was observed for the given speed profiles $c(x)$. Moreover, in all speed profiles $c(x)$, $\hat{\kappa}(\omega)d$ gets close to $\hat{\kappa}_-(\omega)d$ for small values of ω. For every speed profile $c(x)$, the wavenumbers $\hat{\kappa}(\omega)d$ and $\tilde{\kappa}(\omega)d$ are strictly increasing with respect to ω. The numerical results are in complete agreement with the analytical results. Furthermore, we observed that the Perturbation Theory, though formally applicable, does not work for reasonable values of Young's Modulus E and ice thickness h for $\tilde{\kappa}(\omega)d$, i.e., for reasonable values of E and h for ice, the values of $\tilde{\kappa}(\omega)d$ obtained from thick ice in Chapter 4 are far away from the ones obtained from pack ice.

Algorithm 4 The steps of the numerical algorithm for $\tilde{\kappa}(\omega)$

Input: n, ω_0, d, c_-, c_+
Initialize: a discrete function $c(x) = (c_1, c_2, \ldots, c_n)$
for $\omega \in (0, \omega_0)$ **do**
    Evaluate $\beta(\omega)$ according to definition (2.0.22).
    Solve equation (6.1.2) for $\eta_0 > 0$.
    Set initial approximation $\zeta_n = \eta_0/n$.
    Calculate $\tilde{\kappa}_+(\omega)d$ and $\tilde{\kappa}_-(\omega)d$ according to formulas (4.2.15).
    for $i = 1$ to n **do**
        $w_i = \sqrt{\left(\frac{\omega d}{c_n}\right)^2 + n^2\zeta_n^2 - \left(\frac{\omega d}{c_i}\right)^2}$.
    end for
    for $j = 1$ to $n-1$ **do**
        Let $\zeta_j = \frac{w_j}{n}$.
    end for
    for $j = 2$ to n **do**
        Find the 2×2 matrix u_j where
        $u_j(1,1) = \frac{w_{j-1}}{w_j}\left(\frac{1+e^{-2\zeta_{j-1}}}{2}\right)$, $u_j(1,2) = -\frac{w_{j-1}}{w_j}\left(\frac{1-e^{-2\zeta_{j-1}}}{2}\right)$,
        $u_j(2,1) = \left(\frac{1+e^{-2\zeta_{j-1}}}{2}\right)$ and $u_j(2,2) = \left(\frac{1-e^{-2\zeta_{j-1}}}{2}\right)$.
        $u(k,l)$ represents the element of matrix V in the k^{th} row and l^{th} column.
    end for
    Find the product of the matrices $V = \prod_{j=n}^{2} [u_j]$.
    Evaluate $\mathscr{E}(\zeta_n) = \frac{1-e^{-2\zeta_n}}{1+e^{2\zeta_n}}$, and solve the transcendental equation for ζ_n
    $v(1,2)(n\zeta_n - \beta(\omega)d\mathscr{E}(\zeta_n)) - v(2,2)(-n\zeta_n\mathscr{E}(\zeta_n) + \beta(\omega)d) = 0$,
    $v(k,l)$ represents the element of matrix V in the k^{th} row and l^{th} column.
    Calculate $\tilde{\kappa}(\omega)d = \sqrt{\left(\frac{\omega d}{c_n}\right)^2 + n^2\zeta_n^2}$.
end for
Output: $\tilde{\kappa}_+(\omega)d, \tilde{\kappa}_-(\omega)d$ and $\tilde{\kappa}(\omega)d$

The following section will discuss the asymptotic nature of the dimensionless wavenumbers $\hat{\kappa}(\omega)d$ and $\tilde{\kappa}(\omega)d$.

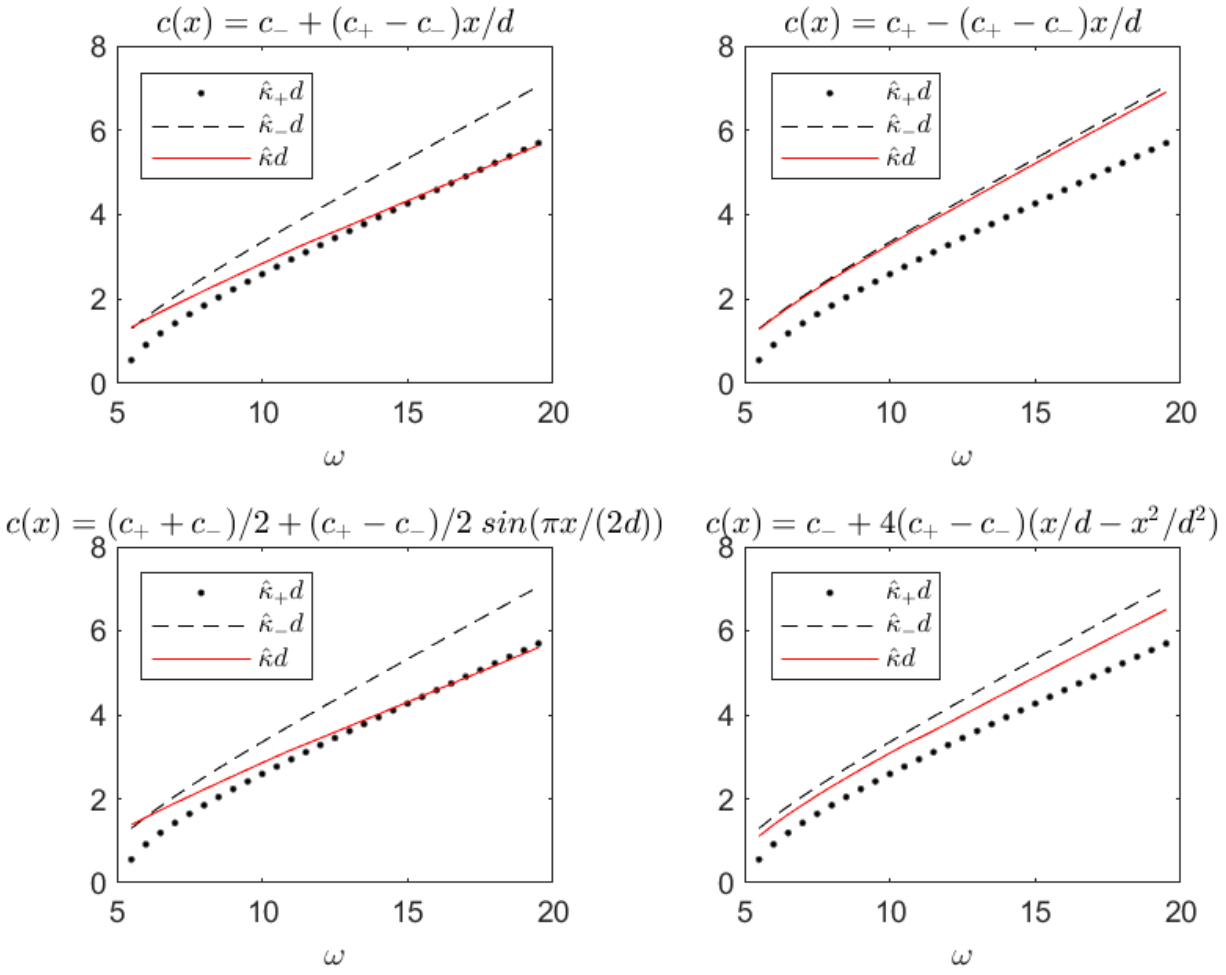

Figure 6.1 Frequency dependence of the dimensionless wavenumber $\hat{\kappa}d$ for different speed profiles

6.3 Asymptotic Considerations

We begin with the function $\beta(\omega)$. If $c(x) >> 1$, then the solution of equation (6.0.2) subject to boundary condition (6.0.3) is $\psi(x) = \cosh(\sqrt{\lambda}x)$. Then from boundary condition (6.0.7),

$$\sqrt{\lambda}\tanh(\sqrt{\lambda}d) = \beta(\omega). \tag{6.3.1}$$

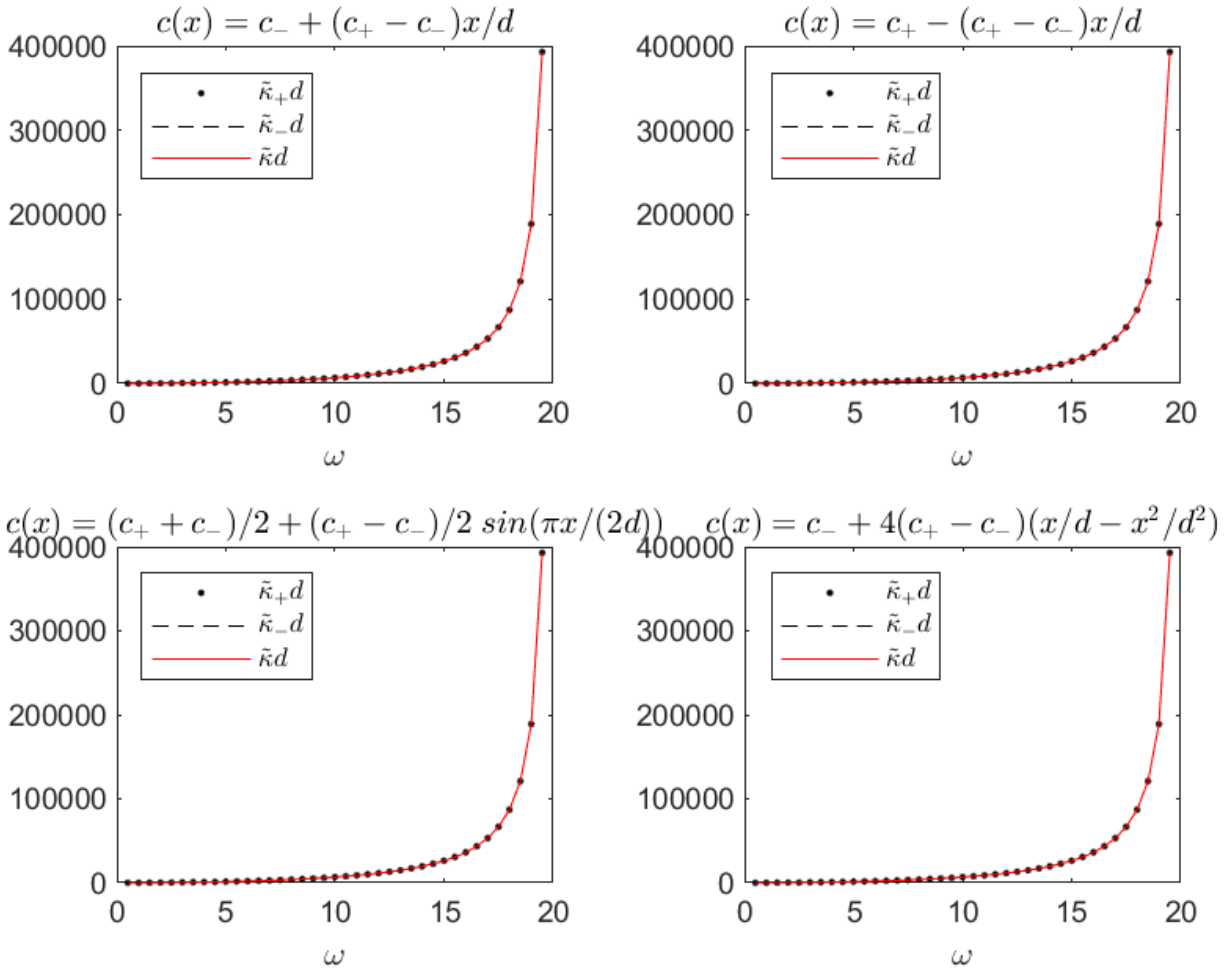

Figure 6.2 Frequency dependence of the dimensionless wavenumber $\tilde{\kappa}d$ for different speed profiles

If, in addition, the ocean is deep, i.e., $d >> 1$, we have $\tanh(\sqrt{\lambda}d) \to 1$. Therefore, the above equation can be approximately represented in the dimensionless form

$$\sqrt{\lambda}d \approx \beta(\omega)d. \tag{6.3.2}$$

Since $\kappa = \sqrt{\lambda}$, the function $\beta(\omega)$ approximately represents the wavenumber.

Remark 6.3.1. The approximate equation (6.3.1) makes sense if $\beta(\omega) > 0$, which is true since we considered $\omega < \omega_0$ for the propagating modes.

Remark 6.3.2. Based on the numerical results, if the frequency ω is not very small, the dimensionless quantity $\beta(\omega)d$ is large, i.e., $\beta(\omega)d >> 1$. Hence, boundary condition (6.0.7) asymptotically becomes $\psi(d) = 0$, which means that the ocean has no ice cover.

From the first equation in (6.1.2),

$$\xi_0 \tan \xi_0 = -\beta(\omega)d.$$

If $\beta(\omega)d >> 1$,

$$\xi_0 \approx \frac{\pi}{2}.$$

Now, the bounds in (3.4.1) can be expressed as

$$\hat{\lambda}_1(\omega, c_+) \approx \frac{\omega^2}{c_+^2} - \frac{\pi^2}{4d^2}, \quad \hat{\lambda}_1(\omega, c_-) \approx \frac{\omega^2}{c_-^2} - \frac{\pi^2}{4d^2}. \tag{6.3.3}$$

Since $\hat{\kappa}d = \sqrt{\hat{\lambda}_1}d$, we obtain

$$\hat{\kappa}_+ d \approx \sqrt{\frac{\omega^2 d^2}{c_+^2} - \frac{\pi^2}{4}}, \quad \hat{\kappa}_- d \approx \sqrt{\frac{\omega^2 d^2}{c_-^2} - \frac{\pi^2}{4}}. \tag{6.3.4}$$

The curves described by the above approximations are very close to the curves in Figure 6.1.

Remark 6.3.3. For the thick ice model, the approximations of $\hat{\kappa}_+ d$ and $\hat{\kappa}_- d$ are given by (5.0.4), which are different from the approximations in (6.3.4). Since the approximations of $\hat{\kappa}_+ d$ and $\hat{\kappa}_- d$ are different in the thick ice and pack ice models, these approximations depend on the type of ice cover.

From the second equation in (6.1.2),

$$\eta_0 \tanh \eta_0 = \beta(\omega) d.$$

If $\beta(\omega)d >> 1$,

$$\eta_0 \approx \beta(\omega) d.$$

Now, the bounds in (3.4.2) can be expressed as

$$\tilde{\lambda}(\omega, c_+) \approx \frac{\omega^2}{c_+^2} + \beta^2(\omega), \qquad \tilde{\lambda}(\omega, c_-) \approx \frac{\omega^2}{c_-^2} + \beta^2(\omega). \tag{6.3.5}$$

Since $\tilde{\kappa} d = \sqrt{\tilde{\lambda}} d$, we obtain

$$\tilde{\kappa}_+ d \approx \sqrt{\frac{\omega^2 d^2}{c_+^2} + \beta^2(\omega) d^2}, \qquad \tilde{\kappa}_- d \approx \sqrt{\frac{\omega^2 d^2}{c_-^2} + \beta^2(\omega) d^2}. \tag{6.3.6}$$

The curves described by the above approximations are very close to the curves in Figure 6.2.

If the parameters of the model satisfy the condition $\beta(\omega)d >> \dfrac{\omega d}{c_\pm}$, then

$$\tilde{\kappa} d \approx \beta(\omega) d, \tag{6.3.7}$$

which is similar to approximation (6.3.2). From the above approximation, we conclude that the wavenumber is almost independent of the speed profile $c(x)$, and this independence was observed in Figure 6.2. Comparing approximations (6.3.4) and (6.3.7), we obtain

$$\tilde{\kappa} d >> \hat{\kappa} d, \tag{6.3.8}$$

which is verified by comparing figures 6.1 and 6.2.

For deep ocean, $d >> 1$, and $c(x) >> 1$, $\beta(\omega) \approx \kappa$. Therefore, from definition (2.0.22), definition of ω_0 in (2.0.19), the fact that $m = \rho_{ice}h$, and by defining $\rho = \rho_2$, we obtain

$$\kappa \approx \frac{\omega^2}{g - \dfrac{\rho_{ice}h\omega^2}{\rho}}, \tag{6.3.9}$$

which is the dispersion relation (equation (3)) presented in [9].

For open water (ice-free), $m = 0$, so equation (2.0.22) becomes

$$\omega^2 = g\beta(\omega). \tag{6.3.10}$$

From equation (6.3.1) and the fact that $\kappa = \sqrt{\lambda}$, we obtain

$$\beta(\omega) = \kappa \tanh(\kappa d). \tag{6.3.11}$$

Substituting equation (6.3.11) in equation (6.3.10), we obtain the dispersion relation (5.0.13). When $d >> 1$, we obtain the dispersion relation (5.0.14).

Now, we consider the first transcendental equation in (6.1.2). From Remark 6.1.1, we can find an asymptotic representation for the solutions ξ_n of this equation as $n \to \infty$. We rewrite the first equation in (6.1.2) as

$$\tan\xi = -\frac{\beta(\omega)d}{\xi}. \tag{6.3.12}$$

$$\implies \quad \xi \sin\xi + \beta(\omega)d\cos\xi = 0. \tag{6.3.13}$$

Since $\xi \sin\xi + \beta(\omega)d\cos\xi$ is entire and has infinitely many zeros, the only point of accumulation is ∞. Since the right side of equation (6.3.12) approaches 0 when $\xi \to \infty$,

$$\tan\xi \approx 0 \implies \xi_n \approx \pi n + \varepsilon_n, \tag{6.3.14}$$

where $\varepsilon_n \to 0$ as $n \to \infty$.

From equation (6.3.12),

$$\tan(\pi n + \varepsilon_n) = -\frac{\beta(\omega)d}{\pi n + \varepsilon_n}.$$

Since $\tan(\pi n + \varepsilon_n) = \tan\varepsilon_n$, we obtain

$$\tan\varepsilon_n = -\frac{\beta(\omega)d}{\pi n + \varepsilon_n}.$$

Since $\varepsilon_n \to 0$ as $n \to \infty$, we can express the above equation asymptotically as

$$\tan\varepsilon_n = -\frac{\beta(\omega)d}{\pi n}.$$

For ε_n small enough, $\tan\varepsilon_n \approx \varepsilon_n$. From the above equation,

$$\varepsilon_n \approx -\frac{\beta(\omega)d}{\pi n}. \tag{6.3.15}$$

Substituting approximation (6.3.15) in approximation (6.3.14), we obtain

$$\xi_n \approx \pi n - \frac{\beta(\omega)d}{\pi n}. \tag{6.3.16}$$

From the above approximation,

$$\xi_n = \pi n + O\left(\frac{1}{n}\right).$$

Now, we will represent the formulas for the minimum and maximum of the dimensionless wavenumber $\hat{\kappa}(\omega)d$. Substituting approximation (6.3.16) in formulas (4.1.12), we obtain

$$\begin{aligned} \hat{\kappa}_+(\omega)d &\approx \sqrt{\left(\frac{\omega d}{c_+}\right)^2 - \left(\pi n - \frac{\beta(\omega)d}{\pi n}\right)^2}; \\ \hat{\kappa}_-(\omega)d &\approx \sqrt{\left(\frac{\omega d}{c_-}\right)^2 - \left(\pi n - \frac{\beta(\omega)d}{\pi n}\right)^2}. \end{aligned} \tag{6.3.17}$$

Remark 6.3.4. In formulas (6.3.17), we note that the corresponding waves propagate only for moderate values of n, i.e., when n is not large enough.

We now consider the second transcendental equation in (6.1.2). From Remark 6.1.1, there is no asymptotic representation for η. Hence, the formulas for the minimum and maximum of the dimensionless wavenumber $\tilde{\kappa}(\omega)d$ are represented by equations in (4.2.15).

CHAPTER 7

Conclusion and Continuing Work

We consider some mathematical aspects of wave propagation in a layered ocean waveguide covered by two different types of ice, thick ice and pack ice. Specifically, we study the application of the Sturm-Liouville problem on acoustic wave propagation in a layered ocean covered by ice. With the help of the separation of variables method, the Sturm-Liouville problem appears at a cross-section of the waveguide. From the theory of the Sturm-Liouville problem, we study the properties of the first two eigenvalues (or the wavenumbers of the propagating modes). Assuming that only the upper and lower bounds of the propagation speed are known, we explicitly find the minimum and maximum values of the first two eigenvalues (or the wavenumbers of the first two modes). We prove that the first eigenvalue is always positive, thus corresponding to propagating mode, and find the cut-off frequency, for which the second eigenvalue is positive. In other words, the first mode transfers energy along the waveguide for all frequencies but the second one transfers energy only for the frequencies above the cut-off frequency.

A fast numerical algorithm is suggested based on the discretization of the speed profile. It represents a version of the formalism of layered media. We use this algorithm for the diverse speed profiles, and we also use it for different values of ice thickness and Young's Modulus. It confirms the analytical results for the first two eigenvalues. Based on the analytical results, it was predicted that the wavenumbers would be independent of the speed profiles and dependent on the ice thickness and Young's Modulus in the case of thick ice. From our observations, in the first algorithm, there is a dependence on the speed profiles but no dependence on the ice thickness and

Young's Modulus for reasonable intervals. In the second algorithm, there is a dependence on the speed profiles, ice thickness, and Young's Modulus.

In the case of pack ice, we used a similar algorithm but did not use the algorithm for different values of ice thickness. Also, the value of Young's Modulus of pack ice was taken as 0 since this is a particular case where the cylindrical rigidity approaches 0. The numerical results were in complete agreement with the analytical results. In the first algorithm, the dependence of the speed profiles on the wavenumber was expected from the numerical results of thick ice. However, in the second algorithm, the observation of no significant dependence on the speed profiles was not expected from the numerical results of thick ice. The numerical results of the first algorithm demonstrate that we can obtain the results of pack ice from thick ice for reasonable values of ice thickness and Young's Modulus, but the numerical results of the second algorithm demonstrate that we cannot obtain the results of pack ice from thick ice for reasonable values of ice thickness and Young's Modulus. In the second algorithm, the wavenumbers obtained from the model of thick ice are far away from the ones obtained from the model of pack ice model for reasonable values of ice thickness and Young's Modulus. Besides numerical results, we develop Asymptotic Analysis for both models, thick ice and pack ice, to find the approximate but explicit formulas for the extreme values of the first two eigenvalues. The results obtained from the pack ice model demonstrate that the pack ice model could be treated as the limiting case of the thick ice model.

We expect that the results of the change in eigenvalues with respect to air temperature will enable studying the influence of global warming on ice covers. With the help of the results from both thick ice and pack ice models, we can extend these results for future work. We can find the numerical results of the wavenumbers with the temperature change. Moreover, one could use the real-world datasets of the recorded air temperature values to estimate the future change in air temperature with the help of the time series and regression models in Machine Learning as done in Section 4.5. Once we have this change in air temperature for the future, we can find the behavior of the wavenumbers for those future temperature values. Besides extending the temperature de-

pendence results, it is possible to apply Spectral Theory and Real Analysis for the thick ice model as done in [14] for the pack ice model. As done in [9], we can find numerical results for normalized wavenumbers with the help of dispersion relations. Our physical model could be extended to higher dimensions by considering the third dimension of the ice cover and other factors that affect the ice thickness, like wind and change in water salinity and water temperature. In this extended model, the separation of variables method would not work. Therefore, we would have to use the finite element method (FEM) or some other rigorous method to find the analytical and numerical results. From the results of our model, we hope to apply the inverse problem methods so that the variation in wavenumbers would yield the values of ice thickness and Young's Modulus of ice to provide some information about the ice cover on the ocean surface in the presence of global warming.

REFERENCES

[1] L. M. Brekhovskikh, *Waves in layered media*, New York: Academic Press, (1980).

[2] V. A. Squire, J. P. Dugan, P. Wadhams, P. J. Rottier, and A. K. Liu, Of ocean waves and sea ice, *Annu. Rev. Fluid Mech*, **27** (1), (1995), 115–168.

[3] N. G. Kuznetsov, V. G. Maz'ia, and B. R. Vainberg, *Linear water waves: A mathematical approach*, New York: Cambridge University Press, (2002).

[4] J. Chu, Waves in the deep, *MIT News*, February 3, (2015).

[5] U. Kadri, Deep ocean water transport by acoustic-gravity waves, *JGR Oceans*, **119** (11), (2014), 7925–7930.

[6] U. Kadri, Wave motion in a heavy compressible fluid: Revisited, *European J. of Mechanics - B/Fluids*, **49** Part A, (2015), 50–57.

[7] O. A. Godin, Acoustic-gravity waves in atmospheric and oceanic waveguides, *The J. of the Acoustical Society of America*, **132** (2), (2012), 657–669.

[8] J. A. Smith, Revisiting oceanic acoustic gravity surface waves, *J. of Physical Oceanography*, **45** (12), (2015), 2593–2598.

[9] C. O. Collins III, W. E. Rogers, and B. Lund, An investigation into the dispersion of ocean surface waves in sea ice, *Ocean Dynamics*, **67**, (2017), 263–280.

[10] D. Ye. Kheisin, *Some non-stationary problems of dynamics of the ice cover*, In: Studies in Ice Physics and Ice Engineering (Ed. Iakolev), Israel Program for Scientific Translations, (1971).

[11] M. H. Meylan, L. G. Bennetts, J. E. M. Mosig, W. E. Rogers, M. J. Doble, and M. A. Peter, Dispersion relations, power laws, and energy loss for waves in the marginal ice zone, *J. of Geophysical Research: Oceans*, **123** (5), (2018), 3322–3335.

[12] B. P. Belinskiy, Wave propagation in the ice-covered ocean waveguide and operator polynomials, *Proceedings of the Second ISAAC Congress*, **2**, (2000), 1319–1333.

[13] B. P. Belinskiy, J. P. Dauer, and Y. Xu, Inverse scattering of acoustic waves in an ocean with ice cover, *Applicable Analysis*, **61** (3-4), (1996), 255–283.

[14] B. P. Belinskiy, D. B. Hinton, L. Weerasena, and M. M. Khan, On the Sturm-Liouville problem describing an ocean waveguide covered by pack ice, *Applicable Analysis*, **101** (5), (2021), 1659–1681.

[15] D. Ye. Kheisin, *Ice cover dynamics*, Leningrad: Hidrometeoizdat (in Russian), (1967).

[16] D. D. Reynolds, *Engineering principles of acoustics*, Boston: Allyn and Bacon Inc., (1981).

[17] R. Feynman, *Lectures on physics*, Volume 1, Addison: Addison Publishing Company, (1969).

[18] B. P. Belinskiy, Boundary value contact acoustic problems, *Applicable Analysis, The Special Issue for the AMS - Chattanooga*, **68** (1-2), (1998), 51–73.

[19] D. Mondal and S. Banerjea, Scattering of waterwaves by an inclined porous plate submerged in ocean with ice cover, *Q. J. Mech. Appl. Math*, **69** (2), (2016), 195–213.

[20] A. Das, S. De, and B. N. Mandal Radiation of waves by a thin cap submerged in ice-covered ocean, *Q. J. Mech. Appl. Math*, **73** (4), (2020), 261–278.

[21] M. Weitz and J. Keller, Reflection of water waves from floating ice in the water of finite depth, *Communications on Pure and Applied Mathematics*, **3** (3), (1950), 305–318.

[22] D. P. Kouzov, Diffraction of a cylindrical hydroacoustic wave at the joint of two semi-infinite plates, *J. Appl. Mathematics and Mechanics*, **33** (2), (1969), 240–250.

[23] A. N. Norris, Acoustic diffraction from the junction of two joined parallel plates, *J. Acoust. Soc. AM*, **99** (3), (1996), 1475–1483.

[24] M. J. Crocker, *Handbook of acoustics*, New York: John Wiley & Sons, Inc., (1998).

[25] M. A. Bilello, *Formation, growth, and decay of sea ice in the Canadian Arctic Archipelago*, Volume 65, US Army Snow Ice and Permafrost Research Establishment, Corps of Engineers, (1960).

[26] W. Li, R. Wang, D. Li, and D. Fang, A model of temperature-dependent Young's modulus for ultrahigh temperature ceramics, *Physics Research International*, **2011**, (2011), 1–3.

[27] J. B. Wachtman Jr, W. E. Tefft, D. G. Lam Jr, and C. S. Apstein, Exponential temperature dependence of Young's modulus for several oxides, *Physics Review*, **122** (6), (1961), 1754–1759.

[28] E. Lotsari, L. Lind, and M. Kämäri, Impacts of hydro-climatically varying years on ice growth and decay in a subarctic river, *Water*, **11** (10), (2019), 2058.

[29] T. Zhang and M. Jeffries, Modeling interdecadal variations of lake-ice thickness and sensitivity to climatic change in northernmost Alaska, *Annals of Glaciology*, **31**, (2000), 339–347.

[30] A. Cardou, Piecewise uniform optimum design for axial vibration requirement, *AIAA J.*, **11** (12), (1973), 1760–1761.

[31] B. P. Belinskiy, J. W. Hiestand, and J. V. Matthews, Piecewise uniform optimal design of a bar with an attached mass, *Electron. J. Diff. Equations*, **2015** (206), (2015), 1–17.

[32] B. P. Belinskiy, J. W. Hiestand and L. Weerasena, Optimal design of a fin in steady-state, *Appl. Mathem. Model.*, **77**, (2020), 1188-1200.

[33] R. H. Byrd, J. C. Gilbert, and J. Nocedal, A trust region method based on interior point techniques for nonlinear programming, *Mathematical Programming*, **89** (1), (2000), 149–185.

[34] R. H. Byrd, M. E. Hribar, and J. Nocedal, An interior point algorithm for large-scale nonlinear programming, *SIAM Journal on Optimization*, **9** (4), (1999), 877–900.

[35] R. A. Waltz, J. L. Morales, J. Nocedal, and D. Orban, An interior algorithm for nonlinear optimization that combines line search and trust region steps, *Mathematical Programming*, **107** (3), (2005), 391–408.

APPENDIX

MATLAB FMINCON ALGORITHM

We discuss the steps of the MATLAB *fmincon* algorithm to solve a nonlinear optimization problem. The 'fmincon' method has five optimization algorithms: 'interior-point,' 'trust-region-reflective,' 'sqp,' 'sqp-legacy,' and 'active-set'. In our study, we used the default algorithm, 'interior-point'.

Comment. In our study, we had the challenge of dealing with imaginary and out-of-bound values. The 'interior-point' algorithm dealt with this challenge since this algorithm satisfies upper and lower bounds at all iterations and can ignore undefined values.

In general, a nonlinear optimization problem can be written as

$$\begin{aligned} &\min f(x) \\ \text{subject to } &g(x) \leq 0 \\ &h(x) = 0 \\ &x \geq 0, \end{aligned} \tag{A1}$$

where f, g, and h are real-valued functions on $X \subseteq \mathbb{R}^n$, $n \in \mathbb{Z}^+$, with at least one of f, g, and h being nonlinear, and $x \in X$.

Comment. If x is a vector, then $x \geq 0$ means that each component of x will be non-negative.

The setup of the 'fmincon' problem is similar. For each $\mu > 0$, the approximate problem is formulated as

$$\begin{aligned} &\forall \mu > 0 \text{ find } \min f_\mu(x,s) = \min f(x) - \mu \sum_{i=1}^{k} \ln(s_i) \\ \text{subject to } &g(x) + s = 0 \\ &h(x) = 0 \\ &x, s \geq 0, \end{aligned} \tag{A2}$$

where s_i are slack variables and k is a positive integer greater than or equal to 1. When μ approaches 0, the minimum of f_μ approaches the minimum of f. The sum of all the logarithmic terms is called the barrier function, and μ is the barrier parameter (see [33] - [35]).

The optimization problem for our problem (4.1.7), (4.1.11), and (4.1.12) can be formulated as

$$\begin{aligned}
&\min a_n \left\{ \alpha_n \left[1 + P(\omega) \left(\frac{\omega^2 d^2}{c_j^2} - n^2 \alpha_j^2 \right)^2 \right] - \beta(\omega) \Delta x \tan \alpha_n \right\} = b_n \left\{ \alpha_n \tan \alpha_n \left[1 + \right. \right. \\
&\left. \left. P(\omega) \left(\frac{\omega^2 d^2}{c_j^2} - n^2 \alpha_j^2 \right)^2 \right] + \beta(\omega) \Delta x \right\}, \quad j = 1, \ldots, n \\
&\text{subject to } \sqrt{\left(\frac{\omega d}{c_n} \right)^2 - n^2 {\alpha_n}^2} - \sqrt{\left(\frac{\omega d}{c_+} \right)^2 - {\xi_0}^2(\omega)} \leq 0 \\
&- \sqrt{\left(\frac{\omega d}{c_n} \right)^2 - n^2 {\alpha_n}^2} + \sqrt{\left(\frac{\omega d}{c_-} \right)^2 - {\xi_0}^2(\omega)} \leq 0 \\
&0 < \alpha_n < \infty.
\end{aligned} \tag{A3}$$

We define the objective function as

$$\begin{aligned}
f(\alpha_n) = a_n \left\{ \alpha_n \left[1 + P(\omega) \left(\frac{\omega^2 d^2}{c_j^2} - n^2 \alpha_j^2 \right)^2 \right] - \beta(\omega) \Delta x \tan \alpha_n \right\} - b_n \left\{ \alpha_n \tan \alpha_n \left[1 + \right. \right. \\
\left. \left. P(\omega) \left(\frac{\omega^2 d^2}{c_j^2} - n^2 \alpha_j^2 \right)^2 \right] + \beta(\omega) \Delta x \right\}, \quad j = 1, \ldots, n.
\end{aligned} \tag{A4}$$

Then the approximate problem is

$$\begin{aligned} &\min f_\mu(\alpha_n, s) = \min f(\alpha_n) - \mu \ln(s_1) - \mu \ln(s_2) \\ \text{subject to } &\sqrt{\left(\frac{\omega d}{c_n}\right)^2 - n^2 {\alpha_n}^2} - \sqrt{\left(\frac{\omega d}{c_+}\right)^2 - {\xi_0}^2(\omega)} + s_1 = 0 \\ &-\sqrt{\left(\frac{\omega d}{c_n}\right)^2 - n^2 {\alpha_n}^2} + \sqrt{\left(\frac{\omega d}{c_-}\right)^2 - {\xi_0}^2(\omega)} + s_2 = 0 \\ &s_1, s_2 \geq 0 \\ &0 < \alpha_n < \infty. \end{aligned} \tag{A5}$$

We define $g_1(\alpha_n)$ and $g_2(\alpha_n)$ as

$$g_1(\alpha_n) = \sqrt{\left(\frac{\omega d}{c_n}\right)^2 - n^2 {\alpha_n}^2} - \sqrt{\left(\frac{\omega d}{c_+}\right)^2 - {\xi_0}^2(\omega)},$$

$$g_2(\alpha_n) = -\sqrt{\left(\frac{\omega d}{c_n}\right)^2 - n^2 {\alpha_n}^2} + \sqrt{\left(\frac{\omega d}{c_-}\right)^2 - {\xi_0}^2(\omega)}.$$

We further define $g = [g_1, g_2]^T$.

From the constraints in (A5),

$$\begin{aligned} s_1 &= \sqrt{\left(\frac{\omega d}{c_+}\right)^2 - {\xi_0}^2(\omega)} - \sqrt{\left(\frac{\omega d}{c_n}\right)^2 - n^2 {\alpha_n}^2}, \\ s_2 &= \sqrt{\left(\frac{\omega d}{c_n}\right)^2 - n^2 {\alpha_n}^2} - \sqrt{\left(\frac{\omega d}{c_-}\right)^2 - {\xi_0}^2(\omega)}. \end{aligned} \tag{A6}$$

We define $s = [s_1, s_2]^T$.

To solve the approximate problem (A5), the 'interior-point' algorithm would either use a direct step or Conjugate Gradient (CG) Step at each iteration. By default, the algorithm uses a direct step. If it fails, the algorithm uses a CG step.

Define

$$\phi_\nu(\alpha_n, s) = f_\mu(\alpha_n, s) + \nu||g(\alpha_n) + s||. \tag{A7}$$

Here, $\phi_\nu(\alpha_n, s)$ is called the merit function and $\nu > 0$ is a penalty parameter (see [34]). If the merit function is not decreased at an attempted step, the algorithm rejects that step and starts with a new step.

Define the Lagrangian function as

$$L(\alpha_n, s, \bar{\lambda}) = f(\alpha_n) - \mu(\ln s_1 + \ln s_2) + \bar{\lambda}^T(g(\alpha_n) + s), \tag{A8}$$

where $\bar{\lambda}_1$ and $\bar{\lambda}_2$ are Lagrange multipliers and $\bar{\lambda} = [\bar{\lambda}_1, \bar{\lambda}_2]^T$ is the Lagrange multiplier vector.

Comment. Here g and s are vectors, so $g + s$ would be a vector. As we take the dot product of this vector with the $\bar{\lambda}$ vector, we obtain a scalar.

The Karush-Kahun-Tucker (KKT) conditions are given by (A9) - (A11):

$$\begin{aligned} \nabla_{\alpha_n} L(\alpha_n, s, \bar{\lambda}) &= 0, \\ \nabla_s L(\alpha_n, s, \bar{\lambda}) &= 0. \end{aligned} \tag{A9}$$

$$\bar{\lambda}_1 g_1(\alpha_n) + \bar{\lambda}_2 g_2(\alpha_n) = 0. \tag{A10}$$

$$\begin{aligned} g_1(\alpha_n) &\leq 0, \\ g_2(\alpha_n) &\leq 0, \\ \bar{\lambda}_1, \bar{\lambda}_2 &\geq 0. \end{aligned} \tag{A11}$$

Comment. Here, the symbol ∇ with an index means the gradient. More specifically, when we take the gradient with respect to α_n, we consider the α_n component of the gradient. In (A12), ${J_g}^T$ is a row vector and $\bar{\lambda}$ is a column vector. Therefore, $\nabla g\bar{\lambda}$ will be a scalar. Moreover, $f(\alpha_n)$ is a function of only one variable, so ∇f will be reduced to the derivative of f with respect to α_n.

Direct Step

The algorithm starts solving the problem (A5) using this step which is called the Newton step (see [34]). In this step, the algorithm attempts to solve the KKT equations (A9) and (A10) for the problem (A5) using a linear approximation.

From definition (A8) and system (A9),

$$\begin{aligned} \nabla_{\alpha_n} L(\alpha_n, s, \bar{\lambda}) &= \nabla f(\alpha_n) + {J_g}^T \bar{\lambda} = 0, \\ \nabla_s L(\alpha_n, s, \bar{\lambda}) &= -\mu S^{-1} + \bar{\lambda} = 0, \end{aligned} \tag{A12}$$

where $J_g = [\nabla g_1, \nabla g_2]^T$ and $S = \text{diag}(s)$.

From system (A12) and the constraints of (A5),

$$\begin{bmatrix} \nabla f + {J_g}^T \bar{\lambda} \\ -\mu S^{-1}\bar{e} + \bar{\lambda} \\ g + s \end{bmatrix} = 0, \tag{A13}$$

where $\bar{e} = [1,1]^T$

From system (A12),

$$\begin{aligned} \nabla^2_{\alpha_n \alpha_n} L(\alpha_n, s, \bar{\lambda}) &= \nabla^2 f(\alpha_n) + \nabla {J_g}^T \bar{\lambda}, \\ \nabla^2_{\alpha_n s} L(\alpha_n, s, \bar{\lambda}) &= 0, \\ \nabla^2_{ss} L(\alpha_n, s, \bar{\lambda}) &= \mu S^{-2}, \end{aligned} \tag{A14}$$

where $\nabla J_g = [\nabla^2 g_1, \nabla^2 g_2]^T$.

Comment. The symbol ∇ with a double index means the second derivative. If the index is α_n, we take the derivative with respect to α_n of the α_n component of the gradient.

From the definition of $f(\alpha_n)$,

$$\nabla f(\alpha_n) = a_n \left[1 + P(\omega) \left(\frac{\omega^2 d^2}{c_j^2} - n^2 \alpha_j^2 \right)^2 - \beta(\omega) \Delta x \sec^2 \alpha_n \right] - b_n (\tan \alpha_n + \alpha_n \sec^2 \alpha_n) \left[1 + P(\omega) \left(\frac{\omega^2 d^2}{c_j^2} - n^2 \alpha_j^2 \right)^2 \right], \quad j = 1, \ldots, n. \quad \text{(A15)}$$

$$\implies \nabla^2 f(\alpha_n) = -2 a_n \beta(\omega) \Delta x \sec^2 \alpha_n \tan \alpha_n - 2 b_n (\sec^2 \alpha_n + \alpha_n \sec^2 \alpha_n \tan \alpha_n) \left[1 + P(\omega) \left(\frac{\omega^2 d^2}{c_j^2} - n^2 \alpha_j^2 \right)^2 \right], \quad j = 1, \ldots, n. \quad \text{(A16)}$$

From the definitions of $g_1(\alpha_n)$ and $g_2(\alpha_n)$,

$$\nabla g_1(\alpha_n) = -\frac{n^2 \alpha_n}{\sqrt{\left(\frac{\omega d}{c_n} \right)^2 - n^2 {\alpha_n}^2}}, \qquad \nabla g_2(\alpha_n) = \frac{n^2 \alpha_n}{\sqrt{\left(\frac{\omega d}{c_n} \right)^2 - n^2 {\alpha_n}^2}}. \quad \text{(A17)}$$

$$\implies \nabla^2 g_1(\alpha_n) = -\frac{n^2 \left(\frac{\omega d}{c_n} \right)^2}{\left[\left(\frac{\omega d}{c_n} \right)^2 - n^2 {\alpha_n}^2 \right]^{3/2}}, \qquad \nabla^2 g_2(\alpha_n) = \frac{n^2 \left(\frac{\omega d}{c_n} \right)^2}{\left[\left(\frac{\omega d}{c_n} \right)^2 - n^2 {\alpha_n}^2 \right]^{3/2}}. \quad \text{(A18)}$$

Substituting the formulas (A16) and (A18) in the first equation of (A14), we obtain

$$\nabla^2_{\alpha_n\alpha_n} L(\alpha_n, s, \bar{\lambda}) = -2a_n\beta(\omega)\Delta x \sec^2\alpha_n \tan\alpha_n - 2b_n(\sec^2\alpha_n + \alpha_n \sec^2\alpha_n \tan\alpha_n)\left[1+ \right.$$

$$\left. P(\omega)\left(\frac{\omega^2 d^2}{c_j^2} - n^2\alpha_j^2\right)^2\right] - \bar{\lambda}_1 \frac{n^2\left(\frac{\omega d}{c_n}\right)^2}{\left[\left(\frac{\omega d}{c_n}\right)^2 - n^2{\alpha_n}^2\right]^{3/2}} + \bar{\lambda}_2 \frac{n^2\left(\frac{\omega d}{c_n}\right)^2}{\left[\left(\frac{\omega d}{c_n}\right)^2 - n^2{\alpha_n}^2\right]^{3/2}}, \quad j = 1, \ldots, n, \tag{A19}$$

which is defined as the Hessian of $L(\alpha_n, s, \bar{\lambda})$.

Applying Newton's method on the system (A13), we obtain

$$\begin{bmatrix} \nabla^2_{\alpha_n\alpha_n} L & 0 & {J_g}^T \\ 0 & \mu S^{-2} & I \\ J_g & I & 0 \end{bmatrix} \begin{bmatrix} \Delta\alpha_n \\ \Delta s \\ \Delta\bar{\lambda} \end{bmatrix} = - \begin{bmatrix} \nabla f + {J_g}^T\bar{\lambda} \\ S\bar{\lambda} - \mu\bar{e} \\ g + s \end{bmatrix}, \tag{A20}$$

where I is the 2x2 identity matrix.

Comment. In the 3x3 matrix above, 0 in the first row is a row vector of size 2 containing 0's, 0 in the second row is a column vector of size 2 containing 0's, and 0 in the third row is a scalar. The first equation contains scalar quantities on both the left and right sides. Since S^{-2} has size 2x2 and s has size 2x1, $\mu S^{-2}\Delta s$ has size 2x1 and $I\Delta\lambda$ has size 2x1 by the same reasoning. Therefore, the size of both the left and right sides in the second equation is 2x1. In the third equation, the size of the left and right sides is 2x1.

By premultiplying Δs with S^{-1}, we can rewrite the above augmented system as

$$\begin{bmatrix} \nabla^2_{\alpha_n\alpha_n} L & 0 & {J_g}^T \\ 0 & S\Lambda & S \\ J_g & I & 0 \end{bmatrix} \begin{bmatrix} \Delta\alpha_n \\ S^{-1}\Delta s \\ \Delta\bar{\lambda} \end{bmatrix} = - \begin{bmatrix} \nabla f + {J_g}^T\bar{\lambda} \\ S\lambda - \mu\bar{e} \\ g + s, \end{bmatrix}, \tag{A21}$$

where $\Lambda = \text{diag}(\bar{\lambda})$ and $\Lambda = \mu S^{-1}$.

The system of equations (A21) represents the direct step. To solve for $(\Delta\alpha_n, \Delta s)$, the algorithm creates an $l\bar{d}l$ factorization of the matrix. In the $l\bar{d}l$ factorization, the matrix is factored as $l\bar{d}l^*$, where l is the unit lower triangular matrix, $\bar{d}$ is the block diagonal matrix, and l^* is the Hermitian transpose of l. Using this factorization, the algorithm checks whether $\nabla^2_{\alpha_n\alpha_n}L$ is positive definite or not to obtain a finite solution of the system (A21). If $\nabla^2_{\alpha_n\alpha_n}L$ is not positive definite, the algorithm uses the CG step.

Update Barrier Parameter

For the problem (A5) to approach the original problem (A3), the barrier parameter μ should get close to 0 with the increase of iterations (see [33] - [35]). The algorithm has two barrier parameter options: 'monotone' and 'predictor-corrector.' The default option is 'monotone,' which we used in this study. In the case of the 'monotone' option, μ decreases by a factor of $1/100$ or $1/5$ if the problem (A5) is solved with sufficient accuracy.

Comment. For the approximate problem to approach the original problem, μ should approach 0. We say that the problem is solved with sufficient accuracy if the problem is solved within the specified tolerance. If the problem (A5) is solved in less than three iterations, then μ is updated by the factor of $1/100$; otherwise, μ is updated by the factor of $1/5$ (see [35]).

The measure of accuracy is determined by (see [35])

$$\max(||\nabla f + {J_g}^T\bar{\lambda}||, ||S\bar{\lambda} - \mu\bar{e}||, ||g + s||) < \mu.$$

Conjugate Gradient Step

We start with the system (A13) obtained by the KKT equations. Multiplying the second equation by S on both sides, we obtain

$$\begin{bmatrix} \nabla f + \nabla g \bar{\lambda} \\ S\bar{\lambda} - \mu \bar{e} \\ g + s \end{bmatrix} = 0. \tag{A22}$$

The algorithm finds the Lagrange multipliers by computing the least squares estimates. The Lagrange multiplier vector $\bar{\lambda}$ would minimize the Euclidean norm of the first two equations of (A22). $\bar{\lambda}$ is found as

$$\bar{\lambda} = \lambda^{LS} = (J^T J)^{-1} J^T \begin{bmatrix} -\nabla f \\ \mu e \end{bmatrix},$$

where $J = [J_g^T, S]^T$ and λ^{LS} refers to the least square estimate of $\bar{\lambda}$.

After computing the Lagrange multipliers, the algorithm applies the sequential quadratic programming method to the problem (A5). The displacement $(\Delta\alpha_n, \Delta s)$ is generated by solving the quadratic subproblem

$$\begin{aligned} &\min \nabla f^T \Delta\alpha_n + \frac{1}{2}\Delta\alpha_n^T \nabla^2_{\alpha_n\alpha_n} L \Delta\alpha_n - \mu \bar{e}^T S^{-1} \Delta s + \frac{1}{2}\Delta s^T S^{-1} \Lambda \Delta s \\ &\text{subject to } J_g \Delta\alpha_n + \Delta s + g + s = r \\ &\qquad (\Delta\alpha_n, \Delta s) \in Y, \end{aligned} \tag{A23}$$

where r is the unknown function and Y is a closed and bounded set that defines a region around α_n such that the quadratic model (the objective function) and linear constraint are good approximations of the problem and that the feasibility of s_1 and s_2 is ensured (see [34]).

Here, $\nabla^2_{\alpha_n\alpha_n} L(\alpha_n, s, \bar{\lambda})$ is the Hessian of the objective function in (A23) with respect to α_n and $\nabla^2_{ss} L(\alpha_n, s, \bar{\lambda})$ is the Hessian of the objective function in (A23) with respect to s or an

approximation to it. With the help of the trust region Y, the algorithm can obtain a finite solution for the subproblem (A23) even when $\nabla^2_{\alpha_n\alpha_n}L$ is not positive definite (see [34]). A step $(\Delta\alpha_n, \Delta s)$ is computed such that it lies inside Y, the objective function in the subproblem (A23) is a good approximation to the objective function in (A5), and the linear constraints in the subproblem (A23) are good approximations to the linear constraints in (A5) (see [34]).

The following bound on the step is imposed.

$$\left\| \begin{bmatrix} \Delta\alpha_n \\ \Delta s \end{bmatrix} \right\| \leq R,$$

where the trust region radius $R > 0$ is updated at every iteration (see [33], [34]).

The step in the slack variables is scaled by S^{-1} to avoid the slack variables from approaching zero (see [33]). The scaled trust region is given as

$$\left\| \begin{bmatrix} \Delta\alpha_n \\ S^{-1}\Delta s \end{bmatrix} \right\| \leq R.$$

The slack variables should also remain positive, so another condition is imposed. This condition is given as

$$s + \Delta s \geq (1-t)s \implies \Delta s \geq -ts,$$

where $t \in (0,1)$ and is usually taken close to 1 (see [33] and [34]).

Normal Step

To find a value of r that makes subproblem (A23) feasible, i.e., the finite solution of (A23) lies within the trust region Y, the algorithm starts by computing the normal step v that lies in the trust region and approximately satisfies the linear constraint of subproblem (A23) in the least squares sense (see [34]). In order to achieve this, we consider the variable $a = (a_{\alpha_n}, a_s)^T$ for the

subproblem (see [34])

$$\begin{aligned} &\min \ ||J_g a_{\alpha_n} + a_s + g + s||^2 \\ &\text{subject to } \ ||(a_{\alpha_n}, S^{-1}a_s)^T|| \leq \zeta R \\ &a_s \geq -ts/2, \end{aligned} \tag{A24}$$

where $\zeta \in (0,1)$.

Define

$$\tilde{a} = (a_{\alpha_n}, \tilde{a_s})^T = (a_{\alpha_n}, S^{-1}a_s)^T. \tag{A25}$$

Performing this transformation on the objective function of subproblem (A24), the algorithm first calculates the Cauchy point $\tilde{a}^{CP}$ of the problem by minimizing the objective along the steepest descent direction starting from $\tilde{a} = 0$ (see [34]). Then it computes the Newton step $\tilde{a}^N$, which is the minimum norm minimizer of the objective (see [34]). The Cauchy and Newton steps define the dogleg path, which consists of two segments from $\tilde{a} = 0$ to $\tilde{a} = \tilde{a}^{CP}$ and from $\tilde{a} = \tilde{a}^{CP}$ to $\tilde{a} = \tilde{a}^N$ (see [34]). After the objective is minimized and the dogleg step is compared with the Newton step truncated to the feasible region, the lower value of the objective function is chosen between these two steps (see [34]). Finally, $\tilde{a}$ is transformed into the original space of variables (see [34]).

Tangential Problem

From the residual of the normal step, we define (see [34])

$$r = J_g a_{\alpha_n} + a_s + g + s.$$

From subproblem (A23),

$$\begin{aligned} &\min \nabla f^T \Delta\alpha_n - \mu \bar{e}^T S^{-1} \Delta s + \frac{1}{2}(\Delta\alpha_n^T \nabla^2_{\alpha_n\alpha_n} L \Delta\alpha_n + \Delta s^T S^{-1} \Lambda \Delta s) \\ &\text{subject to } J_g \Delta\alpha_n + \Delta s = J_g a_{\alpha_n} + a_s \\ &\qquad ||(\Delta\alpha_n, S^{-1}\Delta s)^T|| \leq R \\ &\qquad \Delta s \geq -ts. \end{aligned} \tag{A26}$$

To find an approximate solution of subproblem (A26), we define

$$\Delta_+ = a + b, \tag{A27}$$

where a is the normal step and b is tangent to the scaled constraint gradients.

Using the same change of variables as equation (A25), we define

$$\tilde{\Delta}_+ = (\tilde{\Delta}\alpha_n, \tilde{\Delta}s)^T = (\Delta\alpha_n, S^{-1}\Delta s)^T = (a_{\alpha_n}, \tilde{a_s})^T + (b_{\alpha_n}, \tilde{b_s})^T = \tilde{a} + \tilde{b}. \tag{A28}$$

Define

$$\mathscr{L} = \begin{bmatrix} \nabla^2_{\alpha_n\alpha_n} L & 0 \\ 0 & \Lambda S \end{bmatrix}. \tag{A29}$$

Using equations (A28) and (A29), the objective of subproblem (A26) can be expressed as

$$q(\tilde{a} + \tilde{b}) = (\nabla f^T, -\mu \bar{e}^T)(\tilde{a} + \tilde{b}) + \frac{1}{2}(\tilde{a} + \tilde{b})^T \mathscr{L} (\tilde{a} + \tilde{b}).$$

From the first nonlinear constraint of subproblem (A26),

$$||\tilde{\Delta}_+||^2 = ||\tilde{a} + \tilde{b}||^2 \leq R^2.$$

The algorithm imposes the condition $\tilde{b}^T\tilde{a} = 0$. Therefore, the above inequality can be expressed as

$$||\tilde{b}||^2 \leq R^2 - ||\tilde{a}||^2.$$

Now, subproblem (A26) can be written as

$$\begin{aligned} \min\ & q(\tilde{a}+\tilde{b}) = q(\tilde{a}) + \nabla f^T b_{\alpha_n} - \mu\bar{e}^T\tilde{b_s} + (\mathscr{L}\tilde{a})^T\tilde{b} + \frac{1}{2}(\tilde{b}^T\mathscr{L}\tilde{b})_n \\ \text{subject to}\ & J_g b_{\alpha_n} + S\tilde{b_s} = 0 \\ & ||\tilde{b}||^2 \leq R^2 - ||\tilde{a}||^2 \\ & \tilde{b_s} \geq -t\bar{e} - \tilde{a_s}, \end{aligned} \tag{A30}$$

which is the tangent subproblem.

The CG iteration computes estimates of the minimizer of q by the recursion (see [34])

$$\tilde{b}^+ = \tilde{b} + \alpha p,$$

where the parameter α is chosen to minimize q and p is the direction of the gradient of q.

The algorithm terminates if the projected gradient of q is less than the prescribed tolerance, if the direction of p is one of the negative curvatures, or if the trust-region norm constraint is not satisfied (see [34]). Finally, $\tilde{b}$ is transformed into the original space of variables (see [34]). The merit function (A7) determines whether solution (2.0.13) is acceptable; if not, the trust-region radius R is updated accordingly (see [34]).

VITA

Mohammad Khan was born and raised in Karachi, Pakistan. He received a bachelor's degree in Applied Mathematics from the University of California, Berkeley, in 2016 and a master's degree from California State University, Long Beach, in 2019. He then earned his doctoral degree in Computational Science, with a Computational and Applied Mathematics concentration, at the University of Tennessee at Chattanooga in 2023 under the supervision of Dr. Boris P. Belinskiy and Dr. Lakmali Weerasena.

Khan has experience writing in Python, Java, C/C++, R, and MATLAB. He has worked as a tutor and grader in mathematics during his undergraduate and graduate years and gained middle school and high school teaching experience in mathematics, statistics, and physics. During his senior year of the undergraduate program, he co-authored a physics book for high school students. During his doctoral program, he published a paper with his advisors and Dr. Don Hinton from the University of Tennessee at Knoxville. At the time of submitting this dissertation, he is working on a manuscript for publication along with his advisors. He was an invited speaker at the UTC Research Dialogues Conference in April 2021 and 2022, UTC Technology Symposium in April 2021, and the New York State Regional Graduate Mathematics Conference in April 2021.